DESIGN AND CONTROL OF SOLAR PANEL COMPANION INVERTERS FOR PANEL LEVEL POWER EXTRACTION

by

Prasanth Kumar Sahu

A dissertation submitted to the faculty of
The University of North Carolina at Charlotte
in partial fulfillment of the requirements
for the degree of Doctor of Philosophy in
Electrical Engineering

Charlotte

2019

Approved by:

_____
Dr. Madhav Manjrekar

_____
Dr. Tiefu Zhao

_____
Dr. Abasifreke Ebong

_____
Dr. Maciej Noras

ABSTRACT

PRASANTH KUMAR SAHU. Design and control of solar panel companion inverters for panel level power extraction. (Under the direction of DR. MADHAV MANJREKAR)

Solar Panel Companion Inverters (SPCIs) have been proposed as H-bridge inverters embedded with a PV module. These inverters employ a unique methodology that converts the conventional DC voltage output of a solar panel to switched quasi-square wave voltages with variable pulse width. These SPCIs are connected in series to produce an aggregated superior quality multilevel waveform that can be directly interfaced with the AC grid. This alternative approach offers advantages of micro-inverters in realizing panel-level maximum power point transfer and realization of system-level cost benefits of a central inverter. In this dissertation, dynamic analysis and closed loop controller design of SPCIs is presented. Maximum Power Point Tracking (MPPT) for SPCIs is proposed to demonstrate the panel level maximum power extraction from the solar panels. Simulations are performed using MATLAB Simulink, to demonstrate efficacy of the MPPT algorithm. Reactive power support of SPCIs while maintaining MPPT is explored. Panel level optimization is investigated by performing analysis for synthesizing AC output voltage across each SPCI. Using the analysis, a modified sort and stack algorithm is presented to implement Sorted Stair Case Modulation and Sorted Pulse Width Modulation strategies. A laboratory prototype was constructed to demonstrate the principle of sort and stack algorithm, closed loop current control and grid tie operation. Also, reactive power support while maintaining MPPT is experimentally demonstrated.

DEDICATION

To my parents and brother.

ACKNOWLEDGEMENTS

I would like to express my gratitude towards my parents, my brother for believing in me and making it possible for me to follow my dream of pursuing higher education.

I would like to thank my advisor, Dr. Madhav Manjrekar, for his guidance and encouragement, without which, this dissertation would not have been possible. His words can always inspire me and take me to higher level of thinking in my future endeavors.

It would be my duty to extend my gratitude to the committee members Dr. Tiefu Zhao, Dr. Abasifreke Ebong, and Dr. Maciej Noras for taking time to be on my committee and assess my work.

I am thankful to EPIC (Energy Production and Infrastructure Center) for its generous support. Also, I would like to thank Dr. Ronak Bhatt for his support and valuable inputs provided while building the laboratory prototype.

I should also mention Patrick and Fabian who assisted me, and Dr. Soma, who provided his inputs while establishing my experimental setup. I was fortunate to be surrounded by wonderful colleagues and friends. Pankaj, Nakul and Nisha have been extremely helpful and made my time at the lab so memorable.

Special mentions to Santhosh and Harsha for being my amazing roommates and very good friends. Finally, I would like to thank all my friends who have always been there for me throughout the process.

TABLE OF CONTENTS

LIST OF FIGURES

CHAPTER 1 : INTRODUCTION

1.1. Introduction

This chapter presents a brief introduction and organization of the dissertation. Importance of renewable power generation is presented in Section 1.2. Motivation for the research is presented in Section 1.3. Section 1.4 presents the organization of the dissertation.

1.2. Renewable Power

There has been an increasing demand of energy with the increase in standard of living. Figure 1.1 shows the History of energy consumption in the United States by source of energy generation [1]. Figure 1.2 shows the contribution to the electric power generation by various sources in the recent past [2] with fossil fuels being the major source. The domination of fossil fuels in electric power generation has been one of the primary reasons for the global warming. Also, excessive usage of fossil fuels as the energy source will ultimately lead to extinction of fossil fuels in the years to come. In order to avoid the declination of fossil fuel reserves and combat the global warming hazards, it is important to rely on renewable power like solar power generation using Photo-Voltaic (PV) cells.

1.3. Motivation

The work discussed in this dissertation is an extension of thesis work reported in [3]. According to the U.S. Department of Energy (DOE) a PV system installed at 1$/W, equivalent to 5 cents/kWh, would make solar energy competitive with the wholesale rate

of electricity without additional subsidies. Preliminary DOE analysis of required component costs to reach $1/W installed PV system implies the following breakdown: 50 cents/W for the module, 40 cents/W for the balance of system and installation, and 10 cents/W for power electronics [4]. A typical commercially available solar panel [5] rated for ~30 V DC/8 A DC when operating at its maximum power point, thus establishes a target cost for power electronics at $25-$30 per panel. Towards optimizing capital costs of power electronics on a per watt basis, central photovoltaic inverters have been designed for bulk applications [6]. Strings of solar panels are connected in series to build up DC voltage and then connected in parallel to scale up to required power level before feeding into a single inverter. An alternative approach is to employ a micro-inverter for every solar panel [7]. Such small inverters convert DC electricity produced by a single solar panel and synthesize required ac voltage. Recently, string inverters have been proposed for residential and small commercial systems [8]. They are smaller than central inverters and process power from only one string of solar panels. However, they are larger than micro-inverters and do not interface with each panel on an individual basis. Historically, it has been observed that employment of central inverters for solar power conversion limits energy yields, whereas employment of micro-inverters has not been commercially attractive for larger volumes. A unique methodology has been discussed in [3]. This methodology converts the conventional DC voltage output of a photovoltaic solar panel to switched quasi-square wave voltage with variable pulse width, which when aggregated realizes a superior quality multilevel waveform that can be directly interfaced with the power grid. This alternative approach, termed Solar Panel Companion Inverter (SPCI), offers advantages of micro-inverters in realizing panel-level Maximum Power Point Transfer

(MPPT) and enhanced controllability. Furthermore, bill of materials for each quasi-square wave H-bridge inverter is fractional as compared to micro-inverter, thus enabling realization of system-level cost benefits of a central inverter approach. However, the barrier for this approach is in synthesis and sequencing of individual quasi-square wave outputs in real time based on a) grid synchronization requirements, and b) employment of varying DC voltage/current levels dictated by MPPT algorithms. Despite these challenges associated with control complexity and power circuit minimization, the motive of this dissertation is to investigate a game-changing mechanism for interfacing solar panels with power grid. Simulation results demonstrating the panel level MPPT operation of SPCI had been presented [3]. However, the simulations were performed using an open loop current control approach, and the report was focused on exploring the modulation strategies. This dissertation was started with a motive to implement a closed loop current control working with an MPPT algorithm, to demonstrate the maximum power operation at panel level. Also, the objective was to construct a laboratory prototype of SPCI, demonstrating the principle of operation in open loop. This is followed by closed loop current control of grid connected SPCI using DC power supplies. Demonstration of maximum power extraction of SPCI, by connecting real solar panels to each of the SPCI is also discussed in this dissertation.

1.4. Organization of Dissertation

This section presents an overview of the organization of dissertation as follows.

Chapter 1: Introduction

This chapter presented a brief introduction and organization of the dissertation. Importance of renewable power generation was presented in Section 1.2. Motivation for

the research was presented in Section 1.3. Section 1.4 presented the organization of the dissertation.

Chapter 2: Literature Review of Photo-Voltaic Power Conversion Techniques

This Chapter consists of survey of scholarly survey of various Photo-Voltaic (PV) power conversion techniques. The most popular PV topologies such as central inverter topology, string topology and micro inverter topologies are discussed in Section 2.2. Multilevel topologies for PV power conversion are discussed in Section 2.3. Closed loop control techniques for popular PV converter topologies are presented in Section 2.4. Chapter 2 concludes with a discussion presented in Section 2.5.

Chapter 3: Solar Panel Companion Inverter

This chapter provides a brief overview of Solar Panel Companion Inverters (SPCI). Section 3.2 describes the topology of SPCI. Principle of operation of SPCIs is presented in section 3.3. The principle of Sort and Stack is defined in Section 3.4. Various modulation strategies that have been employed for SPCIs is described in section 3.5. Section 3.6 describes the concept of Master Selector. The chapter concludes with a summary presented in Section 3.7.

Chapter 4: Dynamic Analysis and Controller Design

In this chapter, a closed loop control architecture to control active power, and reactive power generation from grid connected SPCI has been introduced. The control architecture together with the Maximum Power Point Tracking scheme that will be discussed in Chapter 6 will be utilized to inject power into the grid. Section 4.2 presents closed loop control scheme employed for grid connected SPCI. This section also the dynamic modeling of real/reactive power - controller. Current controller design of SPCI and its dynamic

performance is presented in Section 4.3. Section 4.4 concludes the chapter with a brief summary.

Chapter 5: Modeling and Simulation

This chapter presents the model of a grid connected SPCI. Section 5.2 describes a block diagram of grid connected SPCI. Matlab Simulink model of power grid and SPCI is explained in Sections 5.3, and 5.4 respectively. Master controller for Sorted Stair Case Modulation (SSCM) Section 5.5. Simulation results demonstrating the closed loop current control operation of grid connected SPCI, with ideal DC voltage sources connected across the DC bus is presented in Section 5.6. Section 5.7 concludes this chapter with a brief discussion.

Chapter 6: Maximum Power Point Tracking

In this chapter, a Maximum Power Point Tracking (MPPT) algorithm for SPCI is described. MPPT scheme is employed to perform maximum power extraction from the photo-voltaic panels at system level. This algorithm generates magnitude of the reference current such that maximum power is extracted from the system. Discussion in this chapter involves power injection into the grid at unity power factor. In section 6.2, block schematic description which includes the proposed MPPT algorithm is presented. MPPT algorithm employed to extract maximum power is discussed in section 6.3. Simulation results for various operating scenarios are presented in section 6.4. These simulations are performed for both Sorted Staircase Modulation (SSCM) and Sorted Pulse Width Modulation (SPWM) schemes that have been explained in Chapter 3. Section 6.5 concludes this chapter with a brief summary.

Chapter 7: Active and Reactive Power Control

This chapter starts by presenting a conventional case of real power transfer into the grid, along with a discussion on generalized power transfer scenarios in sections 7.2, and 7.3. Simulation results corresponding to real and reactive power flow scenarios for the grid connected SPCIs by implementing sort and stack algorithm together with closed loop MPPT algorithm proposed for SPCI are demonstrated in Section 7.4. This chapter concludes with a summary presented in Section 7.5.

Chapter 8: Panel Level Optimization

In this chapter, to ensure that each panel operates at maximum power, an analytical equation which defines the AC output voltage to be synthesized by each SPCI when operating at MPPT is derived in Section 8.2. Using the derived AC output equation, a control algorithm which ensures the maximum power extraction from SPCI, at panel level is presented in Section 8.3. Simulation results which demonstrate the efficacy of the proposed control scheme is demonstrated in Section 8.4. Section 8.5 ends this chapter with a brief summary.

Chapter 9: Experimental setup

In this chapter the prototype construction of Solar Panel Companion Inverters (SPCIs) and demonstration of principle of operation, grid tied operation and Maximum Power Point Tracking (MPPT) algorithm implementation is presented. Section 9.2 discussed the construction of laboratory prototype to demonstrate the working of SPCI. Grid tie operation of grid connected SPCI system is presented in Section 9.3. Section 9.4 demonstrates the MPPT implementation of grid connected SPCI, as well as the reactive power support. Section 9.5 concludes with a brief summary.

Chapter 10: Conclusion

In this chapter, a summary of the contributions that have been made towards the dissertation are presented. Also, the possible areas of future research have been presented.

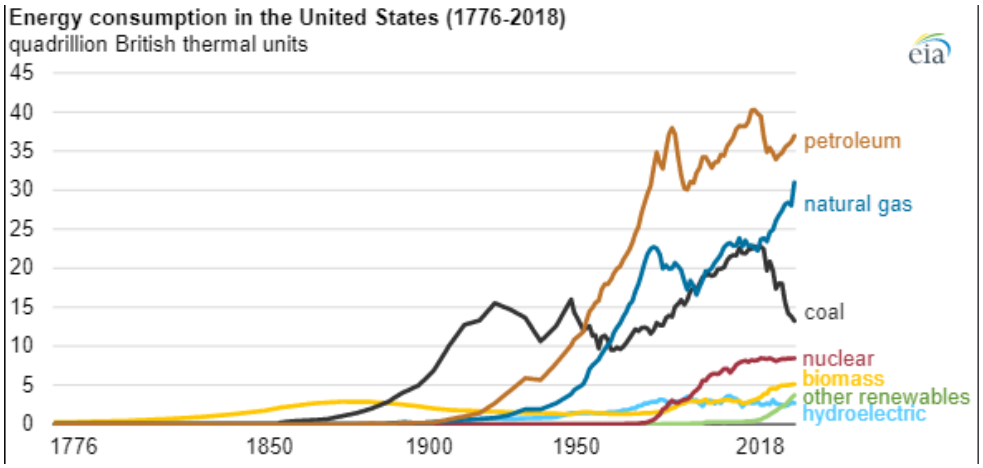

FIGURE 1.1: History of energy consumption in United States [1].

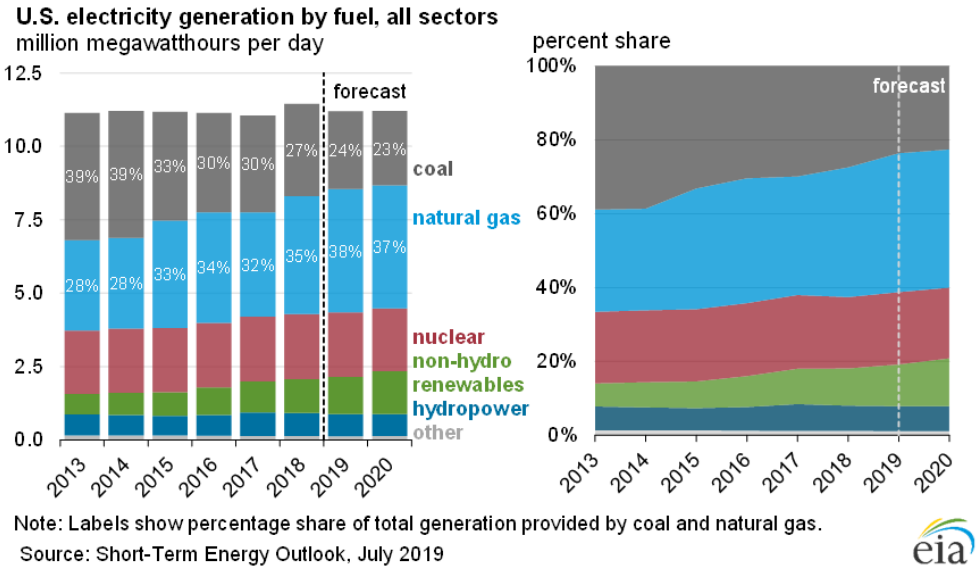

FIGURE 1.2: Electricity generation in United States, by the source of energy [2].

CHAPTER 2 : LITERATURE REVIEW OF PHOTO-VOLTAIC POWER CONVERSION TECHNIQUES

2.1. Introduction

This Chapter consists of survey of scholarly survey of various Photo-Voltaic (PV) power conversion techniques. The most popular PV topologies such as central inverter topology, string topology and micro inverter topologies are discussed in Section 2.2. Multilevel topologies for PV power conversion are discussed in Section 2.3. Closed loop control techniques for popular PV converter topologies are presented in Section 2.4. Chapter 2 concludes with a discussion presented in Section 2.5.

2.2. Classical Photo-Voltaic Power Converter Topologies

Centralized inverter is the commonly used topology for commercial power generation units. As shown in Figure 2.1, central inverter topology consists of several Photo-Voltaic (PV) modules connected in series to form a string and build up the DC voltage comparable to grid voltage. Several such strings are connected in parallel through diodes to build up to the power level, before being fed to an inverter [6, 9, 10]. These inverters can be classical three-phase or single-phase H-bridge inverters, depending on whether the inverters are connected to three-phase or single-phase AC utility grid. This can be referred to as a single stage power conversion. The advantages of such a configuration are: high efficiency (because of single stage power conversion), ease of installation and low cost per watt. Disadvantages of central topology are: high voltage DC cables are required between PV modules and the inverter, maximum power generation from the system is limited by the

module which has the least irradiation and hence offers low yield of output power in case of power mismatch between the panels, there is also a drawback arising from single point of failure.

A variation to the centralized topology could be obtained by introducing a DC-DC power conversion stage before the DC-AC conversion, as shown in Figure 2.2. The DC-DC power conversion stage can be implemented at string level as shown in Figure 2.3, or panel level as shown in Figure 2.4 [7, 11]. These variations can mitigate the effects of power mismatch between the panels and improve the yield. However, the power losses can increase because of the additional DC-DC power conversion stages.

An improved version of central inverter topology is called the string inverter topology which can be seen in Figure 2.5 [8, 9]. In this topology, strings of panels are directly connected to an inverter, which is then interfaced with AC utility grid. There is no need of connecting a string diode. Several such string inverters can be connected to the grid to increase the power level. Maximum power point tracking (MPPT) is implemented on each string. Thus, this methodology offers better yield when compared to that of a central inverter, whenever there is a power mismatch. An improvement to the basic string topology can be implemented by including a DC-DC power converter for each string before the inverter stage. The cost of installation for string topology is more than central inverters, because of the usage of several inverters.

Module level power optimization can be implemented by micro-inverter topology which is shown in Figure 2.6 [7]. In this topology, the inverter is integrated with the PV module and is directly interfaced to the grid. Individual panel-level MPPT can be implemented in this topology, thereby eliminating losses due to power mismatch between

the panels. Usage of DC wiring is eliminated, since the inverters are directly connected to the photovoltaic modules, and the output coming from the inverter is AC. The issue related to single point of failure can be mitigated in this system [12]. Because of its modularity, this topology has an additional advantage of scaling up to the required power level. There are certain drawbacks of micro-inverter topology, as it needs an additional DC-DC boost conversion stage, to step up the module voltage of (usually 30-35 V DC) at maximum power point operation, to match the grid voltage level. This additional DC-DC power conversion stage increases losses in the system. Also, the price on per watt basis is the highest for micro-inverter topology, when compared to central and string inverter topologies.

The inverters employed for classical inverter topologies are two-level or three-level inverters. The power electronic devices utilized for centralized or string topologies will need high voltage ratings, because the DC bus voltage in these topologies are higher. Another class of inverters called multilevel inverters which can utilize power electronic devices rated at low voltage, is discussed in Section 2.3. These inverters are better in terms of performance because they can operate at lower switching frequency and produce superior quality output voltage.

2.3. Multilevel Photo-Voltaic Power Converter Topologies

Various multilevel power converter topologies for PV to improve the performance and efficiency have been proposed [13]. Figure 2.7 shows the diode clamped (also called as neutral point clamped) inverter topology [14-20]. An array of PV modules can be connected to terminals on the DC side of the inverter. The voltage of each array can be controlled to maintain its MPP. Figure 2.8 shows the schematic of a single-phase grid

connected flying capacitor topology for PV power conversion [21-24]. The drawbacks of diode clamped, and flying capacitor topologies topology are non-modularity, and complex controls.

Figure 2.9 shows the schematic of cascaded H-bridge multilevel inverter topology for PV power conversion [25-35]. This topology consists of several single-phase full bridge inverters connected in series on the AC side, and isolated DC power sources (or PV modules) connected on the DC side. Since several such identical H-bridges can be connected in series to build up the voltage on the AC side, this topology has the advantage of being modular. A sinusoidal output voltage can be synthesized by triggering each H-bridge at different voltage levels. Another topology like cascaded H-bridge inverter, called AC stacked inverter has been implemented [36-38]. This topology doesn't synthesize a multilevel output waveform. However, it utilizes high switching frequency scheme to synthesize a sinusoidal voltage at the output of each inverter.

Despite having drawbacks such as complex control algorithms, multilevel inverters have been found to be better in terms of efficiency and performance when compared to classical inverters (two-level or three-level). Multilevel inverters allow the power electronics devices to operate at a low switching frequency and produce an equivalent high switching frequency voltage waveform. These reasons led to a significant research interest in multilevel inverter topologies.

2.4. Closed Loop Control Schemes for Photo-Voltaic Inverters

There can be two approaches towards controlling the grid connected PV inverters. The first approach is called the voltage-mode control which is utilized which is shown in Figure 2.10. This control mode is utilized for FACTS controllers [39-42]. In this mode of control,

the real and reactive power are controlled by controlling the phase angle and amplitude of inverter output AC voltage with respect to the voltage at point of common coupling (PCC). Despite being a simple control implementation, voltage-mode control has a drawback that there is no control over the AC grid current which means the inverter is not protected against the over currents [43].

Another approach called the current-mode control can be implemented wherein, the AC grid current of the inverter is controlled. Figure 2.11 shows a simplified block schematic of current-mode control implementation in dq-frame. In this approach, the active and reactive power are controlled by controlling the phase angle and amplitude of AC grid current with respect to the voltage at PCC. This ensures that the inverter is well protected against sudden variations in the current. This approach also has the advantages of being robust and having a very good dynamic performance [43, 44]. Current control approaches for popular PV inverter topologies are presented in this section.

To have a Maximum Power Point (MPP) operation, the output voltage of PV or the inverter DC input should be maintained constant. The DC terminals of the inverter is usually connected with a DC capacitance to hold the DC bus voltage. For single-stage power converters, this voltage can be controlled by implementing a multi-loop control technique as shown in Figure 2.12 [8, 45, 46]. This figure shows a sample control implementation for single stage centralized topology for PV inverters. It consists of an outer voltage loop which controls the DC bus voltage. Reference to DC bus voltage to this loop is obtained from the Maximum Power Point Tracking (MPPT) block. Algorithms such as Perturb and Observe (P&O), or incremental conductance can be implemented to generate the reference voltage [47-56]. Voltage control loop generates a reference current

which is multiplied with output of Phase Locked Loop (PLL) to inject a current which is in phase with the grid voltage.

For topologies involving two-stage power conversion, MPPT is implemented by DC-DC power conversion stage [57]. This stage is usually in boost configuration, especially for microinverter topology because the panel level voltage must be stepped up to reach the grid voltage level. The inverter controller is a double loop configuration consisting of an outer voltage loop control, which maintains the DC bus voltage at the inverter DC terminals along with the inner current loop control which ensures active power injection into the grid. Figure 2.13 shows the sample schematic of control that can be implemented for a two-stage configuration.

Outer voltage loop controller can be a Proportional-Integral (PI) controller, since the parameters of comparison are DC quantities. However, the actual voltage across the capacitor has 120 Hz ripple. Hence, various control techniques to mitigate this ripple has been researched in the literature [45, 57]. The inner current control loop has a comparison of parameters which are sinusoidal in nature. Controllers for inner loop can be PI, or Proportional-Resonant (PR). While implementing PI controller to control the instantaneous current value, it is challenging to achieve a zero steady state error [58]. On the other hand, PR controller can achieve a zero steady state error because of its high gain at fundamental frequency [59].

2.5. Discussion

From the discussion about various inverter topologies, it can be inferred that there are topologies like the central inverter configuration which are economical. However, these offer a very low yield under non-uniform irradiance conditions because of the absence of

panel level maximum power point tracking realization. On the other hand, there are topologies like the micro-inverter which offer a very good yield under non-uniform irradiance conditions because of the panel level maximum power point tracking realization. However, such configurations are not economical. Solar Panel Companion Inverters (SPCIs) have been proposed where a panel level maximum power point can be realized, by simultaneously reducing the installation costs [60]. But there exists a complexity in the realization of control scheme for the configuration. This research investigates the possibility of existence of such a configuration.

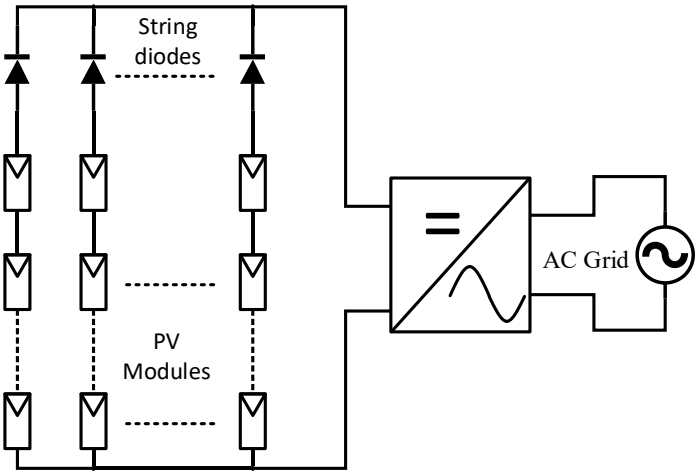

FIGURE 2.1: Simplified circuit schematic showing grid connected central inverter topology.

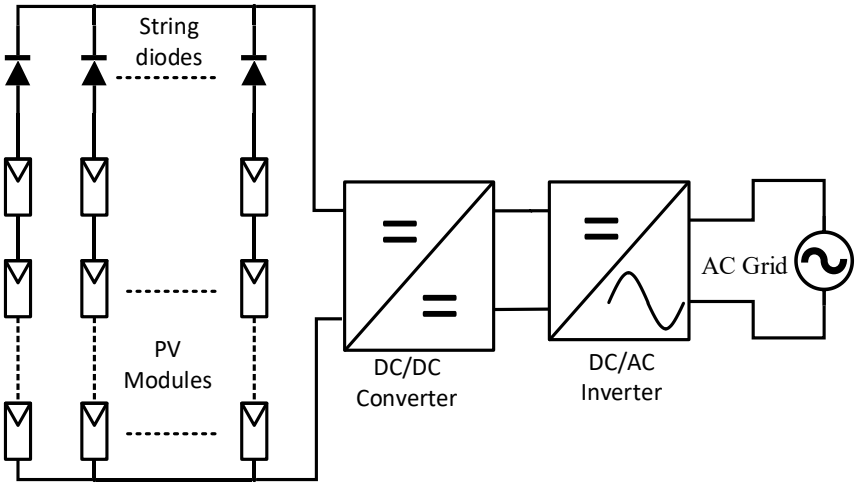

FIGURE 2.2: Simplified circuit schematic showing grid connected central inverter topology with a central DC-DC converter.

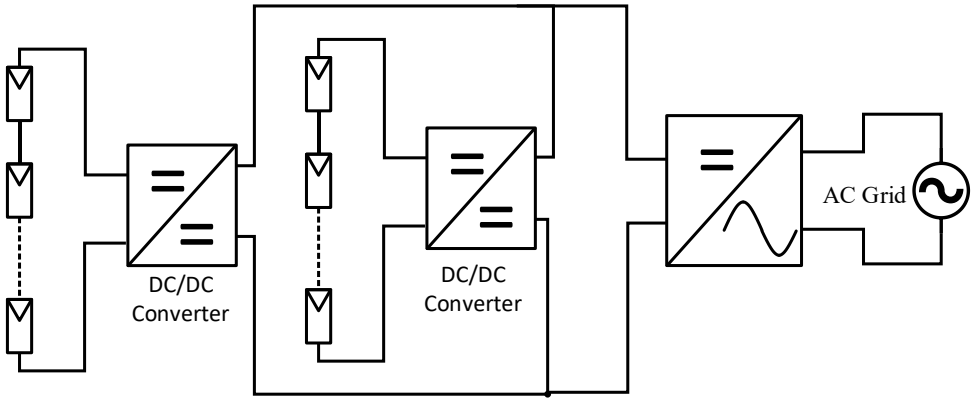

FIGURE 2.3: Simplified circuit schematic showing grid connected central inverter topology with DC optimizers at string level.

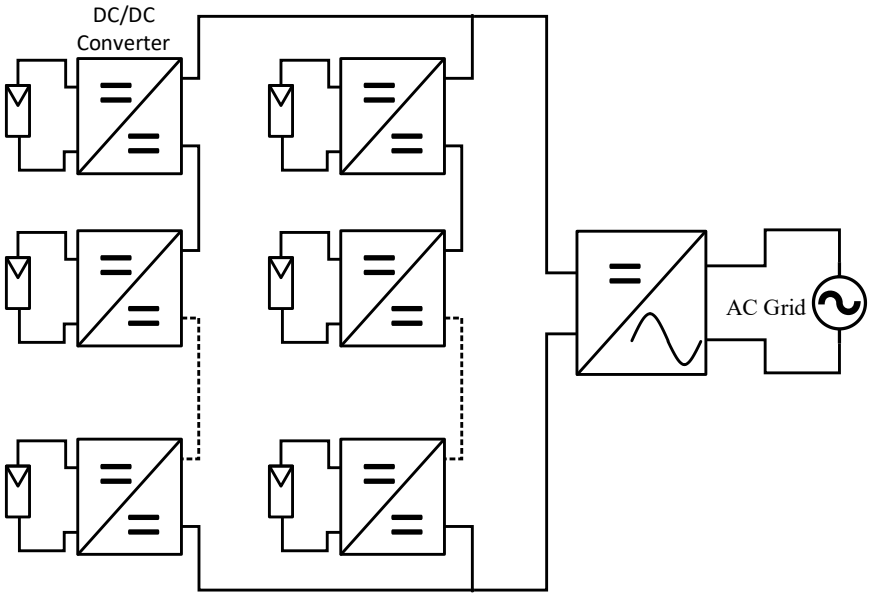

FIGURE 2.4: Simplified circuit schematic showing grid connected central inverter topology with DC optimizers at panel level, which increases the energy yield.

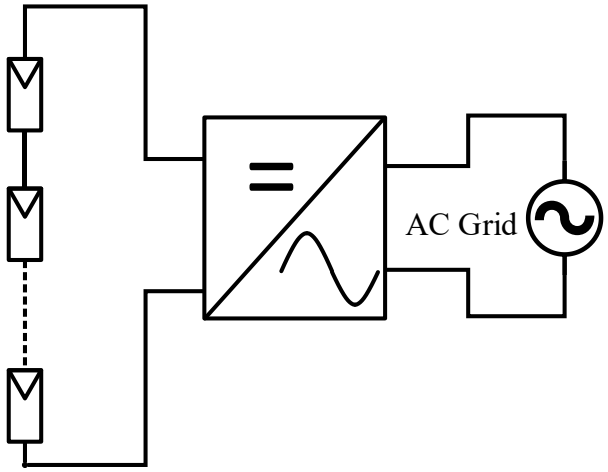

FIGURE 2.5: Simplified circuit schematic showing grid connected string inverter topology.

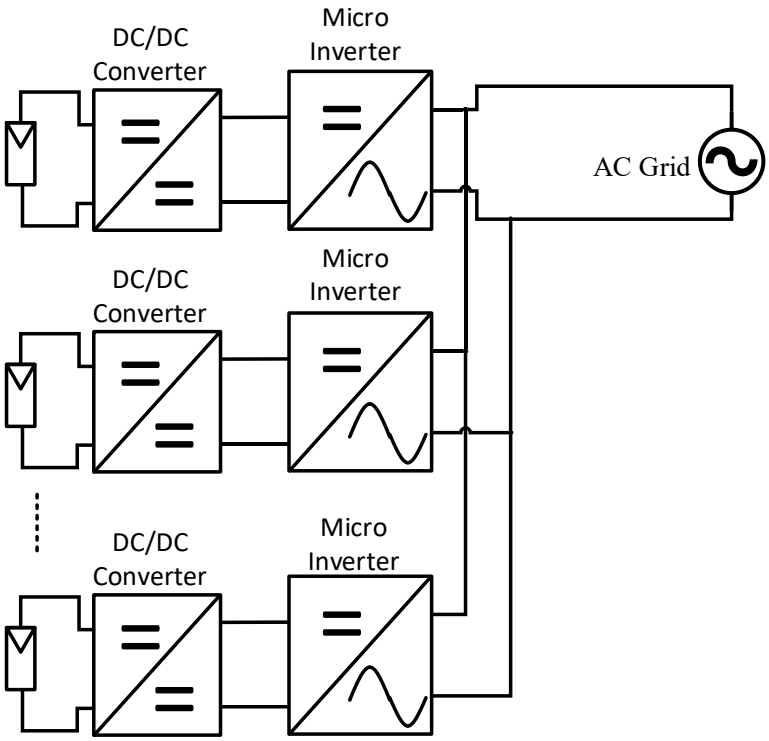

FIGURE 2.6: Simplified circuit schematic showing grid connected string inverter topology.

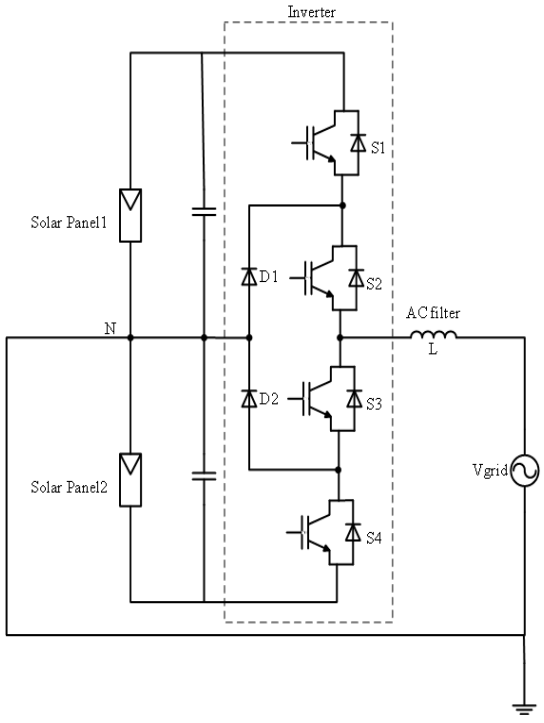

FIGURE 2.7: Simplified circuit schematic showing single-phase grid connected three-level diode clamped inverter topology.

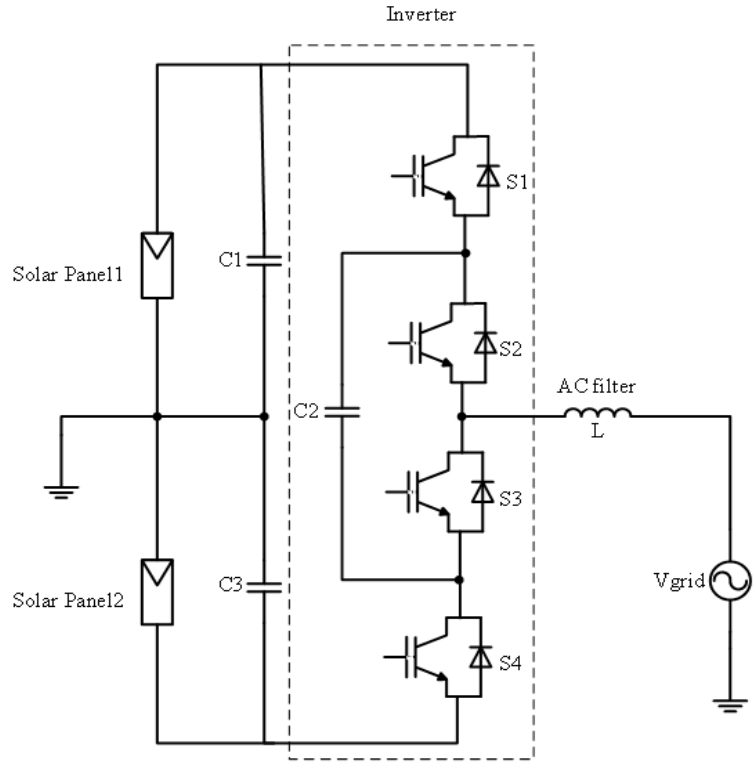

FIGURE 2.8: Simplified circuit schematic showing single-phase grid connected three-level flying capacitor inverter topology.

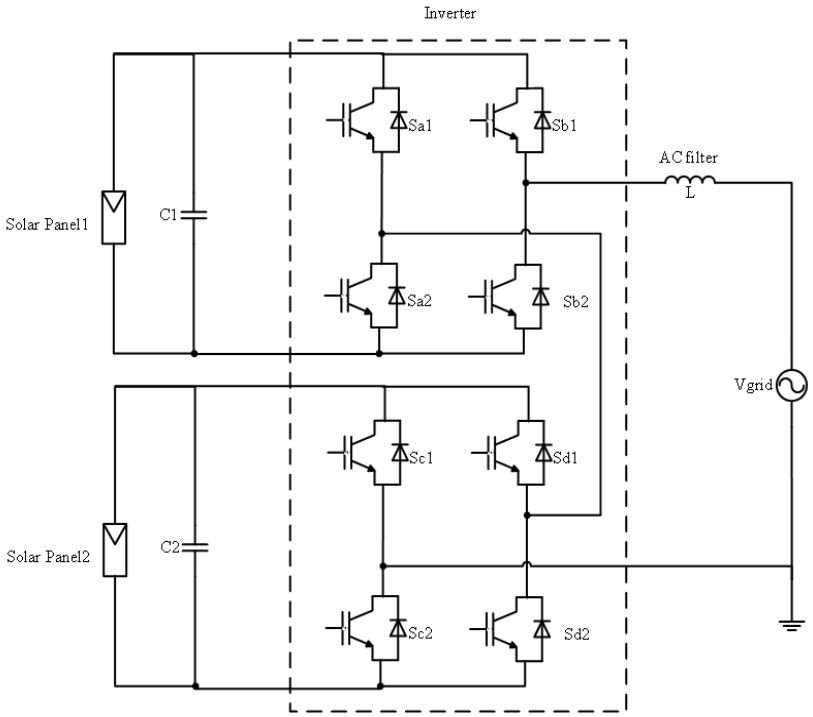

FIGURE 2.9: Simplified circuit schematic showing single-phase grid connected five-level cascaded H-bridge inverter topology.

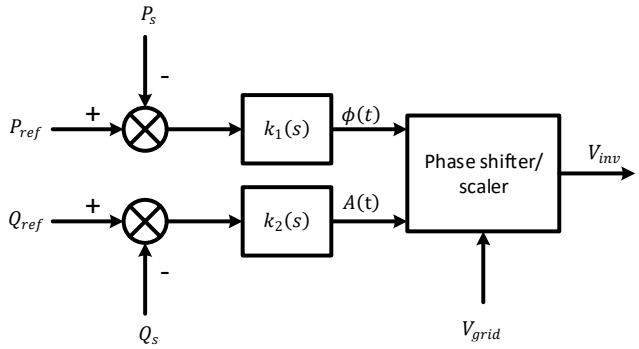

FIGURE 2.10: Simplified block schematic showing voltage mode control for grid tied inverters.

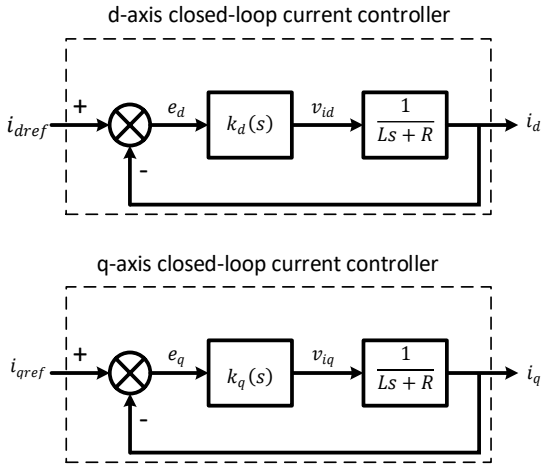

FIGURE 2.11: Simplified block schematic showing current mode control for grid tied inverters.

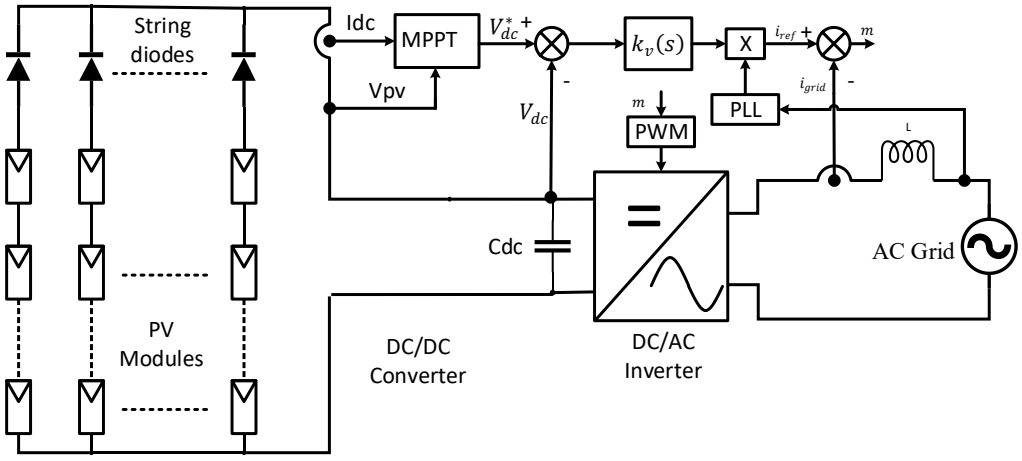

FIGURE 2.12: Schematic showing a typical control scheme employed for single-stage grid connected central inverter topology.

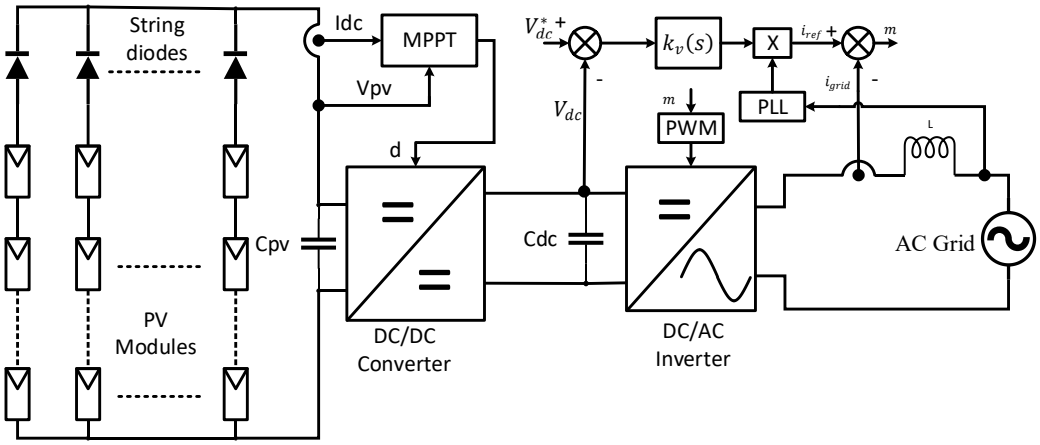

FIGURE 2.13: Schematic showing a typical control scheme employed for two-stage grid connected central inverter topology.

CHAPTER 3 : SOLAR PANEL COMPANION INVERTER

3.1. Introduction

In chapter two, various power conversion topologies, control algorithms for solar power harvesting has been discussed. This chapter provides a summary of the work that has been done in [3]. Section 3.2 describes the topology of SPCI. Principle of operation of SPCIs is presented in section 3.3. The principle of Sort and Stack is defined in Section 3.4. Various modulation strategies that have been employed for SPCIs is described in section 3.5. Section 3.6 describes the concept of Master Selector. The chapter concludes with a summary presented in Section 3.7.

3.2. Topology

Solar Panel Companion Inverter (SPCI) is topologically identical to cascaded H-bridge multilevel inverter [32]. In this topology, several H- bridge inverter modules are connected in series, as shown in Figure 3.1. Each H-bridge inverter module consists of four Metal Oxide Semiconductor Field Effect Transistors (MOSFETs), one microcontroller and a parasitic power supply harvesting energy from the solar panel itself. A DC link capacitor is connected across DC terminals of the inverter. This inverter module is integrated with the solar panel (hence the name Solar Panel Companion Inverter), and depending on the DC voltage of the panel, a quasi-square wave of required duration is synthesized. The principle of quasi-square wave synthesis is described in section 3.4. To realize a required sinusoidal ac voltage, several such panels are connected in series through their companion

inverters. The schematic to synthesize a 120V AC rms voltage is shown in Figure 3.1, wherein six panels, each capable of producing a DC voltage of about 35 V are connected in series through their corresponding companion inverters and are interfaced with the distribution grid via an interfacing reactor. Typically, magnitudes of AC voltages on both sides of the transformer are synchronized such that only real power is supplied from the panels to the grid. However, it is also possible to add a component for reactive power required to support the grid. The output voltage V_0 of the SPCI is the sum of the output voltages across each SPCI. This is synthesized by implementing sort and stack algorithm in which all H-bridge inverter outputs are sorted and sequenced in real-time based on individual panel DC bus voltage of each SPCI.

3.3. Operation of Solar Panel Companion Inverter

Detailed circuit schematic of Solar Panel Companion Inverter (SPCI) is shown in Figure 3.2 [3]. The schematic consists of an SPCI connected to a 120V ac rms grid, a Phase Locked Loop (PLL) block which is used to synchronize the output voltage of SPCI with the grid. The grid voltage is measured and fed into the PLL to construct the image of grid voltage, $V_{gridpll}$. As discussed in Section 3.2, six panels are connected in series through their individual H-bridges. Each H-bridge consists of four MOSFETs, which are closed/opened by means of the triggering pulses given to their gate terminals. G_{11}, G_{12}, G_{13}, and G_{14}, through G_{61}, G_{62}, G_{63}, and G_{64} are the gate signals applied to the MOSFETs in H-bridges connected to Solar Panel1 through Solar Panel6. The master controller controls the pulse generation to close/open the MOSFETs and it is programmed to generate pulses for triggering the MOSFETs. Timing and width of the pulses is determined by the controller, based on input parameters. The input signals to the master controller V_{dc1}, V_{dc2}, V_{dc3}, V_{dc4},

V_{dc5}, and V_{dc6} are the dc voltages measured across Solar Panel1, Solar Panel2, Solar Panel3, Solar Panel4, Solar Panel5, and Solar Panel6 respectively. $V_{gridpll}$, and reference current, I_{ref}, are the two other input signals to the master controller. These eight input signals of the controller are processed in real time and pulses are generated. Its outputs are gate pulses, G_{11} through G_{64}. I_{ref} is the parameter which determines operation of the system at maximum power point. The value of I_{ref} which determines the maximum power point operation varies with the operating scenarios of the SPCI system.

3.4. Principle of Sort and Stack

Principle of sort and stack has been proposed for Solar Panel Companion Inverters (SPCIs), to balance the capacitor voltages, and to ensure panel level maximum power extraction from Photo Voltaic (PV) system. According to this principle, PV panel with the highest should synthesize an ac output quasi-square wave with the highest pulse width. This principle has been implemented by sorting the DC bus voltages together with the modulation schemes that are discussed in section 3.5.

3.5. Modulation Strategies

3.5.1. Unsorted Pulse Width Modulation

Unsorted Pulse Width Modulation (UPWM) is like classical PWM, wherein a comparison is made between sinusoidal reference wave and a high frequency triangular wave, also called carrier wave. Synthesized unsorted pulse width modulated output ac voltage with its sinusoidal reference is shown in Figure 3.3. UPWM is implemented to make a comparative analysis of yields for the Solar Panel Companion Inverter (SPCI) and central inverter topologies. The output voltage generated across all the inverters has the

same phase. However, the amplitude of the output voltage waveform across each inverter might vary and depends on the magnitude of DC bus voltage across the SPCI.

3.5.2. Sorted Stair Case Modulation

Figure 3.5 shows a thirteen-level AC output voltage Stair Case waveform. To synthesize this waveform, Sorted Stair Case Modulation (SSCM) is implemented for Solar Panel Companion Inverter (SPCI) topology [3]. In this strategy, the DC bus voltages of all the PV panels are measured and are sorted in descending order. The inverter connected to the panel with highest DC voltage synthesizes an AC quasi-square wave having the highest pulse width. This action results in drawing maximum current from this panel, thereby consequently decreasing the voltage on the P-V curve of the solar panel. The inverter connected to the panel with the lowest voltage synthesizes an AC quasi-square wave heaving the least pulse width. This action results in drawing minimum current from the panel, thereby increasing the voltage on the P-V curve of this panel. The width of each step is a function of the switching instance in the resulting quasi-square wave. This switching time instance is determined to be that moment at which the reference voltage is greater than the sum of all previous steps plus half of current step. Such a logic results in a symmetrical staircase waveform around any sinusoidal reference. Switching instances for all the steps is shown by a dot on the sine wave, in Figure 3.6.

3.5.3. Sorted Pulse Width Modulation

Figure 3.7 shows a thirteen-level pulse width modulated AC staircase waveform. To synthesize an AC wave as shown in Figure 3.7, Sorted Pulse Width Modulation (SPWM) is implemented for Solar Panel Companion Inverter (SPCI) topology [3]. To synthesize this waveform, Sorted Stair Case Modulation (SSCM) is implemented for Solar Panel

Companion Inverter (SPCI) topology [3].This is like level shifted PWM technique. SPWM is a combination of both SSCM and UPWM strategies. Like SSCM, in SPWM strategy also the DC bus voltages of all the panels are measured, sorted in descending order and the one with the highest voltage synthesizes the first pulse width modulated quasi-square wave having the highest pulse width. This action results in drawing maximum current from this panel, thereby consequently decreasing the voltage on the P-V curve of the solar panel. To synthesize pulse width modulated quasi-square wave, a triangular wave having high frequency (6 kHz) and an amplitude equal to the value of the selected DC bus voltage, is compared to the sine wave reference, as shown in Figure 3.8. The inverter connected to the panel with the lowest voltage synthesizes a pulse width modulated quasi-square wave heaving the least pulse width. This action results in drawing minimum current from the panel, thereby increasing the voltage on the P-V curve of this panel.

3.6. Master Selector

Master Selector has been implemented for the selecting the control scheme which offers maximum yield for a given operating scenario [3]. Figure 3.9 shows the flow chart implementation of the logic for master selector. This is an algorithm which selects one of the modulation strategies described in Section 3.5, depending on the operating scenario. It has been shown that by implementing this strategy the sequence in which all the SPCIs should be switched can be selected in order to improve the performance of the SPCI.

3.7. Summary

Topology of Solar Panel Companion Inverter (SPCI), principle of operation, principle of sort and stack, modulation strategies namely: Unsorted Pulse Width Modulation (UPWM), Sorted Stair Case Modulation (SSCM) and Sorted Pulse Width Modulation

(SPWM), and Master Selector have been summarized in this chapter. Though there are three modulation strategies that have been implemented in [3], the focus of this dissertation will be on implementing SSCM, and SPWM strategies.

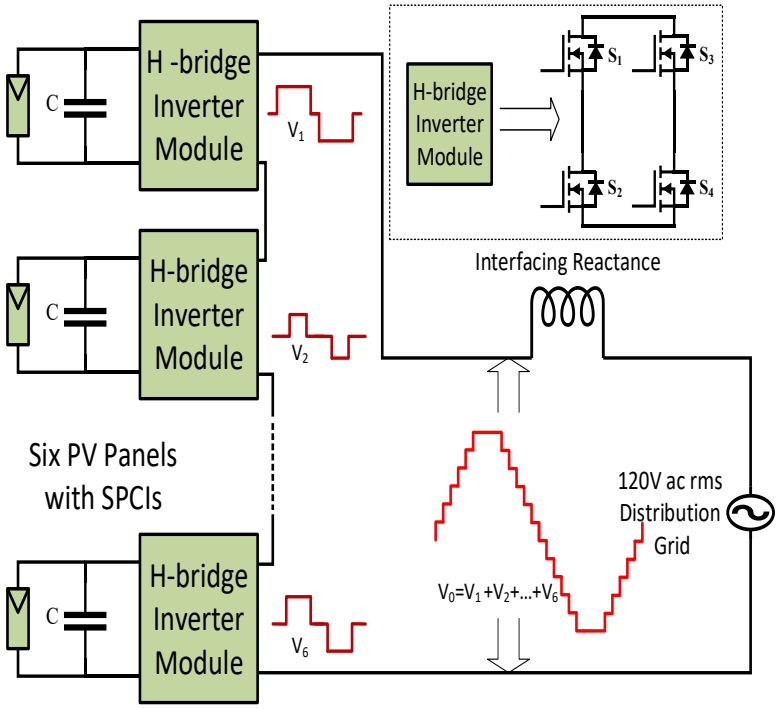

FIGURE 3.1: Simplified schematic of solar panel companion inverter.

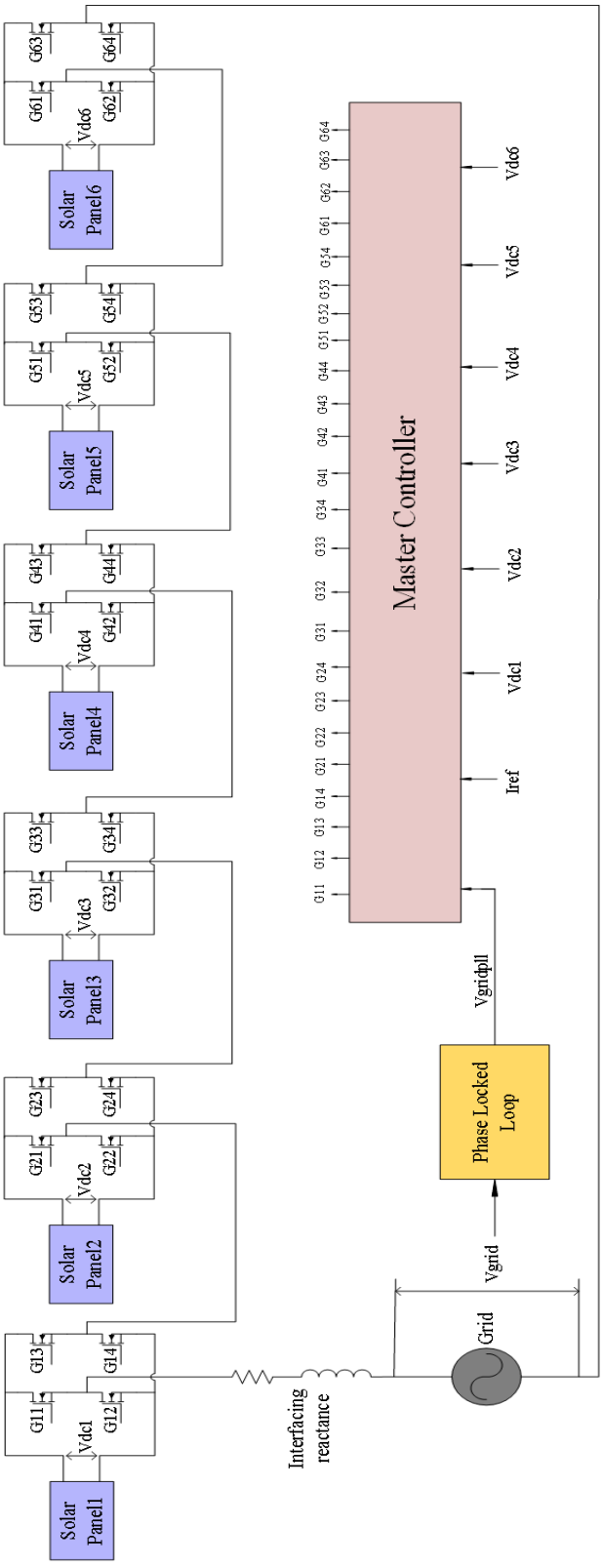

FIGURE 3.2: Detailed circuit schematic of grid tied solar panel companion inverter model capable of synthesizing 120V ac rms voltage [3].

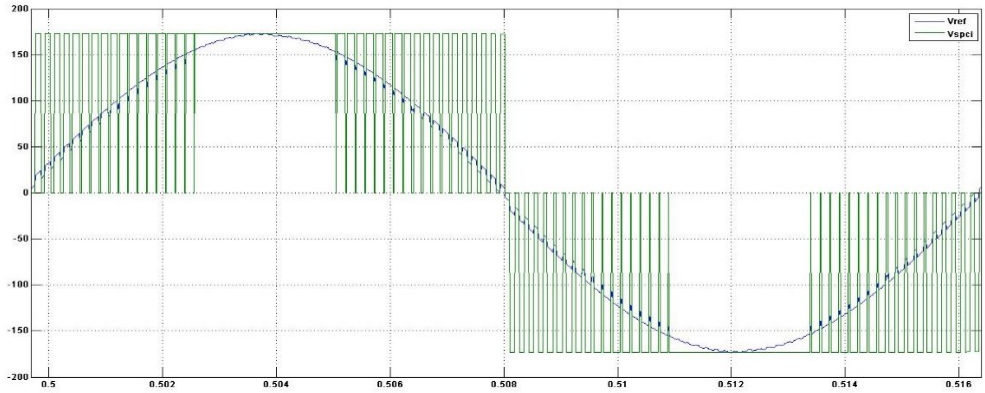

FIGURE 3.3: Unsorted pulse width modulation ac waveform with its sinusoidal ac reference [3].

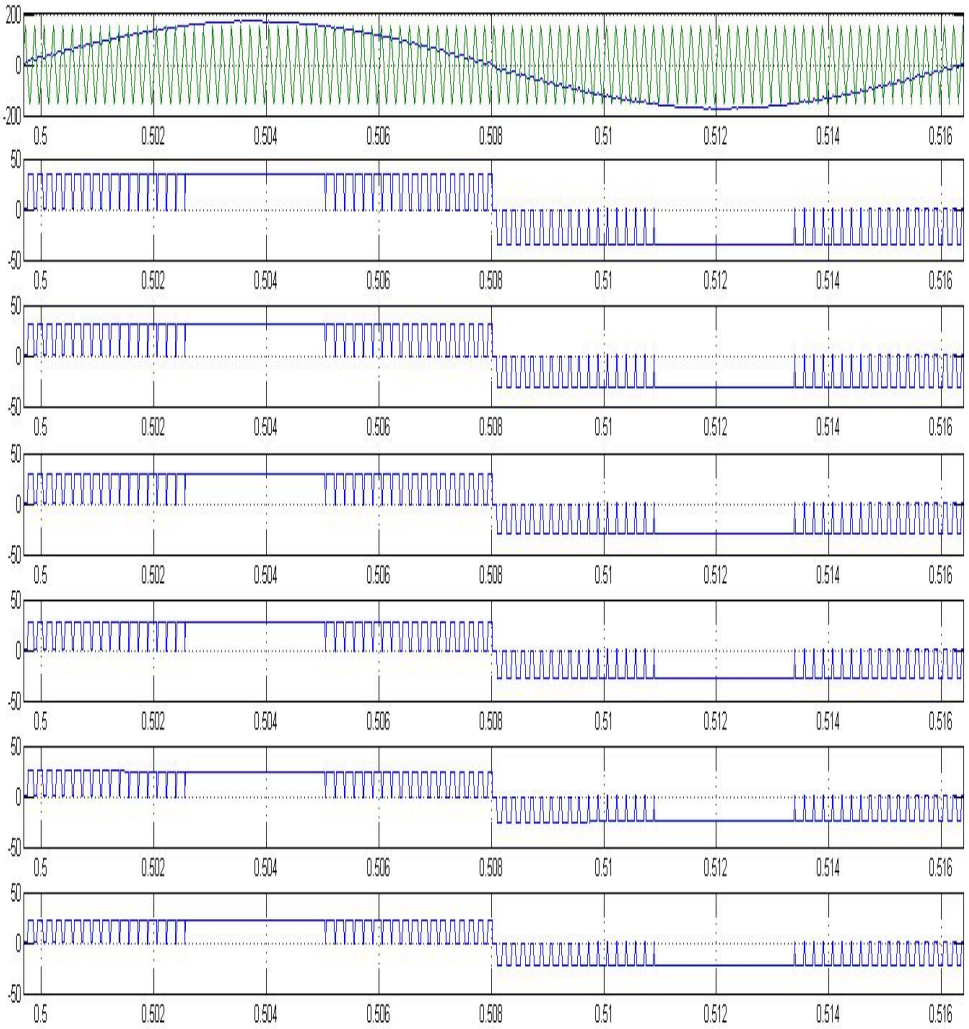

FIGURE 3.4: Unsorted pulse width modulation for a six panel solar panel companion inverter showing synthesis of each step and the corresponding switching instances [3].

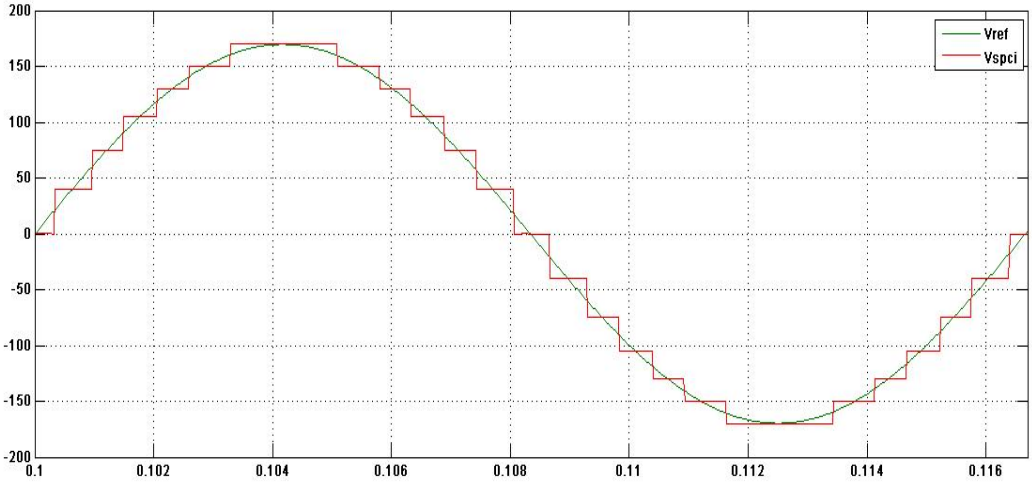

FIGURE 3.5: Sorted stair case modulation ac waveform with its sinusoidal ac reference [3].

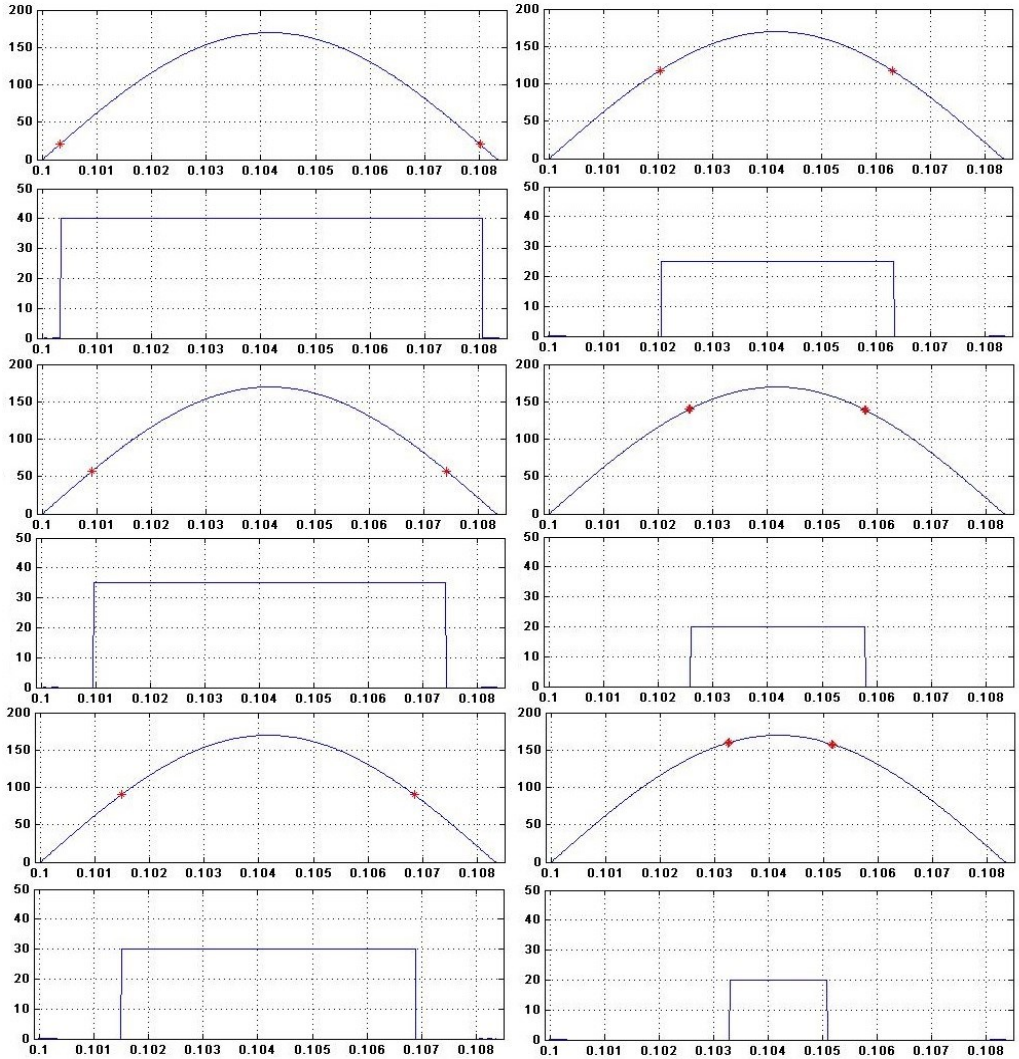

FIGURE 3.6: Sorted stair case modulation for a six-panel solar panel companion inverter showing synthesis of each step and the corresponding switching instances [3].

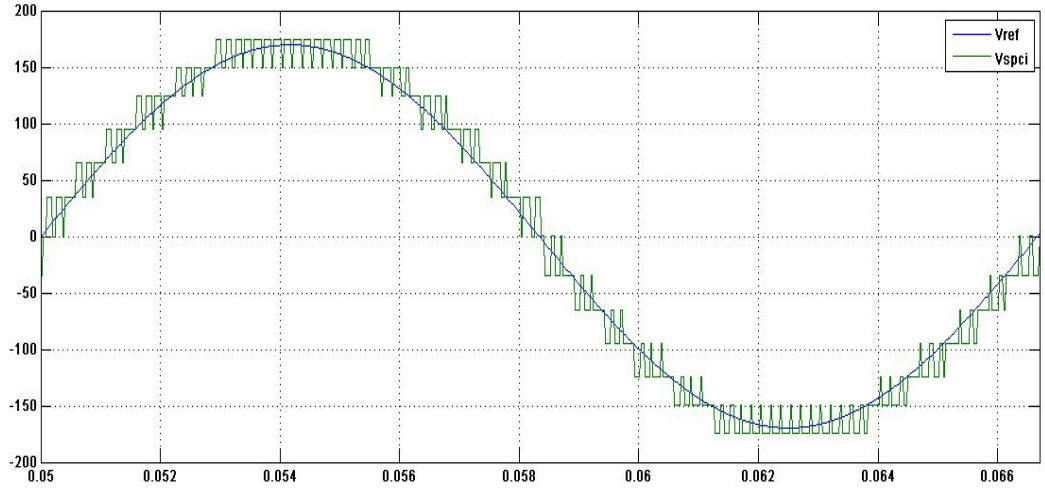

FIGURE 3.7: Sorted pulse width modulation ac waveform with its sinusoidal ac reference [3].

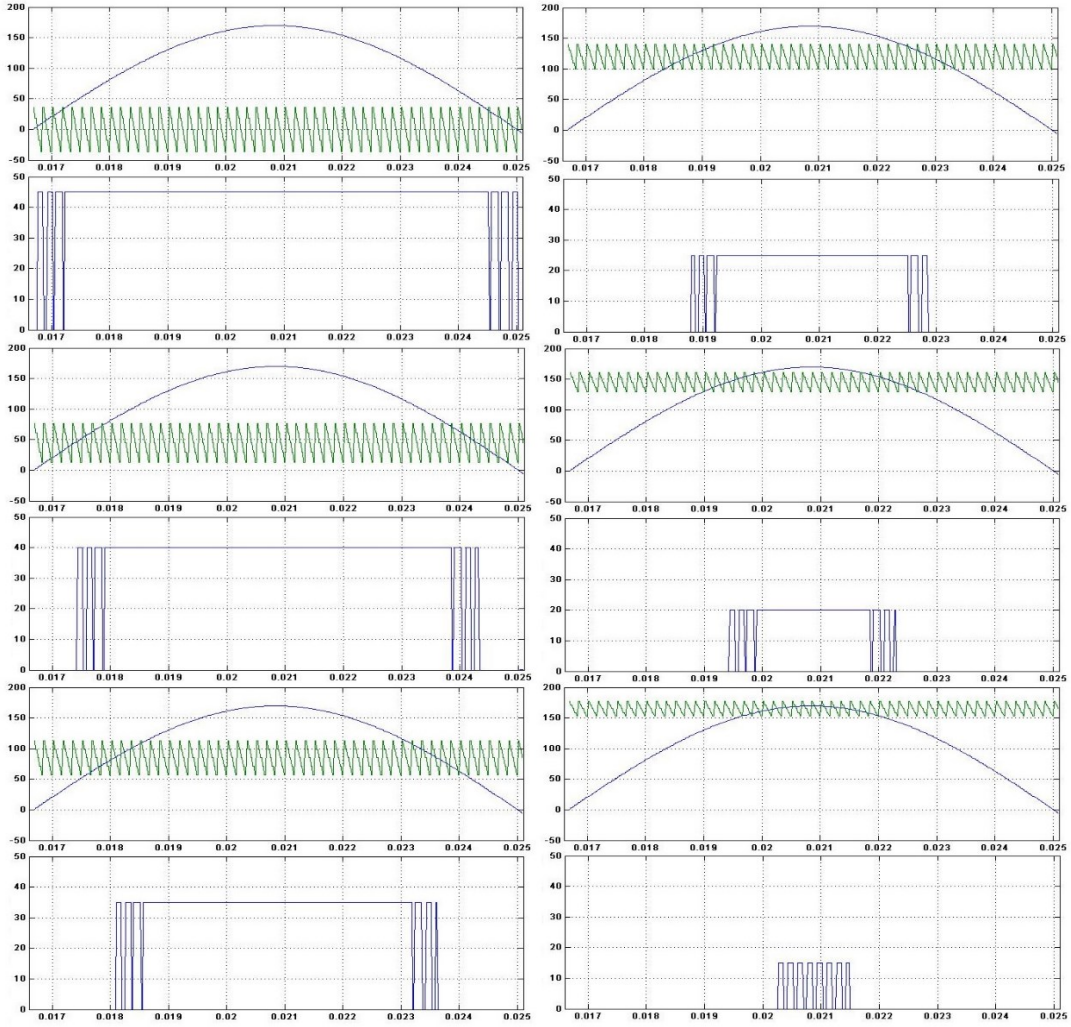

FIGURE 3.8: Sorted pulse width modulation for a six-panel solar panel companion inverter showing synthesis of each step and the corresponding switching instances [3].

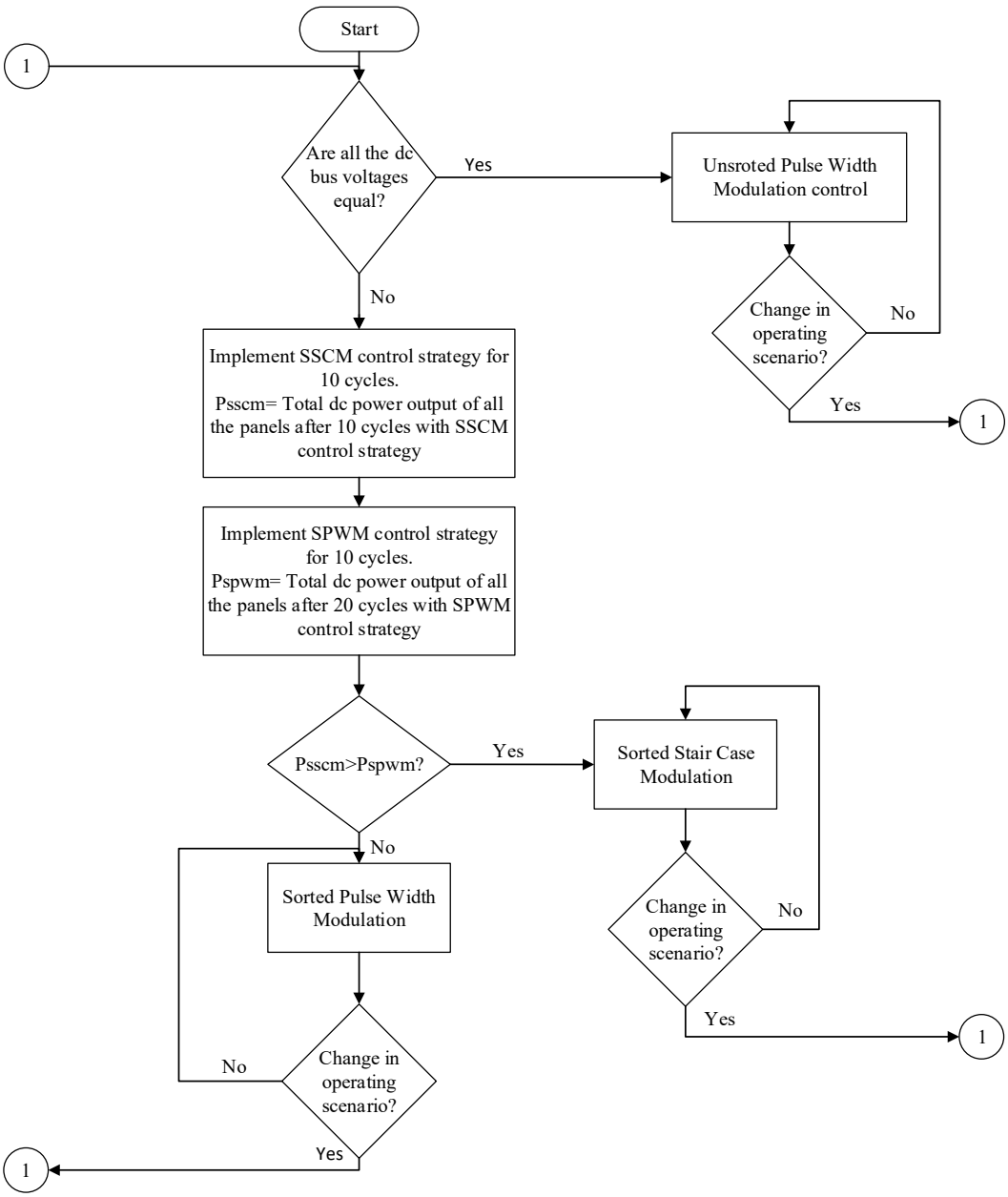

FIGURE 3.9: Flow Chart showing the implementation of master selector logic [3].

CHAPTER 4 : DYNAMIC ANALYSIS AND CONTROLLER DESIGN

4.1. Introduction

In chapter 3, a brief description of Solar Panel Companion Inverters (SPCI) has been presented. Modulation strategies such as Unsorted Pulse Width Modulation (UPWM), Sorted Stair Case Modulation (SSCM), and Sorted Pulse Width Modulation (SPWM) that have been employed for SPCI have been presented. Advantages of SPCI as compared to other popular topologies such as Central and String based topologies have been discussed [3]. So far, the simulations have been performed with an open loop current control approach. In this chapter, a closed loop control architecture to control active power, and reactive power generation from grid connected SPCI has been introduced. The control architecture together with the Maximum Power Point Tracking scheme that will inject power into the AC grid is discussed in Chapter 6. Section 4.2 presents closed loop control scheme employed for grid connected SPCI. This section also presents the dynamic modeling of real/reactive power - controller. Current controller design of SPCI and its dynamic performance is presented in Section 4.3. Section 4.4 concludes the chapter with a brief summary.

4.2. Current Control Scheme

Figure 4.1 shows schematic diagram of current controlled Solar Panel Companion Inverter (SPCI) system. SPCIs are interfaced with AC grid via a series RL branch, at the Point of Common Coupling (PCC). AC grid is stiff and is modeled by an ideal single-phase

voltage source, V_{grid}. The system should be able to exchange active power, P and reactive power, Q with the AC grid, as will be discussed in detail, in Chapter 7. The control objective of grid connected Solar Panel Companion Inverter (SPCI) is to synthesize a sinusoidal AC output voltage (both magnitude and phase angle). Magnitude and phase angle of the synthesized output voltage should be such that a current of specific magnitude and phase angle is injected into the grid. A closed loop current control capable of tracking a sinusoidal reference current can be implemented. This can be referred to as current-mode control scheme. However, tracking a sinusoidal reference input with zero steady-state error is difficult. Hence, the current control scheme is implemented in dq- frame, where a zero steady state error can be achieved by including a Proportional - Integral (PI) compensator, since the control variables are DC quantities. Current control in dq frame is usually implemented in three-phase systems by using Park's transformation. For a single-phase system, the measured current first needs to be converted to static αβ frame [61]. Firstly, a current in quadrature with the measured current is obtained by delaying the measured sinusoidal current by 90^0. SPCI shown in this figure represents a lossless power processor, which converts DC power to AC power. The principle of power conversion for SPCI from DC to AC power has been discussed in Chapter 3. Real and reactive power can be controlled by controlling the amplitude and phase angle of the AC current with respect to AC voltage of the ideal voltage source.

4.2.1. Dynamic Model of Controller

Before proceeding to the dynamic model of the controller, equations involving $\alpha\beta$ to dq transformation are defined. For a space phasor, $\vec{f}(t)$, $\alpha\beta$ to dq transformation is defined by the Equation (4.1).

$$\vec{f}(t) = f_\alpha + jf_\beta = \left(f_d + jf_q\right)e^{j\rho(t)} \tag{4.1}$$

where f_α and f_β are the components of $\vec{f}(t)$ in $\alpha\beta$ – frame, f_d and f_q are DC quantities in dq – frame, and $\rho(t)$ is the phase shift in $\vec{f}(t)$.

Dynamics of AC side of SPCI system of Figure 4.1 is can be described by the Equation (4.2).

$$L\frac{d\vec{\imath}}{dt} = -R\vec{\imath} + \overrightarrow{V_{spc\imath}} - \overrightarrow{V_{gr\imath d}} \tag{4.2}$$

where $\vec{\imath}$ is the grid side AC current phasor, R is the resistance of the interfacing inductor, L is the interfacing inductance, $\overrightarrow{V_{spc\imath}}$ is the phasor output voltage of Solar Panel Companion Inverter, $\overrightarrow{V_{gr\imath d}}$ is the phasor grid voltage.

From Equation (4.1)

$$\vec{\imath} = i_\alpha + ji_\beta = \left(i_d + ji_q\right)e^{i\rho(t)} \tag{4.3}$$

$$\overrightarrow{V_{spc\imath}} = V_{spci\alpha} + jV_{spci\beta} = \left(V_{spcid} + jV_{spciq}\right)e^{i\rho(t)} \tag{4.4}$$

$$\overrightarrow{V_{gr\imath d}} = V_{grid\alpha} + jV_{grid\beta} = \left(V_{gridd} + jV_{gridq}\right)e^{i\rho(t)} \tag{4.5}$$

Equation (4.2) can be rewritten using Equations (4.3), (4.4), and (4.5) as

$$L\frac{d}{dt}\left(i_{dq}e^{i\rho(t)}\right) = -R\left(i_{dq}e^{i\rho(t)}\right) + V_{spcidq}e^{i\rho(t)} - V_{griddq}e^{i\rho(t)} \tag{4.6}$$

where

$$i_{dq} = \left(i_d + ji_q\right) \tag{4.7}$$

$$V_{spcidq} = \left(V_{spcid} + jV_{spciq}\right) \tag{4.8}$$

$$V_{griddq} = \left(V_{gridd} + jV_{gridq}\right) \tag{4.9}$$

Equation 4.6 can be rewritten as

$$L\frac{d}{dt}\left(i_{dq}\right) = -j\left(L\frac{d\rho}{dt}\right)i_{dq} - R\left(i_{dq}\right) + V_{spcidq} - V_{griddq} \tag{4.10}$$

$$L\frac{d}{dt}\left(i_d + ji_q\right) = -j\left(L\frac{d\rho}{dt}\right)\left(i_d + ji_q\right) - R\left(i_d + ji_q\right) + \left(V_{spcid} + jV_{spciq}\right) - \left(V_{gridd} + jV_{gridq}\right) \tag{4.11}$$

Equating the real and imaginary parts of Equation (4.11), we get

$$L\frac{di_d}{dt} = \left(L\frac{d\rho}{dt}\right)i_q - Ri_d + V_{spcid} - V_{gridd} \tag{4.12}$$

$$L\frac{di_q}{dt} = -\left(L\frac{d\rho}{dt}\right)i_d - Ri_q + V_{spciq} - V_{gridq} \tag{4.13}$$

$$\frac{d\rho}{dt} = \omega \tag{4.14}$$

If ω_0 is the frequency of AC grid, and $\rho(t) = \omega_0 t + \theta_0$, then Equations (4.12) and (4.13) can be rewritten as

$$L\frac{di_d}{dt} = L\omega_0 i_q - Ri_d + V_{spcid} - V_{gridd} \tag{4.15}$$

$$L\frac{di_q}{dt} = -L\omega_0 i_d - Ri_q + V_{spciq} - V_{gridq} \tag{4.16}$$

Equations (4.15) and (4.16) describe a second-order linear system with V_{gridd} and V_{gridq} as constant inputs. If V_{spcid} and V_{spciq} are DC quantities, i_d and i_q are also DC quantities in steady state. $\rho(t) = \omega_0 t + \theta_0$ is ensured by implementing a Phase Locked Loop (PLL) algorithm. This implementation is presented in Chapter 5.

4.2.2. Current Control

The current control in dq-frame is based on Equations (4.15) and (4.16). In these equations, i_d and i_q are state variables, V_{spcid} and V_{spciq} are control inputs, and V_{gridd} and V_{gridq} are disturbance inputs. The dynamics of i_d and i_q are coupled due to the presence of reactance terms ($L\omega_0$) in the Equations (4.15) and (4.16). Decoupling the dynamics of i_d and i_q is performed by introducing two control inputs V_{id} and V_{iq}.

$$V_{id} = L\omega_0 i_q + V_{spcid} - V_{gridd} \tag{4.17}$$

$$V_{iq} = -L\omega_0 i_d + V_{spciq} - V_{gridq} \tag{4.18}$$

Hence, Equations (4.15) and (4.16) can be rewritten as

$$L\frac{di_d}{dt} = -Ri_d + V_{id} \tag{4.19}$$

$$L\frac{di_q}{dt} = -Ri_q + V_{iq} \tag{4.20}$$

Equations (4.19) and (4.20) represent two decoupled, first-order linear systems. It can be seen from these equations that the quantities i_d and i_q can be controlled by controlling V_{id} and V_{iq} respectively. Rewriting Equations (4.19) and (4.20) in s-domain representation, we get

$$LsI_d(s) = -RI_d(s) + V_{id}(s) \tag{4.21}$$

$$LsI_q(s) = -RI_q(s) + V_{iq}(s) \tag{4.22}$$

Transfer functions of the systems described by Equations (4.21) and (4.22) respectively are

$$\frac{I_d(s)}{V_{id}(s)} = \frac{1}{Ls + R} \tag{4.23}$$

$$\frac{I_q(s)}{V_{iq}(s)} = \frac{1}{Ls + R} \tag{4.24}$$

From Equations (4.23) and (4.24) it can be said that the plants represented in *d*-axis and *q*-axis are identical. Figure 4.2 shows the simplified block diagram of open loop system represented by Equations (4.19) and (4.20). The control objective for such systems would be to regulate the output currents i_d and i_q at their corresponding specified reference values. Figure 4.3 shows a closed loop current control block schematic wherein, i_d is controlled by comparing i_{dref} with i_d to generate an error signal e_d. This error signal is fed into a compensator $k_d(s)$, and control input signal, V_{id} is generated. Similarly, i_q is

controlled by comparing i_{qref} with i_q to generate an error signal e_q. This error signal is fed into a compensator $k_q(s)$, and control input signal, V_{iq} is generated. The outputs of the controllers along d-axis and q-axis is fed into the sort and stack algorithm, and pulse generator, as discussed in chapter 3. All the signals are DC quantities in steady state operation. Also, the control plants along d-axis and q-axis control loops are identical. Therefore, the corresponding compensators can also be identical. For both the current control loops, the compensators can be a proportional-integral (PI) compensator, since the reference signals are DC quantities. The PI compensator for d-axis current control loop can be described by the Equation (4.25).

$$k_d(s) = k_p + \frac{k_i}{s} \tag{4.25}$$

where k_p is proportional gain, and k_i is integral gain. The integral term of Equation (4.25) guarantees that i_d tracks i_{dref}, with zero steady-state error. Equation (4.25) can be rewritten as

$$k_d(s) = \frac{k_p s + k_i}{s} \tag{4.26}$$

The control system loop gain can be written as:

$$l_d(s) = \left(\frac{k_p}{Ls}\right)\left(\frac{s + \frac{k_i}{k_p}}{s + \frac{R}{L}}\right) \tag{4.27}$$

The plant pole is at $s = -R/L$. For an ideal case, resistance of the interfacing inductor is ≈ 0. For a non-zero resistance, though the pole is on the left half of s-plane, it is close to origin, and hence the natural response of the system is slow. Pole of the plant can be cancelled by zero of compensator by selecting k_p and k_i such that

$$\frac{k_i}{k_p} = \frac{R}{L} \tag{4.28}$$

Loop gain becomes

$$l_d(s) = \frac{k_p}{sL} \tag{4.29}$$

Hence, the closed loop transfer function can be written as

$$\frac{I_d(s)}{I_{dref}(s)} = G_{id}(s) = \frac{1}{s(L/k_p) + 1} \tag{4.30}$$

A parameter called time constant $\tau_i$by the Equation (4.31)

$$\tau_i = \frac{L}{k_p} \tag{4.31}$$

Therefore, Equation (4.30) can be rewritten as

$$\frac{I_d(s)}{I_{dref}(s)} = G_{id}(s) = \frac{1}{s\tau_i + 1} \tag{4.32}$$

Equation (4.32) represents a first-order transfer function with unity gain. Choice of τ_i is a design problem. For a faster response, τ_i should be small. $1/\tau_i$ defines the bandwidth of closed loop control system. Bandwidth of the control system should be selected such that it is at least 10 times smaller than the switching frequency. The compensator for q-axis will be the same as that specified by Equation (4.25).

$$k_q(s) = k_p + \frac{k_i}{s} \tag{4.33}$$

and the closed loop transfer function for q-axis current control loop can be written as

$$\frac{I_q(s)}{I_{qref}(s)} = G_{id}(s) = \frac{1}{s\tau_i + 1} \tag{4.34}$$

4.3. Current Controller Design and Dynamic Performance

Interfacing inductance, L value is assumed to be 17 mH, and the series resistance is assumed to be 1 ohm. For a six modules of Solar Panel Companion Inverters (SPCI), the effective switching frequency is (4*6*60) = 1440 Hz. Therefore, the bandwidth of the current controller is chosen to be $1/\tau_i$ = 144 Hz. Therefore, the time constant, $\tau_i \approx 6$ ms. From Equations (4.28) and (4.31), k_p = 2.448, and k_i = 144. Therefore, the transfer functions of the compensators along d-axis and q-axis control loops can be written as

$$k_d(s) = k_q(s) = \frac{2.448s + +144}{s} \tag{4.35}$$

The plant transfer functions from Equations (4.23) and (4.24) can be written as

$$\frac{I_d(s)}{V_{id}(s)} = \frac{I_q(s)}{V_{iq}(s)} = \frac{1}{0.017s + 1} \tag{4.36}$$

Closed loop control system described by Equations (4.35) and (4.36) has been built in MATLAB Simulink as shown in Figure 4.4, to study the step response of the system. The input to the system is i_{dref} and output is i_d. The system is subjected to following sequence of events: i_{dref} is initially set to the 19.5 (which is the rated i_d value) until 0.15 s. At t = 0.15 s, i_{dref} is subjected to a step change from 19.5 to 10. Figure 4.5 illustrates the time response of the system to the changes in the input signal. It can be seen that i_d tracks the i_{dref}. The step response of i_d is a first order exponential function that reaches its final value after about 0.05 s. As the control loops along d-axis and q-axis are same, the step response of i_q when subjected to a step change in i_{qref} would also be the same as that of i_d response.

4.4. Summary

In this chapter, current control scheme that can be employed for single-phase grid connected Solar Panel Companion Inverter (SPCI) has been presented. The controller design and dynamic performance of the current controller has been discussed. Implementation of the closed loop control of Solar Panel Companion Inverters (SPCI) will be discussed in Chapter 5.

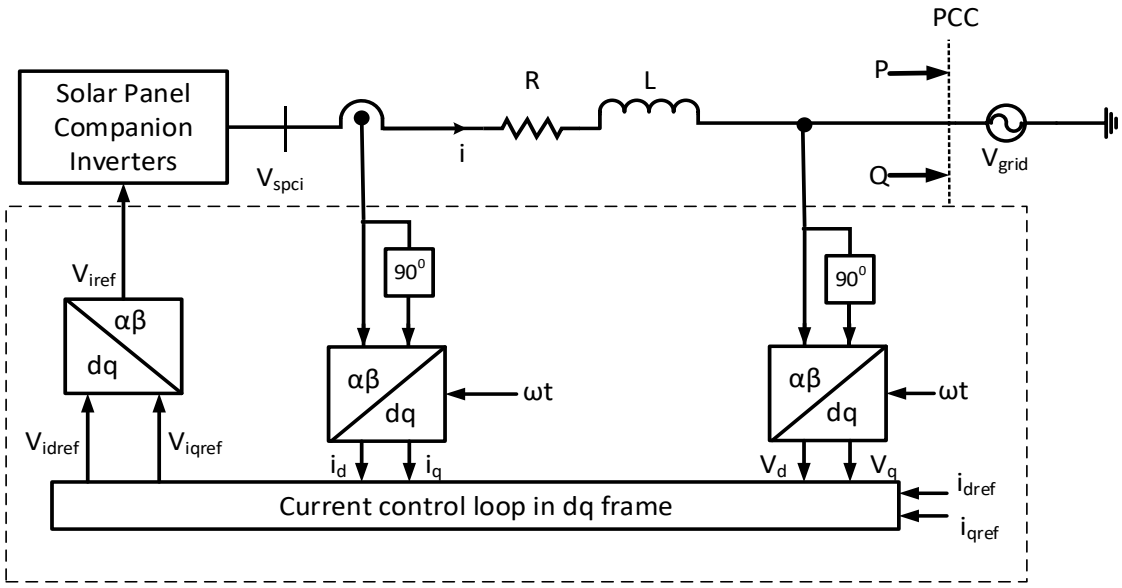

FIGURE 4.1: Schematic of current controlled Solar Panel Companion Inverters (SPCI) interfaced to the grid at Point of Common Coupling (PCC).

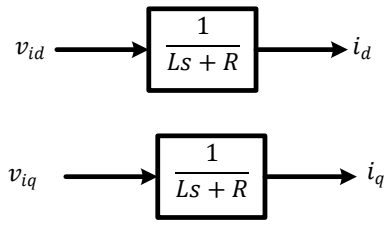

FIGURE 4.2: Simplified block schematic showing open loop control model of grid connected SPCI.

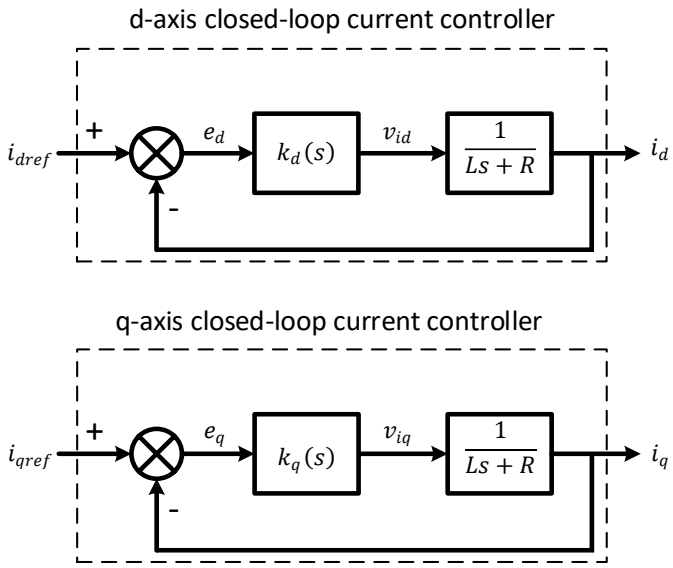

FIGURE 4.3: Simplified block schematic showing closed loop current control in of grid connected SPCI in dq - frame.

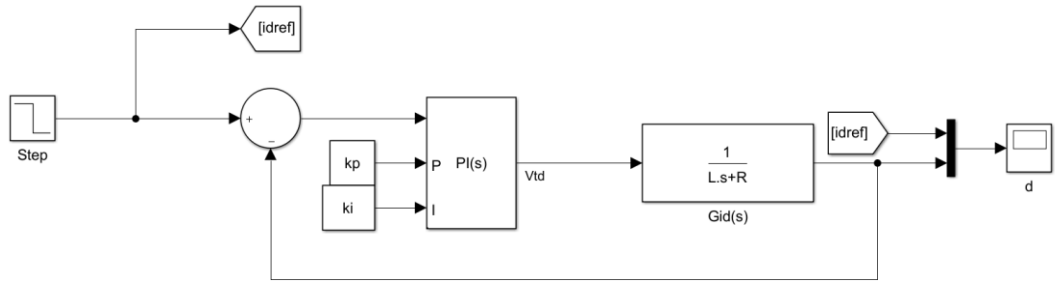

FIGURE 4.4: Simplified block schematic showing d-axis current control loop implemented in MATLAB Simulink.

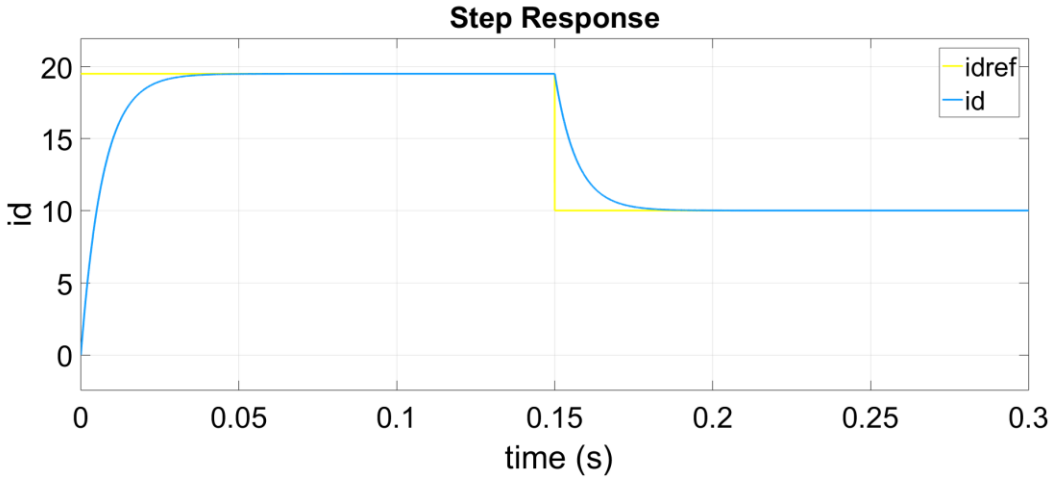

FIGURE 4.5: Dynamic response of closed loop current controller.

CHAPTER 5 : MODELING AND SIMULATION

5.1. Introduction

Chapter 4 described dynamic analysis and closed loop current control will be employed for a grid connected Solar Panel Companion Inverter (SPCI). This chapter presents the model of a grid connected SPCI. Section 5.2 describes a block diagram of grid connected SPCI. Matlab Simulink model of power grid and SPCI is explained in Sections 5.3, and 5.4 respectively. Master controller for Sorted Stair Case Modulation (SSCM) Section 5.5. The Master controller implementation for SSCM in this dissertation is different from the one that has been implemented in [3]. Simulation results demonstrating the closed loop current control operation of grid connected SPCI, with ideal DC voltage sources connected across the DC bus is presented in Section 5.6. Section 5.7 concludes this chapter with a brief discussion.

5.2. Block Diagram of Grid Connected Solar Panel Companion Inverter

A simplified block diagram of grid connected Solar Panel Companion Inverter (SPCI) is shown in Figure 5.1. As discussed in Chapter 3, six solar panels having similar ratings are selected. Each solar panel is connected to an H-bridge and the AC output terminals of all the H-bridges are connected in series to form a two-terminal AC output. This two-terminal AC output is connected to the grid via an interfacing reactor. Phase Locked Loop (PLL) is used to construct an image of the grid voltage and its phase. Closed loop current control scheme is implemented to generate a reference voltage. DC bus voltage signals and

reference voltage signal are fed as inputs into the controller block. The controller block is programmed to process the input signals and synthesize the desired ac output voltage.

5.3. Model of Power Grid

Power grid is modelled in Matlab Simulink as an ideal AC voltage source, with a series impedance. The ac voltage is set to 120 V AC rms and the frequency is set to 60Hz. Interfacing impedance consists of resistive and inductive components (modelled for the resistance and leakage reactance of the interfacing transformer), as shown in Figure 5.2.

5.4. Solar Panel Companion Inverter Model

Simplified circuit schematic of Solar Panel Companion Inverter (SPCI) which can produce a three-level output ac voltage is shown in Figure 5.3 [3]. SPCI system model is built to be able to produce ac output voltage of 120V ac rms. To be able to reach the peak voltage of $120\sqrt{2}$ V, six solar panel models built in Simulink are connected to six H-bridges. As may be seen from Figure 5.4, six H-bridge inverters are connected in series to form a two-wire single phase output. Each H-bridge inverter consists of four MOSFETs. Each module derives power from the PV module that is modelled in Simulink. Each MOSFET is closed/opened by the high/low pulse received at the gate terminal. The twenty-four MOSFETs in the proposed system are driven by a master controller. The working of the controller varies with the type of control strategy employed for SPCI. These controller models are described in the following sections.

5.5. Master Controller for Sorted Stair Case Modulation

Figure 5.5 shows the logic employed for Sorted Stair Case Modulation (SSCM). Sort and stack algorithm to synthesize a staircase output waveform is implemented in this block. Figure 5.6 shows the detailed current control scheme and block schematic of sort and stack

algorithm implementation. The sorting logic takes in the DC bus voltages of all the PV panels, and sorts the voltages in descending order. If $U^*$is the magnitude of reference voltage, and $V_{dc}[0]$ is the DC bus voltage of the panel corresponding to the highest voltage, then switching instance, $\theta[0]$ of the corresponding inverter can be obtained by the following equation.

$$U^* sin\theta[0] = \frac{V_{dc}[0]}{2} \tag{5.1}$$

Therefore, the switching instance of inverter with the largest voltage can be written as

$$\theta[0] = arcsin\left[\frac{\frac{V_{dc}[0]}{2}}{U^*}\right] \tag{5.2}$$

Similarly, the switching instance for SPCI with second largest DC bus voltage can be obtained by the Equation (5.3)

$$U^* sin\theta[1] = V_{dc}[0] + \frac{V_{dc}[1]}{2} \tag{5.3}$$

where $V_{dc}[1]$ is the second largest DC bus voltage, $\theta[1]$ is the switching instance of the corresponding SPCI which can be written as

$$\theta[1] = arcsin\left[\frac{\frac{V_{dc}[1]}{2} + V_{dc}[0]}{U^*}\right] \tag{5.4}$$

If $V_{dc}[i]$ is the DC bus voltage of the ith inverter after sorting, then the corresponding inverters switching instance for an n inverter configuration can be written as:

$$\theta[i] = arcsin\left[\frac{\frac{V_{dc}[i]}{2} + \sum_{i=1}^{n} V_{dc}[i-1]}{U^*}\right] \quad (5.5)$$

The master controller for SSCM is modelled as a triggered system to reproduce effects of a digital controller. As maybe seen in Figure 5.8, the inputs to this controller are six dc bus voltages of the solar panels, AC grid voltage and AC grid current. The outputs of the controller are twenty-four gate signals that are given to individual MOSFETs.

The master controller shown in Figure 5.9 consists of logic employed to sort the dc bus voltages, generate pulses for individual H – bridges, and identify the panel inverters corresponding to the sorted dc bus voltages. It may also be observed that triggered sort is one of the subsystems inside the master controller wherein DC bus voltages of the solar panels are taken as input and are sorted in descending order, whenever the system is triggered. The system is triggered either when the reference voltage is zero or when the slope of the reference voltage is zero i.e., the sorting is performed every quarter cycle of the reference voltage. The outputs of triggered sort subsystem are arrays of sorted DC bus voltages, and the indices corresponding to the dc bus voltages. Sorted dc bus voltages from large to small, and the corresponding voltage indices coming out from the triggered sort subsystem is fed into a MATLAB function block, where switching instance is calculated using the Equation (5.5). These switching instances are fed into the modulators which generate the switching pulses for all the inverter switches. The modulator subsystems also take inputs from the output of the Phase Locked Loop (PLL) along with the phase information of the generated reference voltage from the current control loop. The magnitude and phase angle of reference voltage is generated from the current control loop as shown in Figure 5.10.

5.6. Simulations Demonstrating Closed Loop Current Control

The DC terminals of each H-bridge inverter module is connected to an ideal DC voltage source. The magnitude of DC voltage of each DC voltage source is set to 36.3 V (voltage at maximum power point for the solar panel modules considered in Chapter 6). AC grid voltage is set to 120 V AC rms. Control scheme as described in Chapter 4, as well as the control parameters obtained have been used to study the dynamic performance of grid connected SPCI, with ideal DC voltage sources connected to the DC terminals. Simulation parameters are described in Table 5.1. The interfacing inductance and resistance values assumed in Chapter 4 have been used. Simulations have been performed to verify the control system performance for step changes in input, for Sorted Stair Case Modulation (SSCM). Demonstration of controller performance when both active and reactive power is injected into the grid is shown in Figure 5.11. Initial references for grid current along d-axis, 'idref' and along q-axis, 'iqref' are set to zero till t=0.5 s. At t=0.5 s, 'idref' is set to 17 A. Reference current along q-axis, 'iqref' is zero till t=1 s. At t=1s, 'iqref' is set to 5A. It may be seen from Figure 5.11 that the actual current along q-axis, 'iq' reaches steady state in about 0.2 s. At t=2 s, 'iqref' is again changed to 8 A, and system reaches the steady state in about 0.2 s. Figure 5.12.a shows the simulation waveforms of the AC quantities measured on the grid side, when only active power is injected into the grid, with 'idref'=17 A. It may be seen that the grid current, 'Igrid' is in phase with the grid voltage, 'Vgrid'. 'Vspci' is the thirteen-level output voltage synthesized by the Solar Panel Companion Inverter (SPCI). Figure 5.12.b and Figure 5.12.c shows the simulation waveforms of AC quantities measured for reactive power injection. It may be seen that the grid current, 'Igrid' is not in phase with the grid voltage, 'Vgrid' because in this case, along

with active power, reactive power is also being injected into the grid. The magnitude of the grid current should be the resultant of magnitude of the active and reactive components of current.

5.7. Discussion

This chapter described in detailed the modeling of closed loop current controlled grid connected Solar Panel Companion Inverter (SPCI). Sorted Stair Case Modulation (SSCM) has been specifically described while modeling because the modulation algorithm has been simplified from the one described in [3]. The simulation model for SPWM remains the same as in [3], with an addition of current control loop. These models are used in Chapter 6, and Chapter 7 to demonstrate the simulation results.

Table 5.1: Simulation Parameters

Parameter	***Value***
DC bus voltage	36.3 V
DC bus Capacitance for each inverter	10 mF
Interfacing resistance	1 Ω
Interfacing inductance	17 mH
AC Grid Voltage	120 V AC rms

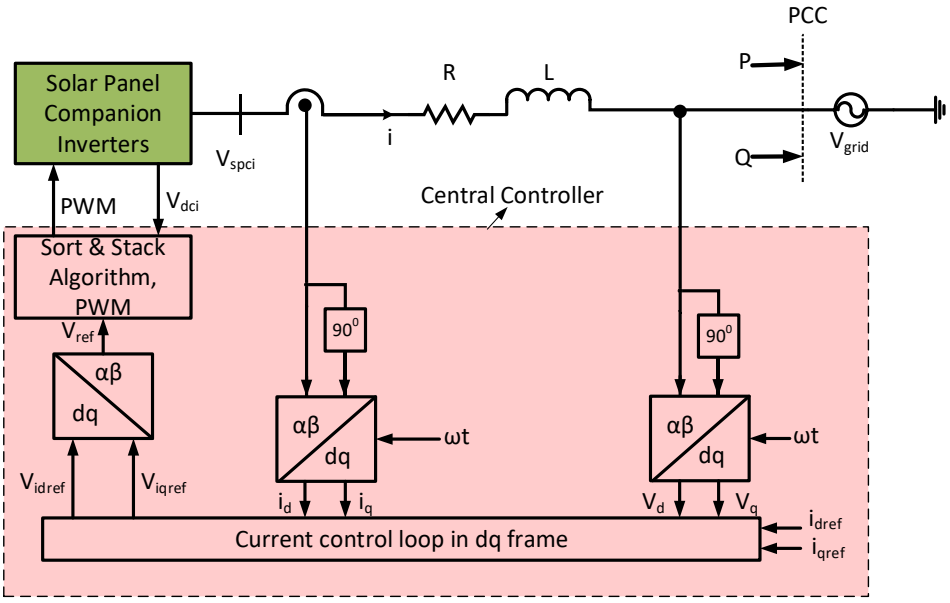

FIGURE 5.1: Simplified block diagram of grid connected solar panel companion inverter.

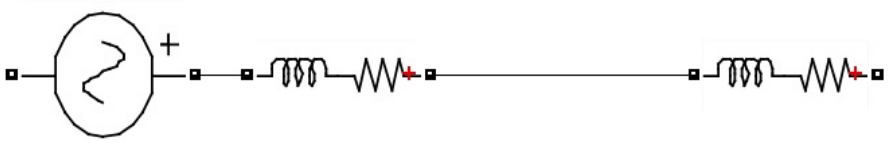

FIGURE 5.2: Simplified circuit schematic showing ac grid modelled as an ideal ac voltage source with a series impedance, connected to an interfacing impedance.

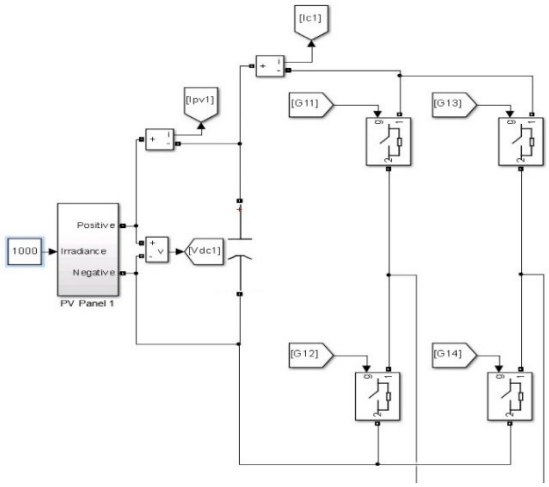

FIGURE 5.3: Simplified circuit schematic of a solar panel companion inverter.

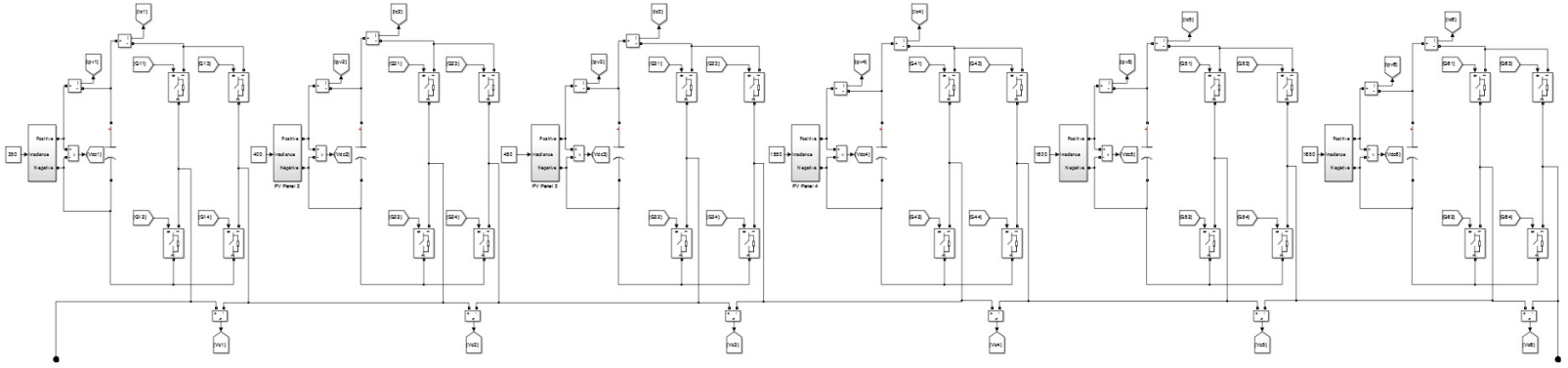

Figure 5.4: Simplified circuit schematic of a proposed 13-level solar panel companion inverter system for 120Vac applications.

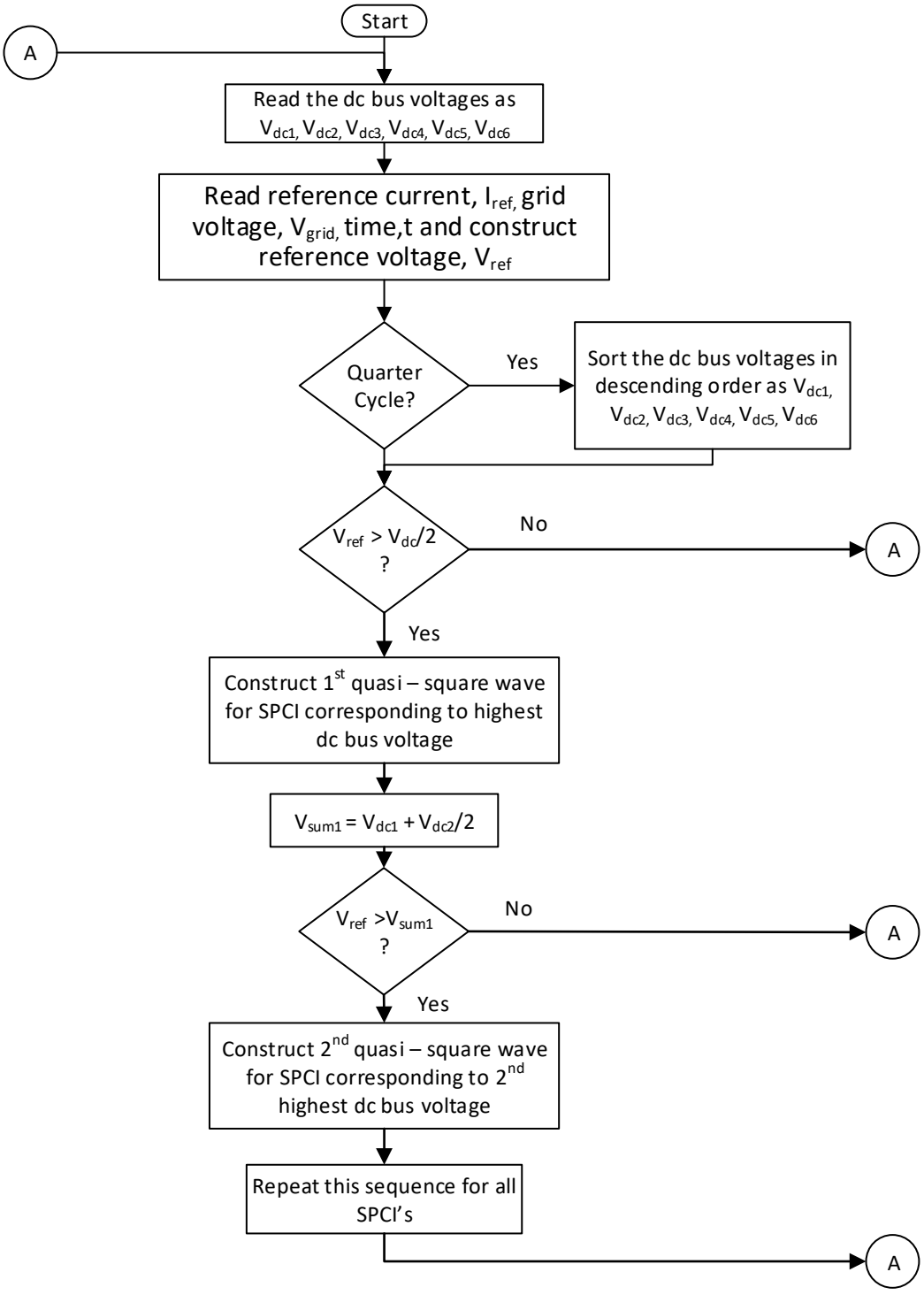

FIGURE 5.5: Flow chart for implementation of sorted stair case modulation [3].

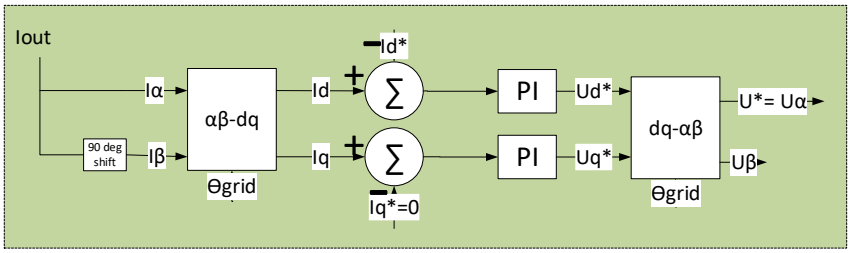

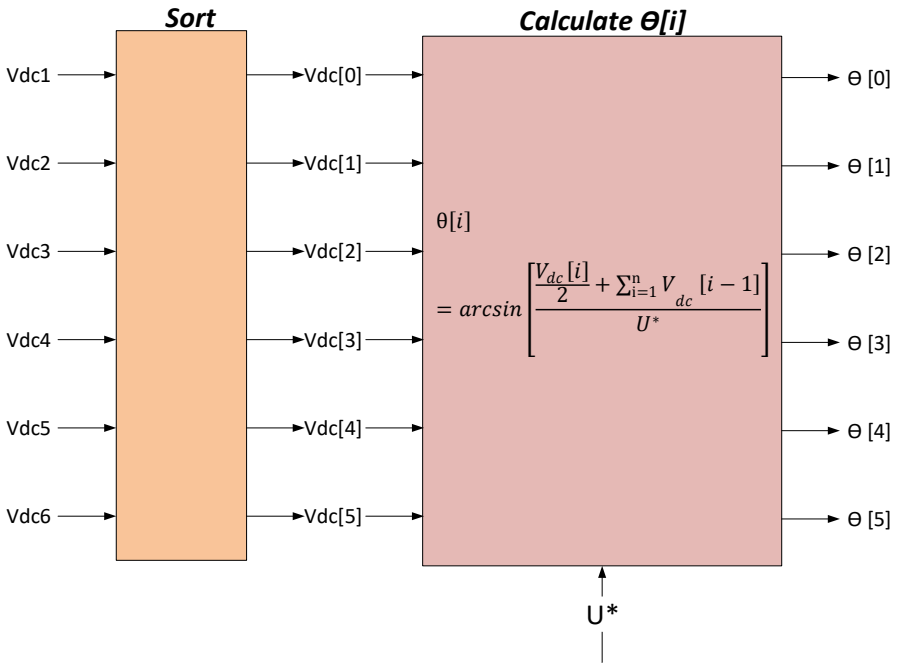

FIGURE 5.6: Simplified block schematic showing implementation of sort and stack algorithm in MATLAB Simulink.

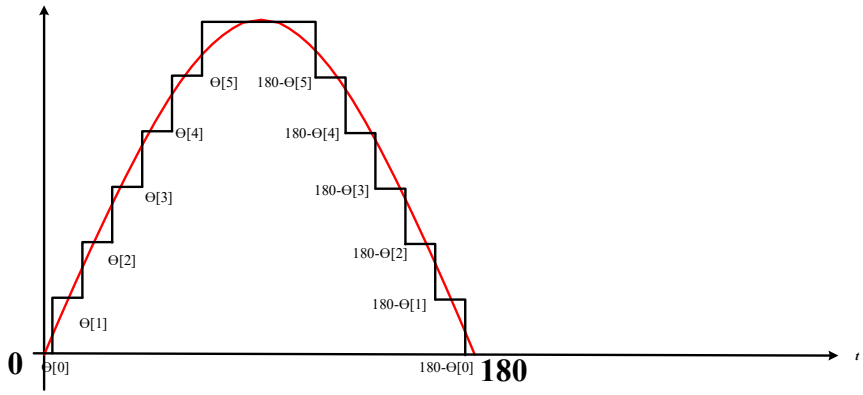

FIGURE 5.7: Schematic showing switching instances of staircase waveform over the reference sinusoidal voltage waveform.

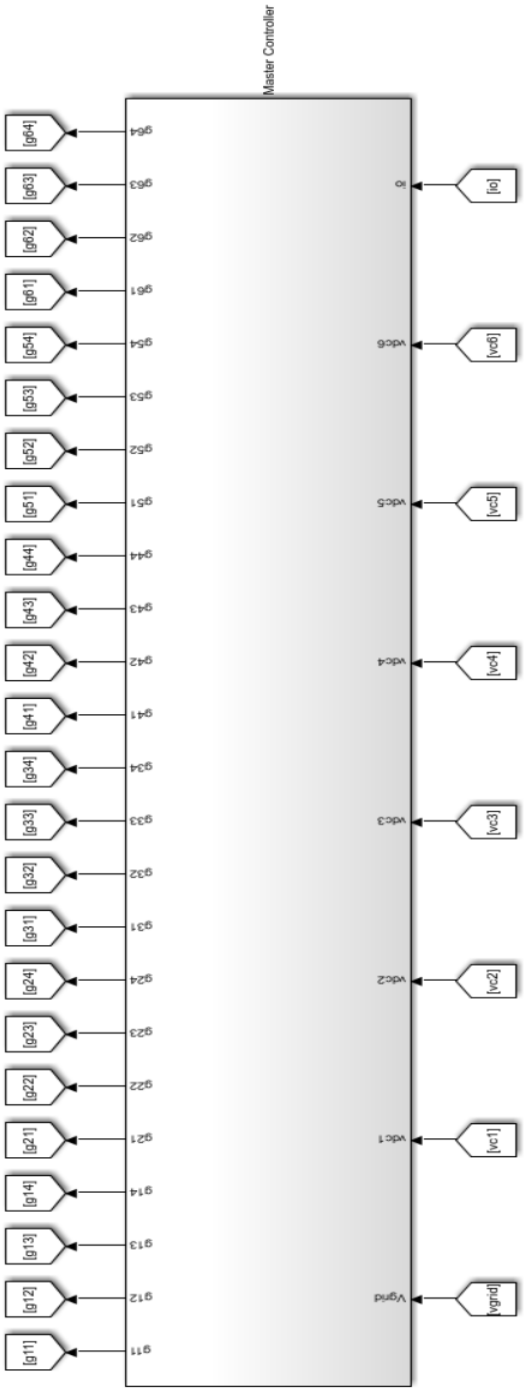

FIGURE 5.8: Central controller for sorted stair case modulation.

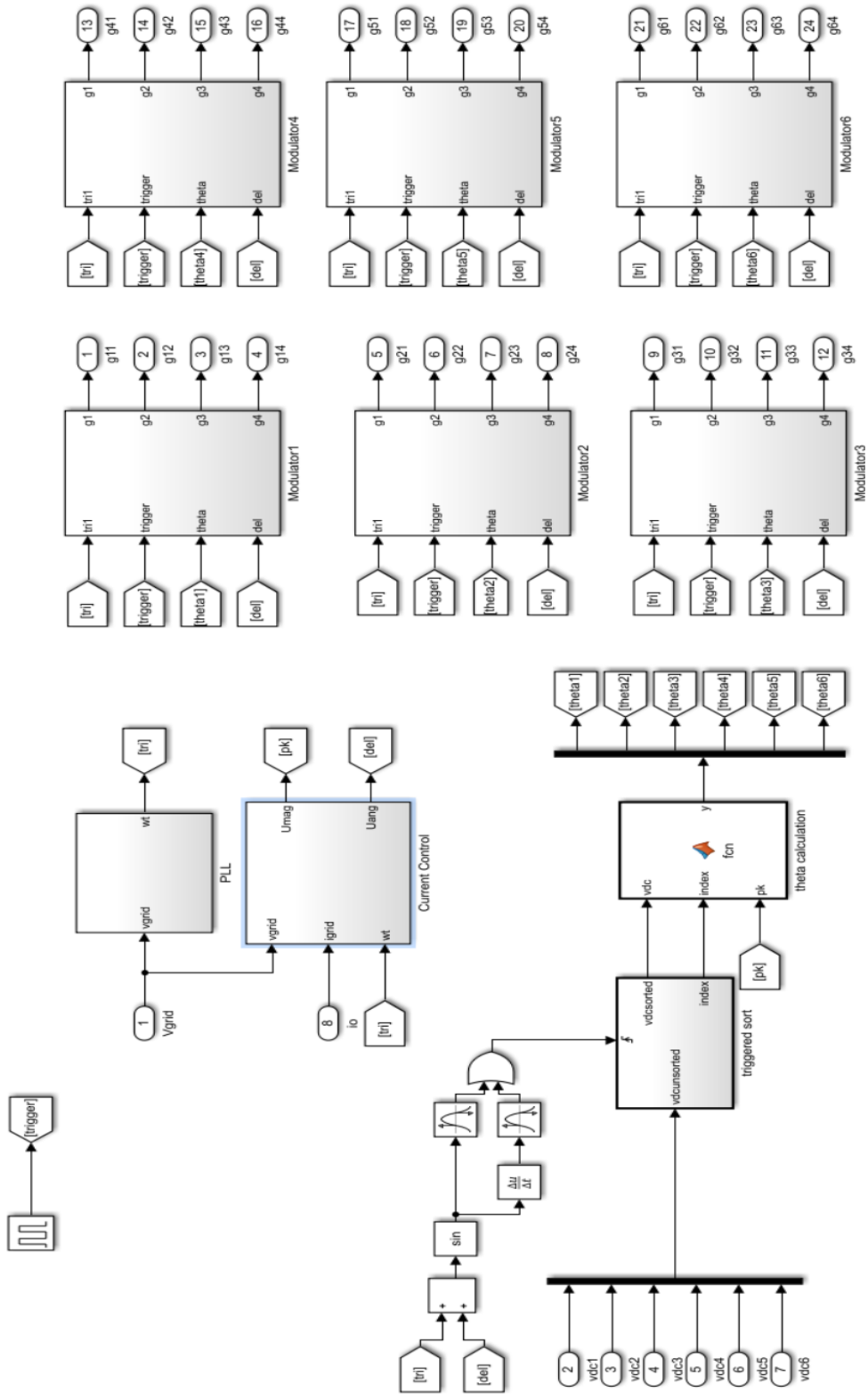

FIGURE 5.9: Simplified block schematic showing Simulink subsystem of master controller for Sorted Stair Case Modulation (SSCM).

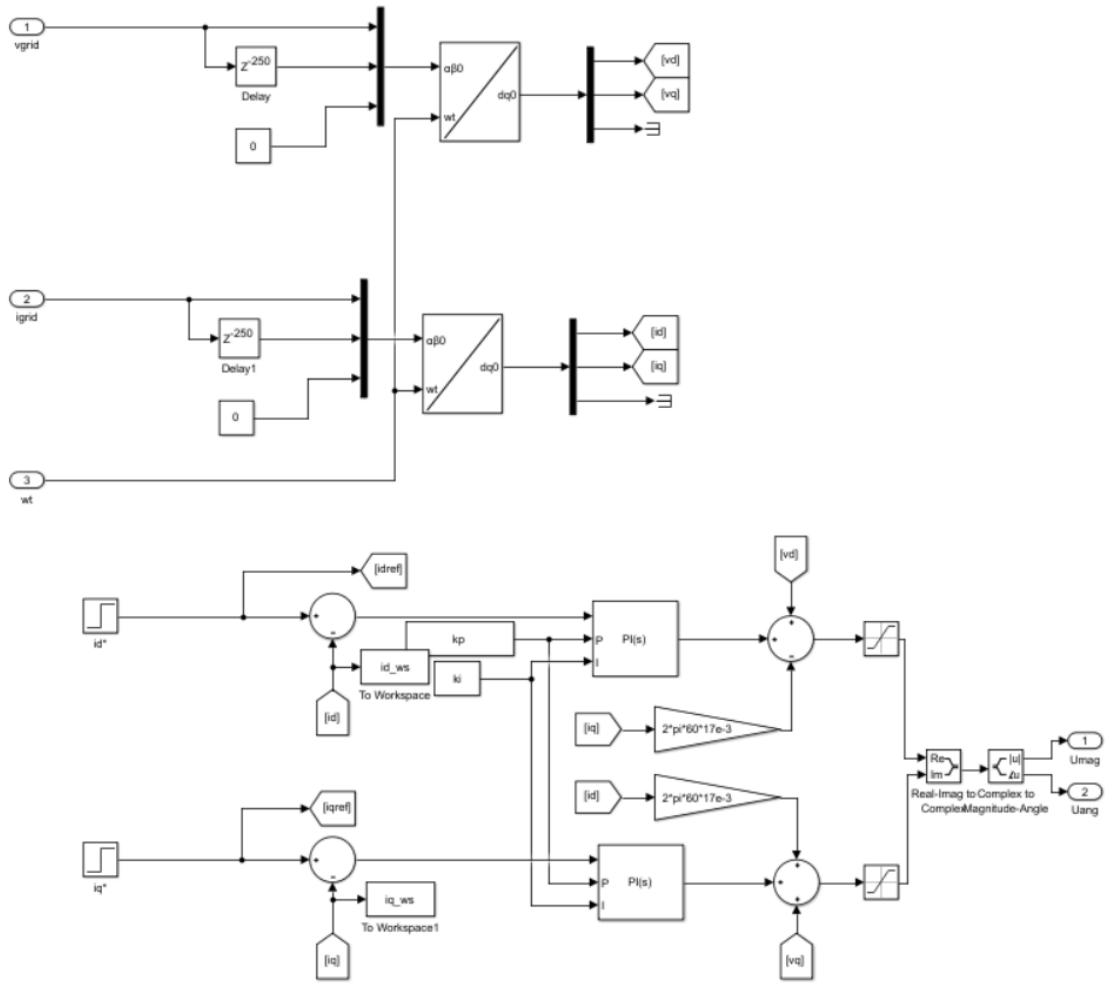

FIGURE 5.10: Simplified block schematic showing Simulink subsystem of master controller for Sorted Stair Case Modulation (SSCM).

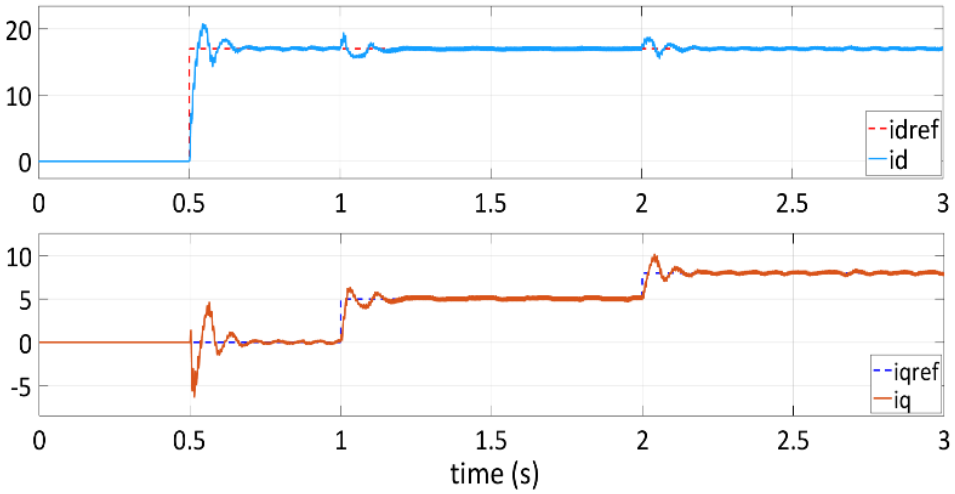

FIGURE 5.11: Simulation waveforms showing the controller performance of grid connected Solar Panel Companion Inverter (SPCI) system with ideal DC sources connected to the DC terminals of each H-bridge module, when both active and reactive power into the grid are controlled.

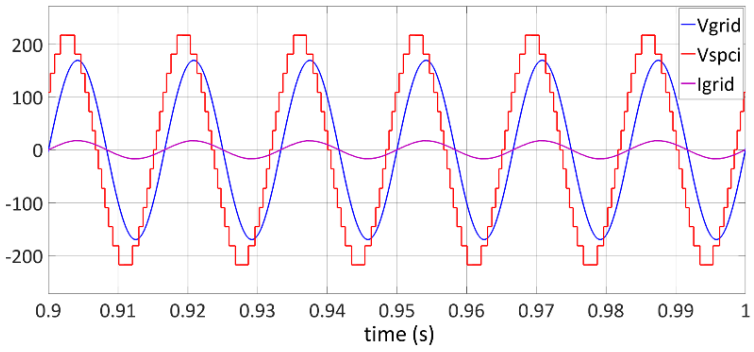

a.

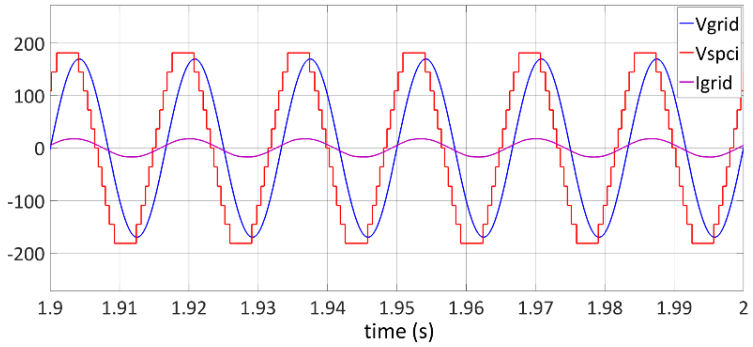

b.

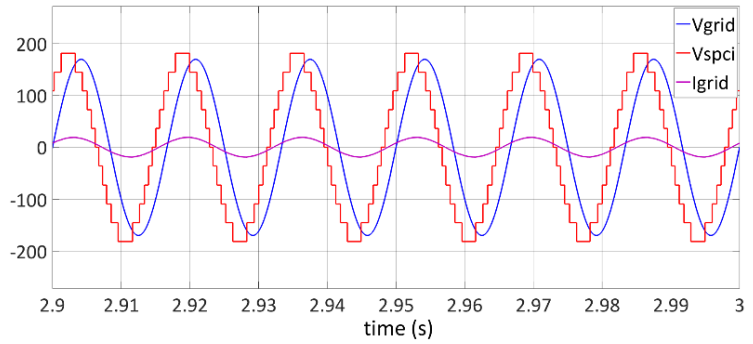

c.

FIGURE 5.12: Simulation waveforms showing the controller performance of grid connected Solar Panel Companion Inverter (SPCI) system with ideal DC sources connected to the DC terminals of each H-bridge module, when both active and reactive power into the grid are controlled.
a. Reference currents along d-axis and q-axis are set to 17A and 0 A respectively.
b. Reference currents along d-axis and q-axis are set to 17A and 5 A respectively.
c. Reference currents along d-axis and q-axis are set to 17A and 8 A respectively.

CHAPTER 6 : MAXIMUM POWER POINT TRACKING

6.1. Introduction

Chapter 4 discussed closed loop control architecture to control active power, and reactive power injection into the grid. Modeling and simulation of closed loop current control for grid connected Solar Panel Companion Inverter (SPCI) has been presented in Chapter 5. Chapter 6 is adapted from [62]. In this chapter, a Maximum Power Point Tracking (MPPT) algorithm for SPCI is described. MPPT scheme is employed to perform maximum power extraction from the photo-voltaic panels at system level. This algorithm generates magnitude of the reference current such that maximum power is extracted from the system. Discussion in this chapter involves power injection into the grid at unity power factor. In section 6.2, block schematic description which includes the proposed MPPT algorithm is presented. MPPT algorithm employed to extract maximum power is discussed in section 6.3. Simulation results for various operating scenarios are presented in section 6.4. These simulations are performed for both Sorted Staircase Modulation (SSCM) and Sorted Pulse Width Modulation (SPWM) schemes that have been explained in Chapter 3. Section 6.5 concludes this chapter with a brief summary.

6.2. Block Schematic Description

A block schematic of the grid connected Solar Panel Companion Inverter (SPCI) is shown in figure 6.1. The schematic consists of SPCIs connected to grid via the interfacing reactance. Grid voltage 'V_{grid}' is measured and fed as an input to the Phase Locked Loop (PLL) block. A PLL algorithm as described in is implemented to generate image of the

grid voltage, 'V_{grid}', and phase of the grid voltage, 'ωt'. MPPT block consists of MPPT algorithm implementation that is described in section 6.3. This block takes in direct axis component of the grid voltage 'V_d', and direct axis component of the grid current 'I_d', from the current control block. Output of MPPT block is direct axis component of the reference grid current, 'I_d*'. The current control loop block consists of the closed loop current control architecture as described in chapter 4. The inputs to this block are 'V_{grid}', 'ωt', and 'I_d*'.

6.3. System Level Maximum Power Point Tracking

Proposed MPPT algorithm generates direct axis component of reference grid current, 'I_d^*'. This 'I_d^*' is fed into closed loop PI controller to generate a reference voltage as discussed in previous sub-section. This proposed algorithm follows a bisection scheme in approaching the maximum power point. An initial minimum current, 'i_d^{min}' of 1A is assumed. A maximum current, 'i_d^{max}' is assumed as the maximum current rating of the SPCI system. As the algorithm is executed, a new reference current is calculated by bisecting 'i_d^{min}', and 'i_d^{max}'. Reference current 'I_d^*' generated each time is bound within 'i_d^{min}', and 'i_d^{max}'. Each time the bisection is implemented, 'i_d^{min}', and 'i_d^{max}' are updated. Detailed flowchart schematic of the implementation can be seen in figure 6.2. In this algorithm, firstly, the initial output power, $P^{[0]}$, power computed at 'n^{th}' iteration, '$P^{[10]}$', initial value of direct axis component of current, '$I_d^{[0]}$', direct axis component of current computed at 'n^{th}' iteration, '$I_d^{[10]}$', change in power between the iterations, 'dP', maximum output power, 'P^{max}', change in reference current, 'dI_d', and count, 'n', are initialized to zero. Depending on the modulation strategy employed, a sampling time, 'T_s' is employed. It takes in calculated output power, 'P_{cal}', and the sampling time, 'T_s' as inputs. P_{cal} can be computed by using equation (1), or by using the DC bus voltages and dc currents

information. Using equation (1) for calculating the power extracted can eliminate the need of additional dc current sensors for sensing the current. If n is equal to zero, i_d^{min} is assigned to $I_d^{[0]}$, and P_{cal} is assigned to P_{max}. At each sampling time, n is incremented by 1, and P_{cal} is assigned to $P_{[n-1]}$, change of power is calculated and assigned to dP. The following are the set of logics applied in implementing the Maximum Power Point Tracking algorithm:

i. If dP is greater than zero, and if $dI_d > 0$, $I_d^{[n-1]}$ is assigned to i_d^{min}, and, $P^{[n-1]}$ is assigned to P^{max}.

ii. If dP is greater than zero, and if $dI_d < 0$, $I_d^{[n-1]}$ is assigned to i_d^{max}, and, $P^{[n-1]}$ is assigned to P^{max}.

iii. If dP is lesser than zero, $I_d^{[n-1]}$ is assigned to i_d^{max}.

iv. $I_d^{[10]}$ is updated by bisecting i_d^{min}, and i_d^{max}.

v. dI_d is computed by subtracting $I_d^{[n-1]}$ from $I_d^{[10]}$.

vi. The updated $I_d^{[10]}$ is assigned to the reference current, I_d*. This I_d* is fed as an input to the current control loop, as discussed in the previous sub-section.

6.4. Simulation Results

MATLAB Simulink is used to perform simulations and demonstrate the maximum power operation of solar panels. The Maximum Power Point Tracking (MPPT) algorithm is implemented together with Sorted Stair Case Modulation (SSCM) and Sorted Pulse Width Modulation (SPWM) respectively. The simulations are performed for various scenarios of uniform and non – uniform irradiance. Six representative operating scenarios for SSCM and SPWM have been selected to demonstrate the efficacy of MPPT algorithm. These scenarios are as follows:

Scenario 1: Uniform irradiation of 200 W/m^2 on all the panels.

Scenario 2: Uniform irradiation of 600 W/m^2 on all the panels.

Scenario 3: Uniform irradiation of 1000 W/m^2 on all the panels.

Scenario 4: Non-uniform irradiation (950 W/m^2, 800 W/m^2, 650 W/m^2, 500 W/m^2, 350 W/m^2, 200 W/m^2)

Scenario 5: Non-uniform irradiation (1000 W/m^2, 900 W/m^2, 800 W/m^2, 700 W/m^2, 600 W/m^2, 500 W/m^2)

Scenario 6: Non-uniform irradiation (1000 W/m^2, 950 W/m^2, 900 W/m^2, 850 W/m^2, 800 W/m^2, 750 W/m^2)

6.4.1. Sorted Stair Case Modulation

Maximum Power Point Tracking (MPPT) algorithm is implemented together with Sorted Stair Case Modulation (SSCM). Figures 6.3 through 6.8 are simulation results corresponding to uniform irradiation conditions. Figure 6.3 shows P-V characteristics of the solar panel model when operating at an irradiation of 200 W/m^2 (operating scenario 1). This scenario corresponds to low available power and can be considered as representation of a cloudy day. Since all solar panels are operating under uniform irradiation, P-V characteristics of all the panels are overlapped. The portion highlighted in red of the P-V curve in figure 6.3 shows steady state operating points of all solar panels, upon reaching the maximum power point, with SSCM strategy implemented. Figure 6.4 shows waveforms of grid voltage, V_{grid}, output voltage, V_{spci}, grid current, I_{grid}, for six cycles when operating in scenario 1, with SSCM strategy implemented. Figure 6.5 shows P-V characteristics of the solar panel model when operating at an irradiation of 600 W/m^2 (operating scenario 2). This scenario corresponds to moderately available power and can be considered as representation of partial daylight. The portion highlighted in red of the P-

V curve in figure 6.6 shows steady state operating points of all solar panels, upon reaching the maximum power point, with SSCM strategy implemented. Figure 6.6 shows waveforms of grid voltage, V_{grid}, output voltage, V_{spci}, grid current, I_{grid}, for six cycles in when operating in scenario 2, with SSCM strategy implemented. Also, it may be seen that magnitude of the grid current in scenario 2 is greater than that of scenario 1 because, more power is available in scenario 2 than in scenario 1. Figure 6.7 shows P-V characteristics of the solar panel model when operating at an irradiation of 1000 W/m^2 (operating scenario 3). This scenario corresponds to maximum available power and represents a perfect sunny day. The portion highlighted in red of the P-V curve in figure 6.7 shows steady state operating points of all the solar panels, upon reaching the maximum power point, with SSCM. Figure 6.8 shows waveforms of grid voltage, V_{grid}, output voltage, V_{spci}, grid current, I_{grid}, for six cycles in when operating in scenario 3 with SSCM. It may be observed that magnitude of the grid current in scenario 3 is the highest when compared to scenario 1, and scenario 2, with SSCM strategy. This is because system is operating under conditions where the power availability is maximum. Also, in all the three scenarios corresponding to uniform irradiance, current is injected into the grid at unity power factor.

Figures 6.9 through 6.14 are simulation results corresponding to non-uniform irradiation conditions. Figure 6.9 shows P-V characteristics of all solar panels in operating scenario 4. In scenario 4, solar panel irradiations are set to $950W/m^2$, $800W/m^2$, $650W/m^2$, $500W/m^2$, $350W/m^2$, $200W/m^2$, and this represents a significant disparity of irradiation incident on all the solar panels. The portion highlighted in red of P-V curves in figure 6.9 shows the steady state operating points of all solar panels, upon reaching the maximum power point, with SSCM strategy implemented. It may be seen that all the panels are

operating at their corresponding maximum power points. Figure 6.10 shows waveforms of grid voltage, V_{grid}, output voltage, V_{spci}, grid current, I_{grid}, for six cycles in when operating in scenario 4, with SSCM strategy. Figure 6.11 shows P-V characteristics of all the solar panels in operating scenario 5. In scenario 5, solar panel irradiations are set to 1000W/m^2, 900W/m^2, 800W/m^2, 700W/m^2, 600W/m^2, 500W/m^2, and this represents a moderate disparity of irradiation incident on all the solar panels. The portion highlighted in red of the P-V curves in figure 6.11 shows steady state operating points of all solar panels, upon reaching the maximum power point, with SSCM strategy. It may be seen that all the panels are operating at their corresponding maximum power points. Figure 6.12 shows the waveforms of grid voltage, V_{grid}, output voltage, V_{spci}, grid current, I_{grid}, for six cycles in when operating in scenario 5. Figure 6.13 shows P-V characteristics of all the solar panels in operating scenario 6. In scenario 6, solar panel irradiations are set to 1000W/m^2, 950W/m^2, 900W/m^2, 850W/m^2, 800W/m^2, 750W/m^2, and this represents a case with minimum disparity of irradiation incident on all the solar panels. The portion highlighted in red of the P-V curves in figure 6.13 shows steady state operating points of all the solar panels, upon reaching the maximum power point, with SSCM implemented. It may be seen that all the panels are operating at their corresponding maximum power points. Figure 6.14 shows the waveforms of grid voltage, V_{grid}, output voltage, V_{spci}, grid current, I_{grid}, for six cycles in when operating in scenario 6. For the considered non-uniform irradiance scenarios, as the disparity in irradiance is increases, the available power in the system decreases (assuming that1000W/m^2 being the highest irradiance possible). Hence, it may be observed from figure 6.10, figure 6.12, and figure 6.13 that magnitude of the grid current

increases, as the disparity in irradiance decreases. Also, for the scenarios involving non-uniform irradiance, the current is injected into the grid at unity power factor.

6.4.2. Sorted Pulse Width Modulation

Maximum Power Point Tracking (MPPT) algorithm is implemented together with Sorted Pulse Width Modulation (SPWM). Figures 6.15 through 6.20 are simulation results corresponding to uniform irradiation conditions. Figure 6.15 shows P-V characteristics of the solar panel model when operating at an irradiation of 200 W/m^2 (operating scenario 1). This scenario corresponds to low available power and can be considered as representation of a cloudy day. Since all solar panels are operating under uniform irradiation, P-V characteristics of all the panels are overlapped. The portion highlighted in red of the P-V curve in figure 6.15 shows steady state operating points of all solar panels, upon reaching maximum power point, with SPWM strategy implemented. Figure 6.16 shows waveforms of grid voltage, V_{grid}, output voltage, V_{spci}, grid current, I_{grid}, for six cycles when operating in scenario 1, with SPWM strategy implemented. Figure 6.17 shows P-V characteristics of the solar panel model when operating at an irradiation of 600 W/m^2 (operating scenario 2). This scenario corresponds to moderately available power and can be considered as representation of partial daylight. The portion highlighted in red of the P-V curve in figure 6.17 shows steady state operating points of all the solar panels, upon reaching the maximum power point, with SPWM strategy implemented. Figure 6.18 shows waveforms of grid voltage, V_{grid}, output voltage, V_{spci}, grid current, I_{grid}, for six cycles in when operating in scenario 2, with SPWM strategy implemented. Also, it may be seen that magnitude of the grid current in scenario 2 is greater than that of scenario 1 because, more power is available in scenario 2 than in scenario 1. Figure 6.19 shows the P-V

characteristics of the solar panel model when operating at an irradiation of 1000 W/m^2 (operating scenario 3). This scenario corresponds to maximum available power and represents a perfect sunny day. The portion highlighted in red of the P-V curve in figure 6.19 shows steady state operating points of all the solar panels, upon reaching the maximum power point, with SPWM strategy implemented. Figure 6.20 shows waveforms of grid voltage, V_{grid}, output voltage, V_{spci}, grid current, I_{grid}, for six cycles in when operating in scenario 3 with SPWM strategy implemented. It may be observed that magnitude of the grid current in scenario 3 is at its highest when compared to scenarios 1 and 2, with SPWM strategy. This is because the system is operating under conditions where power availability is maximum. Also, in all the three scenarios corresponding to uniform irradiance, current is injected into the grid at unity power factor.

Figures 6.21 through 6.26 are the simulation results corresponding to non-uniform irradiation conditions. Figure 6.21 shows P-V characteristics of all the solar panels in operating scenario 4. In scenario 4, solar panel irradiations are set to 950W/m^2, 800W/m^2, 650W/m^2, 500W/m^2, 350W/m^2, 200W/m^2, and this is a representation of significant disparity of irradiation incident on all the solar panels. The portion highlighted in red of the P-V curves in figure 6.21 shows steady state operating points of all the solar panels, upon reaching maximum power point, with SPWM strategy implemented. It may be seen that all panels are operating at their corresponding maximum power points. Figure 6.22 shows waveforms of grid voltage, V_{grid}, output voltage, V_{spci}, grid current, I_{grid}, for six cycles in when operating in scenario 4, with SPWM strategy. Figure 6.23 shows P-V characteristics of all solar panels in operating scenario 5. In scenario 5, solar panel irradiations are set to 1000W/m^2, 900W/m^2, 800W/m^2, 700W/m^2, 600W/m^2, 500W/m^2, and

this represents a moderate disparity of irradiation incident on all the solar panels. The portion highlighted in red of the P-V curves in figure 6.23 shows steady state operating points of all the solar panels, upon reaching maximum power point, with SPWM strategy. It may be seen that all the panels are operating at their corresponding maximum power points. Figure 6.24 shows waveforms of grid voltage, V_{grid}, output voltage, V_{spci}, grid current, I_{grid}, for six cycles in when operating in scenario 5. Figure 6.25 shows P-V characteristics of all the solar panels in operating scenario 6. In scenario 6, solar panel irradiations are set to 1000W/m^2, 950W/m^2, 900W/m^2, 850W/m^2, 800W/m^2, 750W/m^2, and this represents a minimum disparity of irradiation incident on all the solar panels. The portion highlighted in red of the P-V curves in figure 6.25 shows steady state operating points of all the solar panels, upon reaching maximum power point, with SPWM implemented. It may be seen that all panels are operating at their corresponding maximum power points. Figure 6.26 shows the waveforms of grid voltage, V_{grid}, output voltage, V_{spci}, grid current, I_{grid}, for six cycles in when operating in scenario 6. For the considered non-uniform irradiance scenarios, as disparity in irradiance is increases, available power in the system decreases (assuming that1000W/m^2 being the highest irradiance possible). Hence, it may be observed from figure 6.22, figure 6.24, and figure 6.26 that magnitude of grid current increases, as the disparity in irradiance decreases. Also, for the scenarios involving non-uniform irradiance, current is injected into the grid at unity power factor.

6.5. Summary

In this chapter, a system level Maximum Power Point Tracking (MPPT) algorithm has been proposed. The proposed algorithm has been implemented for Sorted Stair Case Modulation (SSCM) and Sorted Pulse Width Modulation (SPWM). The PV curves

demonstrating the steady state operating point of SPCI when operating in uniform and non-uniform irradiation have been obtained. Maximum power extraction at panel level has been shown irrespective of whether the sunlight is uniform or non-uniform. Both the modulation strategies, SSCM and SPWM have been found to perform maximum power extraction at panel level. The MPPT algorithm that has been used in this chapter is also used in Chapter 9 to demonstrate the MPPT operation of the laboratory prototype.

Table 6.1: Simulation Parameters

Parameter		***Value***
Solar Panel model: Bosch Solar Energy c-Si P 72 NA21126 (Parameters at irradiation of 1000 W/m^2, and temperature of 25^{o}C .)	Maximum Power	285.3 W
	Voltage at maximum power	36.3 V
	Current at maximum power	7.86 A
DC bus Capacitance for each inverter		4.7 mF
Interfacing inductance		17 mH

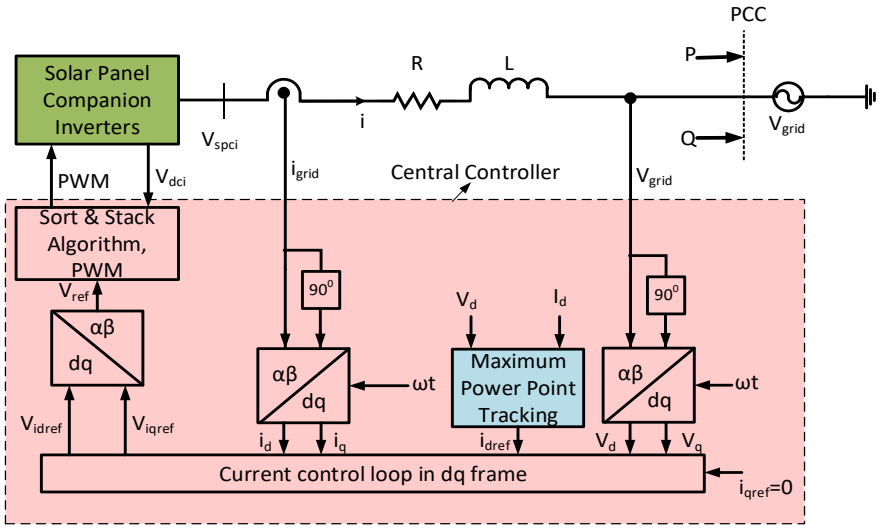

FIGURE 6.1: Block schematic of grid connected solar panel companion inverter (SPCI) with maximum power point tracking (MPPT)

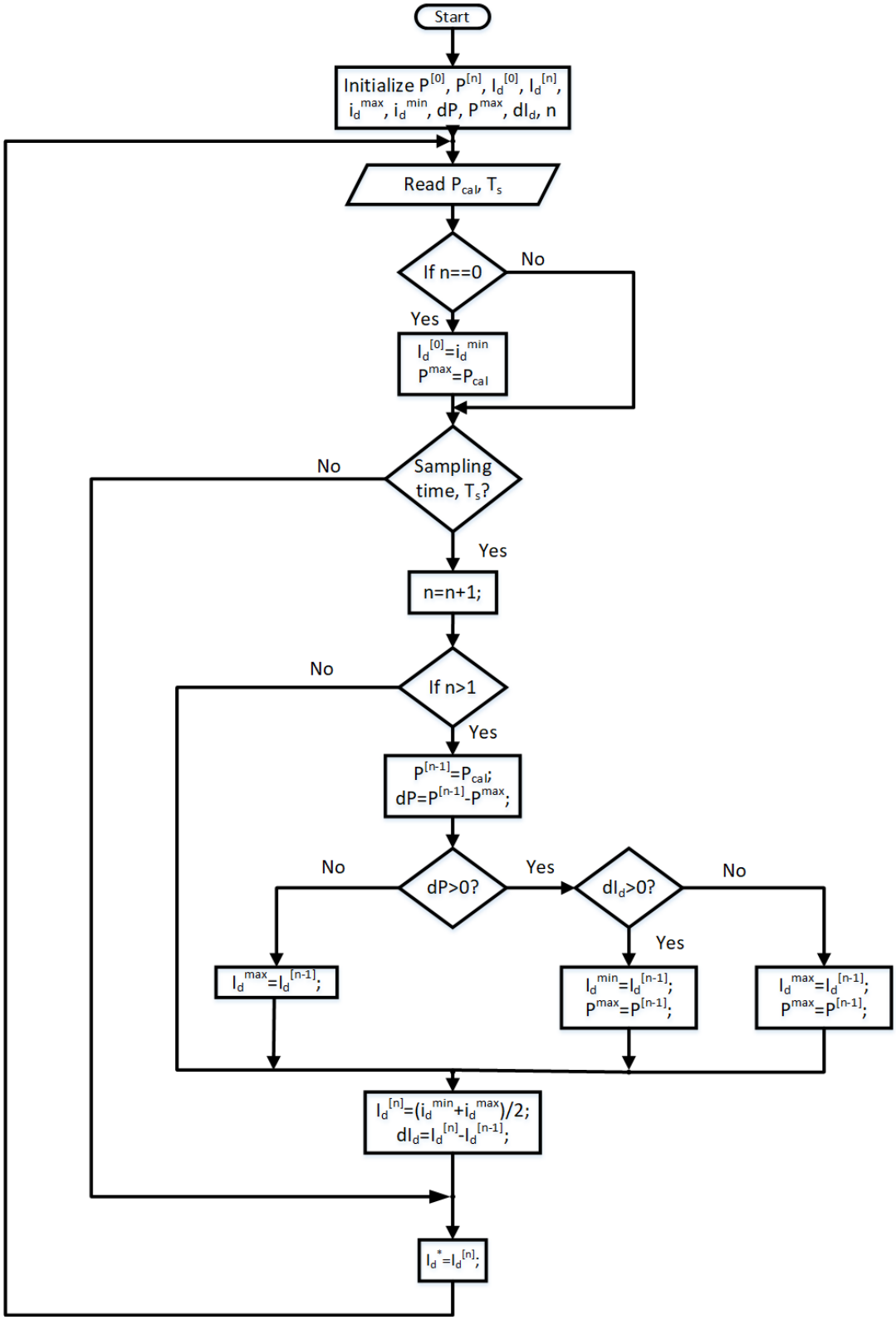

FIGURE 6.2: Schematic showing the flowchart of Maximum Power Point Tracking (MPPT) algorithm.

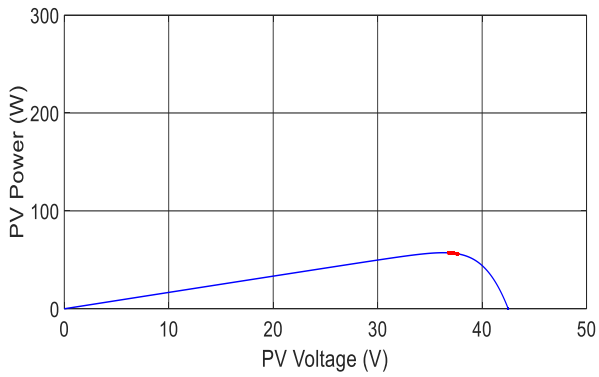

FIGURE 6.3: P-V curve showing the maximum power point operation of all the PV panels highlighted in red, operating under uniform irradiation of 200 W/m^2-operating scenario 1, with Maximum Power Point Tracking (MPPT) algorithm implemented for Sorted Staircase Modulation (SSCM).

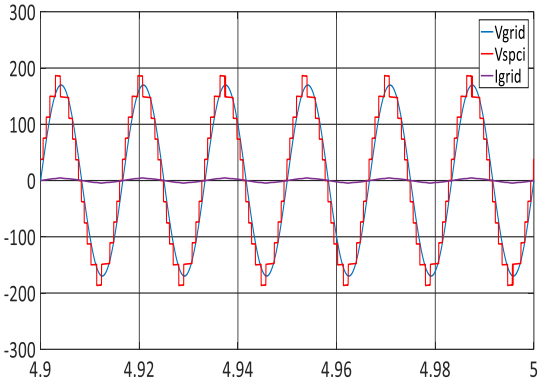

FIGURE 6.4: Simulation waveforms when the inverters are operating under uniform irradiation of 200 W/m^2-operating scenario 1, with Maximum Power Point Tracking (MPPT) algorithm implemented for Sorted Staircase Modulation (SSCM).

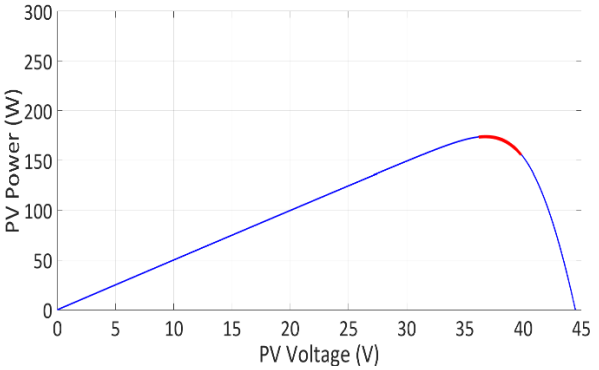

FIGURE 6.5: P-V curve showing the maximum power point operation of all the PV panels highlighted in red, operating under uniform irradiation of 600 W/m^2-operating scenario 2, with Maximum Power Point Tracking (MPPT) algorithm implemented for Sorted Staircase Modulation (SSCM).

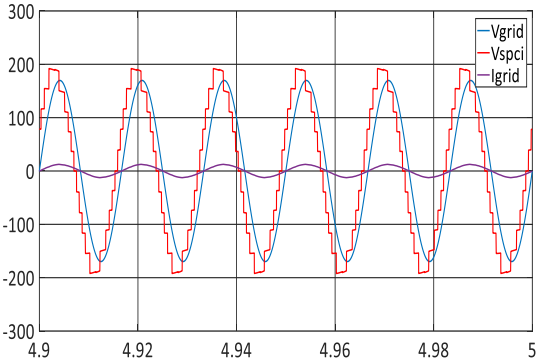

FIGURE 6.6: Simulation waveforms when the inverters are operating under uniform irradiation of 600 W/m^2-operating scenario 2, with Maximum Power Point Tracking (MPPT) algorithm implemented for Sorted Staircase Modulation (SSCM).

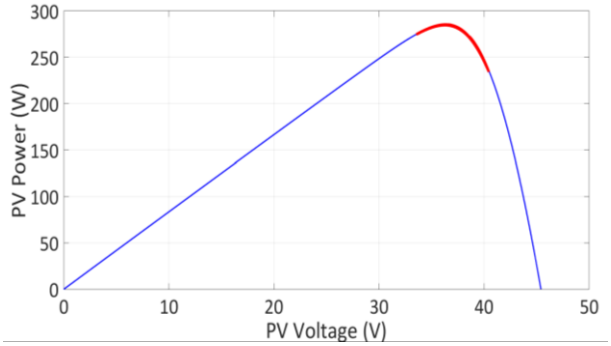

FIGURE 6.7: P-V curve showing the maximum power point operation of all the PV panels highlighted in red, operating under uniform irradiation of 1000 W/m^2-operating scenario 3, with Maximum Power Point Tracking (MPPT) algorithm implemented for Sorted Staircase Modulation (SSCM).

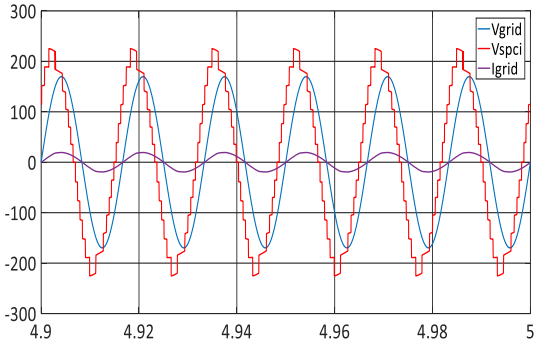

FIGURE 6.8: Simulation waveforms when the inverters are operating under uniform irradiation of 1000 W/m^2-operating scenario 1, with Maximum Power Point Tracking (MPPT) algorithm implemented for Sorted Staircase Modulation (SSCM).

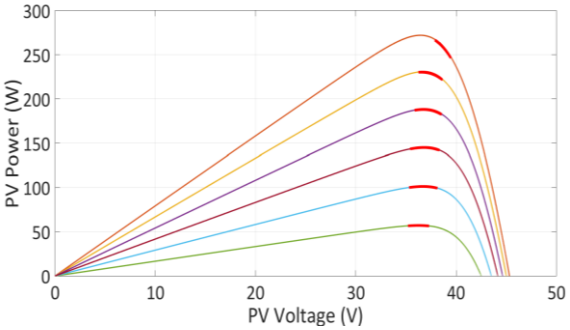

FIGURE 6.9: P-V curves showing the maximum power point operation of all the PV panels highlighted in red, operating under non - uniform irradiation. (950W/m^2, 800W/m^2, 650W/m^2, 500W/m^2, 350W/m^2, 200W/m^2-operating scenario 4.), with Maximum Power Point Tracking (MPPT) algorithm implemented for Sorted Staircase Modulation (SSCM).

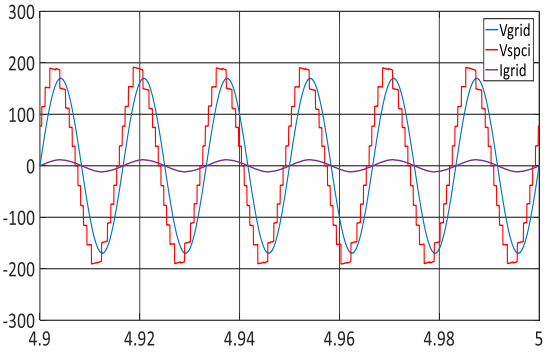

FIGURE 6.10: Simulation waveforms when the inverters are operating under non - uniform irradiation. (950W/m^2, 800W/m^2, 650W/m^2, 500W/m^2, 350W/m^2, 200W/m^2-operating scenario 4.), with Maximum Power Point Tracking (MPPT) algorithm implemented for Sorted Staircase Modulation (SSCM).

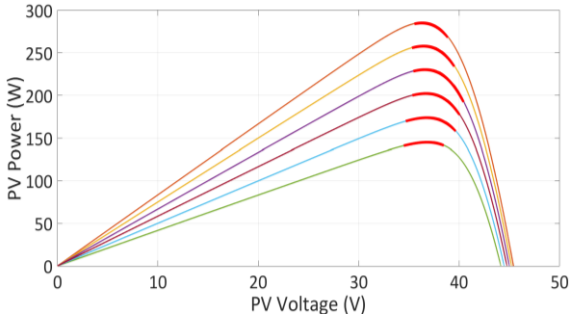

FIGURE 6.11: P-V curves showing the maximum power point operation of all the PV panels highlighted in red, operating under non - uniform irradiation. (1000W/m^2, 900W/m^2, 800W/m^2, 700W/m^2, 600W/m^2, 500W/m^2-operating scenario 5.), with Maximum Power Point Tracking (MPPT) algorithm implemented for Sorted Staircase Modulation (SSCM).

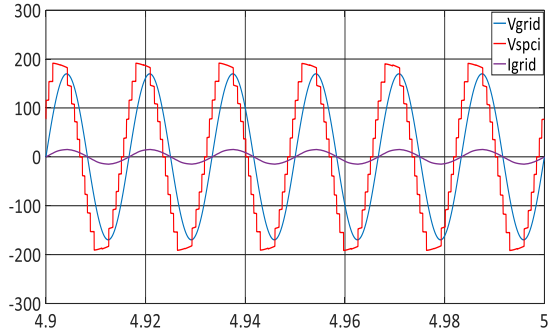

FIGURE 6.12: Simulation waveforms when the inverters are operating under non - uniform irradiation. (1000W/m^2, 900W/m^2, 800W/m^2, 700W/m^2, 600W/m^2, 500W/m^2-operating scenario 5.), with Maximum Power Point Tracking (MPPT) algorithm implemented for Sorted Staircase Modulation (SSCM).

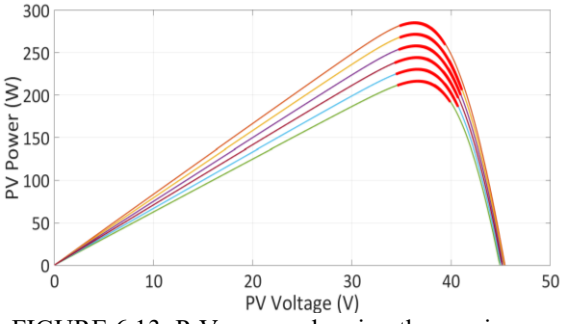

FIGURE 6.13: P-V curves showing the maximum power point operation of all the PV panels highlighted in red, operating under non - uniform irradiation. (1000W/m^2, 950W/m^2, 900W/m^2, 850W/m^2, 800W/m^2, 750W/m^2-operating scenario 6.), with Maximum Power Point Tracking (MPPT) algorithm implemented for Sorted Staircase Modulation (SSCM).

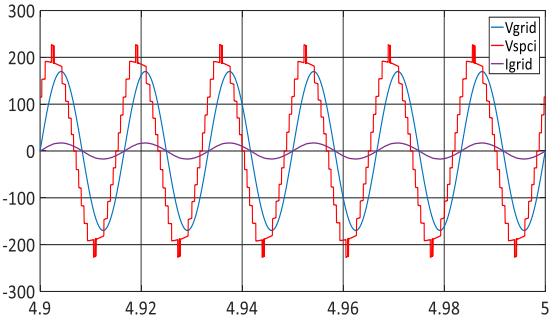

FIGURE 6.14: Simulation waveforms when the inverters are operating under non - uniform irradiation. (1000W/m^2, 950W/m^2, 900W/m^2, 850W/m^2, 800W/m^2, 750W/m^2-operating scenario 6.), with Maximum Power Point Tracking (MPPT) algorithm implemented for Sorted Staircase Modulation (SSCM).

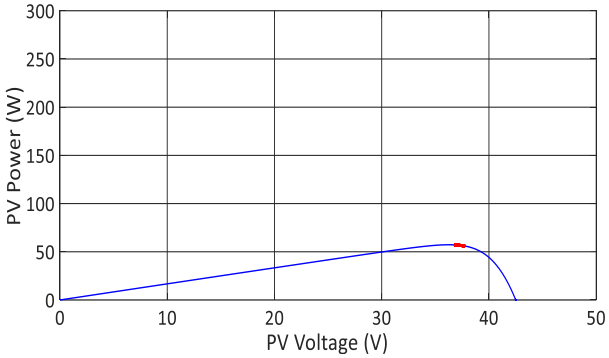

FIGURE 6.15: P-V curve showing the maximum power point operation of all the PV panels highlighted in red, operating under uniform irradiation of 200W/m^2-operating scenario 1, with Maximum Power Point Tracking (MPPT) algorithm implemented for Sorted Pulse Width Modulation (SPWM).

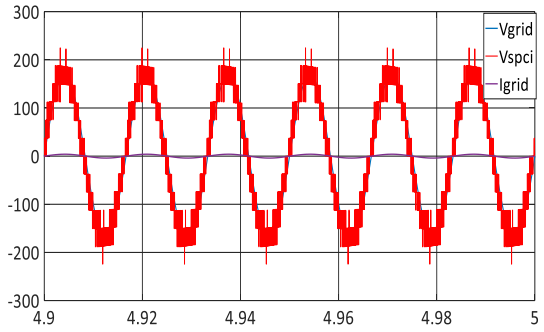

FIGURE 6.16: Simulation waveforms when the inverters are operating under uniform irradiation of 200W/m^2-operating scenario 1, with Maximum Power Point Tracking (MPPT) algorithm implemented for Sorted Pulse Width Modulation (SPWM).

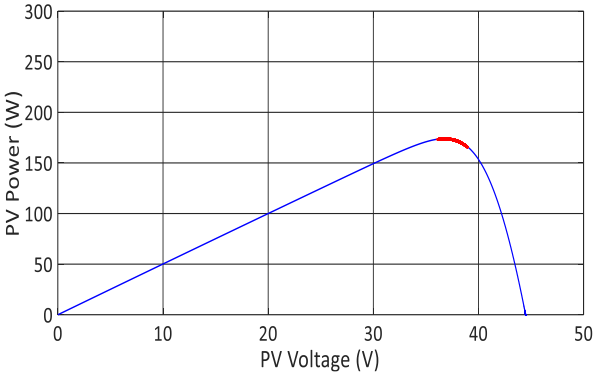

FIGURE 6.17: P-V curve showing the maximum power point operation of all the PV panels highlighted in red, operating under uniform irradiation of 600W/m^2-operating scenario 2, with Maximum Power Point Tracking (MPPT) algorithm implemented for Sorted Pulse Width Modulation (SPWM).

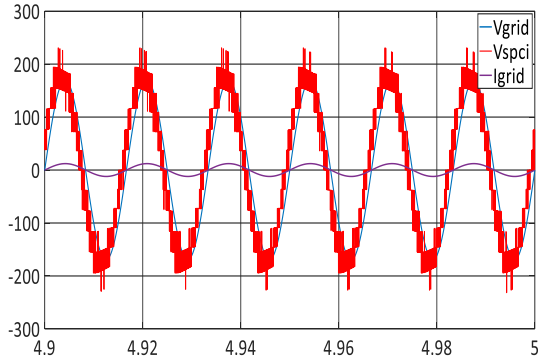

FIGURE 6.18: Simulation waveforms when the inverters are operating under uniform irradiation of 600W/m^2-operating scenario 2, with Maximum Power Point Tracking (MPPT) algorithm implemented for Sorted Pulse Width Modulation (SPWM).

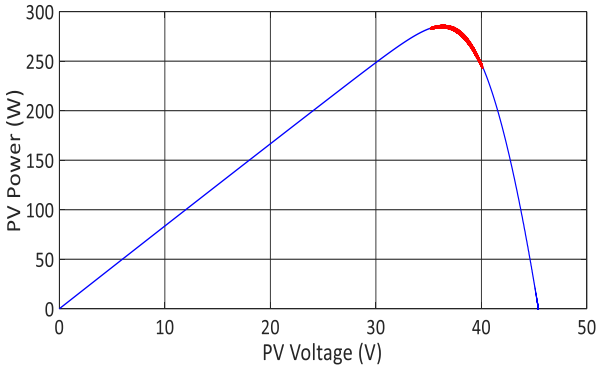

FIGURE 6.19: P-V curve showing the maximum power point operation of all the PV panels highlighted in red, operating under uniform irradiation of 1000W/m^2-operating scenario 3, with Maximum Power Point Tracking (MPPT) algorithm implemented for Sorted Pulse Width Modulation (SPWM).

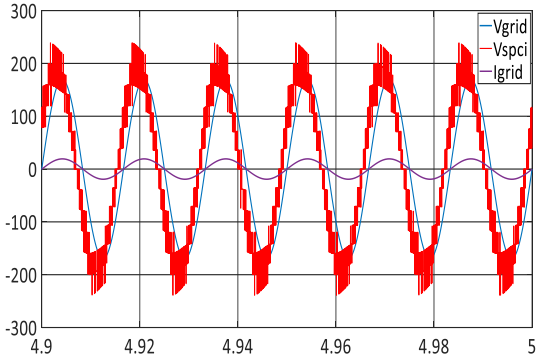

FIGURE 6.20: Simulation waveforms when the inverters are operating under uniform irradiation of 1000W/m^2-operating scenario 3, with Maximum Power Point Tracking (MPPT) algorithm implemented for Sorted Pulse Width Modulation (SPWM).

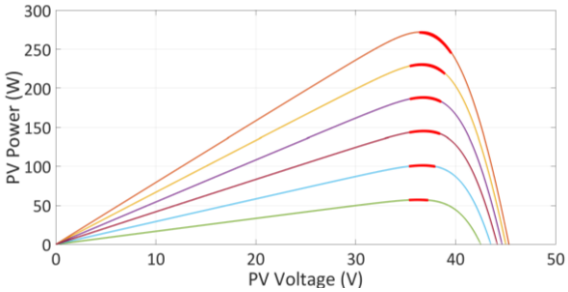

FIGURE 6.21: P-V curves showing the maximum power point operation of all the PV panels highlighted in red, operating under non - uniform irradiation. (950W/m^2, 800W/m^2, 650W/m^2, 500W/m^2, 350W/m^2, 200W/m^2-operating scenario 4.), with Maximum Power Point Tracking (MPPT) algorithm implemented for Sorted Pulse Width Modulation (SPWM).

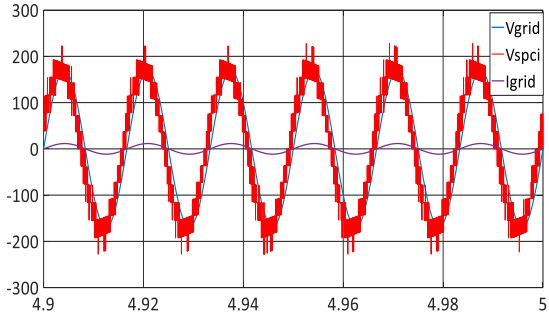

FIGURE 6.22: Simulation waveforms when the inverters are operating under non - uniform irradiation. (950W/m^2, 800W/m^2, 650W/m^2, 500W/m^2, 350W/m^2, 200W/m^2-operating scenario 4.), with Maximum Power Point Tracking (MPPT) algorithm implemented for Sorted Pulse Width Modulation (SPWM).

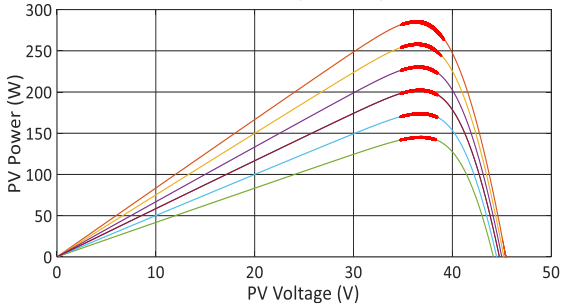

FIGURE 6.23: P-V curves showing the maximum power point operation of all the PV panels highlighted in red, operating under non - uniform irradiation. (1000W/m^2, 900W/m^2, 800W/m^2, 700W/m^2, 600W/m^2, 500W/m^2-operating scenario 5.), with Maximum Power Point Tracking (MPPT) algorithm implemented for Sorted Pulse Width Modulation (SPWM).

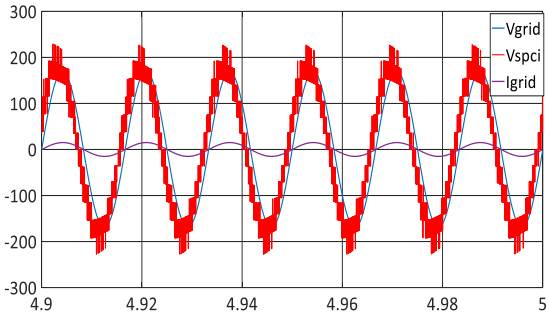

FIGURE 6.24: Simulation waveforms when the inverters are operating under non - uniform irradiation. (1000W/m^2, 900W/m^2, 800W/m^2, 700W/m^2, 600W/m^2, 500W/m^2-operating scenario 5.), with Maximum Power Point Tracking (MPPT) algorithm implemented for Sorted Pulse Width Modulation (SPWM).

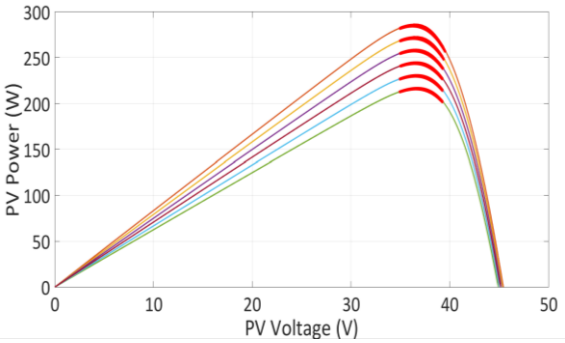

FIGURE 6.25: P-V curves showing the maximum power point operation of all the PV panels highlighted in red, operating under non - uniform irradiation. (1000W/m^2, 950W/m^2, 900W/m^2, 850W/m^2, 800W/m^2, 750W/m^2-operating scenario 6.), with Maximum Power Point Tracking (MPPT) algorithm implemented for Sorted Pulse Width Modulation (SPWM).

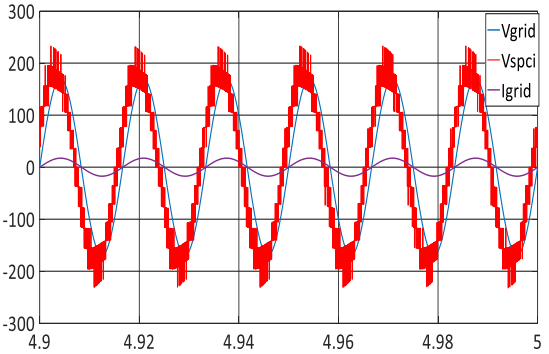

FIGURE 6.26: Simulation waveforms when the inverters are operating under non - uniform irradiation. (1000W/m^2, 950W/m^2, 900W/m^2, 850W/m^2, 800W/m^2, 750W/m^2-operating scenario 6.), with Maximum Power Point Tracking (MPPT) algorithm implemented for Sorted Pulse Width Modulation (SPWM).

CHAPTER 7 : ACTIVE AND REACTIVE POWER CONTROL

7.1. Introduction

Chapter 6 demonstrated the maximum power extraction of Solar Panel Companion Inverters (SPCIs) at panel level. However, the power injection into the grid was performed only at unity power factor, irrespective of the sunlight available on the solar panels. Power injection at unity power factor represents a conventional case of power transfer scenario. The SPCI is expected to perform reactive power support by fully utilizing the power rating of the power electronic devices. This chapter is adapted from [63] and starts by presenting a conventional case of real power transfer into the grid, along with a discussion on generalized power transfer scenarios in sections 7.2, and 7.3. Simulation results corresponding to real and reactive power flow scenarios for the grid connected SPCIs by implementing sort and stack algorithm together with closed loop MPPT algorithm proposed for SPCI are demonstrated in Section 7.4. This chapter concludes with a summary presented in Section 7.5.

7.2. Conventional Case of Real Power Transfer

Let P_{max} be the maximum power extractable from the Solar Panel Companion Inverter (SPCI) system, for a given ambient temperature and insolation conditions. Assuming no losses in the inverter, we can write the power transferred to the grid as:

$$P_{max}=V_{grid}*I_{grid}*\cos\theta \tag{7.1}$$

where θ is the angle between V_{grid} and I_{grid}.

A commonly followed practice is to transfer this power to the grid at unity power factor. This is done to accomplish power transfer with minimum current stress on the power devices in the inverter. The phasor representation for unity power factor operation on the grid is presented in Figure 7.1. It may be seen that the voltage required to be synthesized by the inverter V_{inv} is a vector sum of the grid voltage V_{grid} and the voltage drop V_x across the interfacing reactance. Mathematically, this can be written as:

$$\overline{V_{inv}} = \overline{V_{grid}} + \overline{V_x} \tag{7.2}$$

Although the methodology shown in Figure 7.1 and expressed by equation (2) conforms to the lowest current stress scheme, this presents only one of the cases in the generalized power transfer space for the candidate grid connected PV inverter. This aspect is discussed in detail in the next section.

7.3. Generalized Power Transfer Scenarios

A generalized equation for power transfer between the inverter and grid is given by:

$$P = \frac{|V_{inv}| * |V_{grid}| * \sin\delta}{X} \tag{7.3}$$

where ‘δ’ is the angle between V_{inv} and V_{grid}.

This power transfer is bound on the upper side by the amount of power available in the system for the given ambient temperature and insolation conditions. Thus, it becomes evident that for a given grid voltage V_{grid}, if the component of grid current I_{grid} in phase with grid voltage V_{grid} is constant, then one can be assured of delivering all the available power from the PV module to the grid. In other words, if $I_{grid} * \cos\theta$ is constant, then within the constraints of device current and voltage ratings in the inverter, one can source any current Igrid in a family of grid currents by synthesizing the corresponding V_{inv} from the

family of inverter voltages and keep $P = P_{max} = V_{grid}*I_{grid}*\cos\theta$. This is shown in Figure 7.2. It may be observed from Figure 7.2 that, in accordance with equation (3), the real power transfer P from the PV system to the grid is kept invariant (P_{max}) by compensating the variations in the magnitude of V_{inv} by changing angle δ. One may also note that once the constraint that I_{grid} and V_{grid} should be in phase is relinquished, while real power P is transferred from PV module to the grid, there is finite non-zero amount of reactive power Q that is transferred from the grid to the inverter. This is given by:

$$Q=V_{grid}*I_{grid}*\sin\theta \tag{7.4}$$

As may be seen from Figure 7.3, because the grid current and grid voltage are no longer in phase, while the real power transfer is still the same as earlier ($V_{grid}\ I_{grid}\ \cos\theta$), there is also non-zero reactive power ($V_{grid}\ I_{grid}\ \sin\theta$) transferred from the grid to the PV inverter system. Now, this principle can be further extended to source (instead of sink) finite non-zero reactive power from PV inverter into the grid. This scenario is shown in Figure 7.4. As may be seen from Figure 7.4, while real power transfer is identical to that in Figure 7.3, reactive power has changed direction because $I_{grid}\ \sin\theta$ is reversed. Finally, family of grid currents and corresponding inverter voltages in such scenarios where reactive power is sourced is presented in Figure 7.5.

7.4. Simulation Results

The simulation results representing conventional case of real power transfer as described in Section 7.2 is presented in Figures 7.6 through 7.11. The irradiation on all the panels is set to 1000 W/m^2. This is representative of a scenario where maximum power is available in the system. Sorted Stair Case Modulation (SSCM) scheme is implemented to inject active power into the grid. Figure 7.6 shows the waveforms of grid voltage, V_{grid},

output voltage, V_{spci}, grid current, I_{grid}, for six cycles when operating under uniform irradiation with SSCM scheme. The portion highlighted in red of the P-V curves in Figure 7.7 shows the steady state operating points of all the solar panels, upon reaching the maximum power point with SSCM scheme. Figure 7.8 shows active power is injected into the grid and there is no reactive power injection. This represents the unity power factor operation of the grid connected SPCI.

Sorted Pulse Width Modulation (SPWM) scheme has been implemented to inject active power into the grid. Figure 7.9 shows the waveforms of grid voltage, V_{grid}, output voltage, V_{spci}, grid current, I_{grid}, for six cycles when operating under uniform irradiation with SPWM scheme. The portion highlighted in red of the P-V curves in Figure 7.10 shows the steady state operating points of all the solar panels, upon reaching the maximum power point with SPWM scheme. Figure 7.11 shows active power is injected into the grid and there is no reactive power injection.

Simulations representing scenarios corresponding to low available power in the PV system have been performed. These simulations have been performed to demonstrate generalized power transfer scenarios as described in Section 7.3, and reactive power is injected into the grid from SPCI. A scenario for non-uniform irradiation is considered where in solar panel irradiations are set to 1000W/m^2, 950W/m^2, 900W/m^2, 850W/m^2, 800W/m^2, and, 750W/m^2. Figures 7.12 through 7.14 show the corresponding waveforms when operating in non-uniform irradiation, with Sorted Stair Case Modulation (SSCM) strategy. Figure 7.12 shows the waveforms of grid voltage, V_{grid}, output voltage, V_{spci}, grid current, I_{grid}, for six cycles when operating under non-uniform irradiation, with SSCM scheme. The portion highlighted in red of the P-V curves in Figure 7.13 shows the steady

state operating points of all the solar panels, upon reaching the maximum power point, with SSCM. Figure 7.14 shows active and reactive power injected into the grid, with SSCM scheme. The total generation capacity of the system is 1.7kW. Out of this, 1.461kW is the injected active power into the grid, and a reactive power of 897 Var is injected into the grid (1700 ≈ sqrt ((1461^2) + (897^2))).

Figures 7.15 through 7.17 show the waveforms when operating in non-uniform irradiation, with Sorted Pulse Width Modulation (SPWM) strategy. Figure 7.15 shows the waveforms of grid voltage, V_{grid}, output voltage, V_{spci}, grid current, I_{grid}, for six cycles when operating under non-uniform irradiation, with SPWM scheme. The portion highlighted in red of the P-V curves in Figure 7.16 shows the steady state operating points of all the solar panels, upon reaching the maximum power point, with SPWM scheme. Figure 7.17 shows active and reactive power injected into the grid, with SPWM. The total generation capacity of the system is 1.7kW. Out of this, 1.48 kW is the injected active power into the grid, and a reactive power of 811 Var is injected into the grid (1700 ≈ sqrt ((1480^2) + (811^2))).

A scenario for uniform irradiation is considered where in solar panel irradiations are set to 600W/m2. This scenario is also created to demonstrate generalized power transfer scenarios described in section 7.3, but reactive power is drawn from the grid into SPCI. Figures 7.18 through 7.20 show the corresponding waveforms when operating in uniform irradiation, with Sorted Stair Case Modulation (SSCM) strategy. Figure 7.18 shows the waveforms of grid voltage, Vgrid, output voltage, Vspci, grid current, Igrid, for six cycles when operating under uniform irradiation, with SSCM scheme. The portion highlighted in red of the P-V curves in Figure 7.19 shows the steady state operating points of all the solar panels, upon reaching the maximum power point, with SSCM scheme. Figure 7.20 shows

active and reactive power injected into the grid. The total generation capacity of the system is 1.7kW. Out of this, 0.744kW is the injected active power into the grid, and reactive power of 1374 Var is drawn from the grid (1700 ≈ sqrt ((744^2) + (1374^2))).

Figures 7.21 through 7.23 show the waveforms when operating in uniform irradiation, with Sorted Pulse Width Modulation (SPWM) strategy. Figure 7.21 shows the waveforms of grid voltage, V_{grid}, output voltage, V_{spci}, grid current, I_{grid}, for six cycles when operating under uniform irradiation, with SPWM scheme. The portion highlighted in red of the P-V curves in Figure 7.22 shows the steady state operating points of all the solar panels, upon reaching the maximum power point, with SPWM scheme. Figure 7.23 shows active and reactive power injected into the grid, with SPWM scheme. The total generation capacity of the system is 1.7kW. Out of this, 0.975kW is the injected active power into the grid, and a reactive power of 1366 Var is drawn from the grid (1700 ≈ sqrt ((975^2) + (1366^2))).

7.5. Summary

This chapter started with the conventional case of power transfer for grid tied Solar Panel Companion Inverters (SPCI), where the power was injected to the grid only at unity power factor. Also, a discussion on generalized power transfer scenarios has been presented, wherein the SPCIs should be able to participate in reactive power exchange with the AC grid, especially when the available power is less (either the sunlight is less, or there is a non-uniformity distribution of sunlight over the solar panels). Simulations have been performed to demonstrate the generalized case of power transfer of SPCI, along with the case where SPCI is able to participate in reactive power exchange with the grid, when available power is less. This functionality has also been demonstrated experimentally, in Chapter 9.

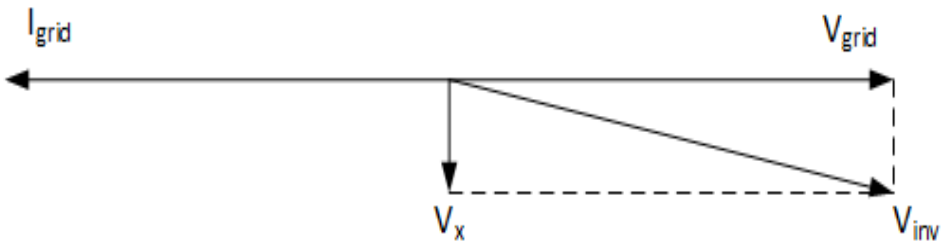

FIGURE 7.1: Maximum real power transfer from PV inverter to the grid in the candidate system under unity power factor operation on the grid side.

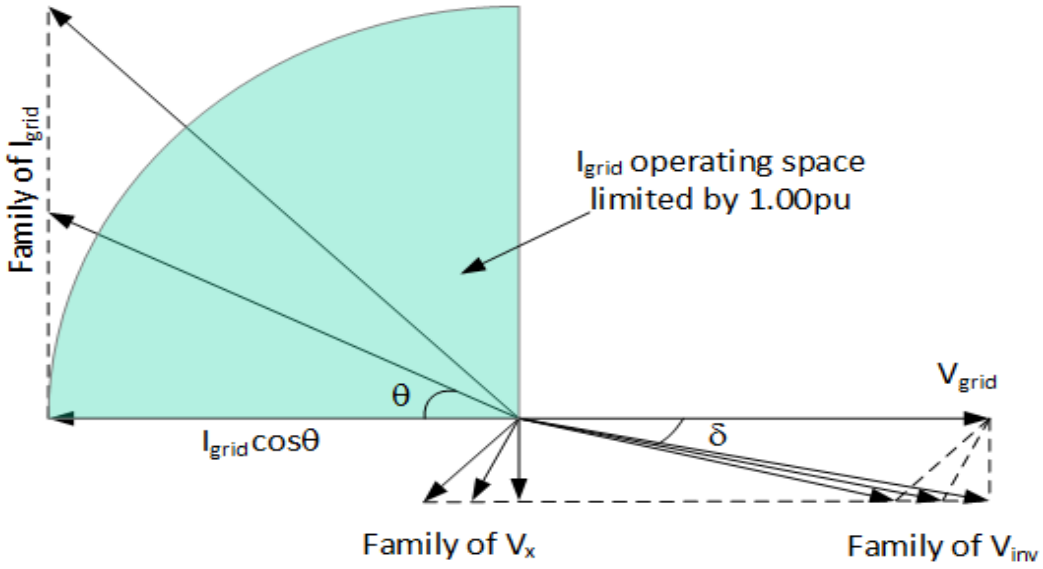

FIGURE 7.2: Various power transfer scenarios under which the real power transferred from PV module to the grid is same and reactive power flows from the grid to the inverter.

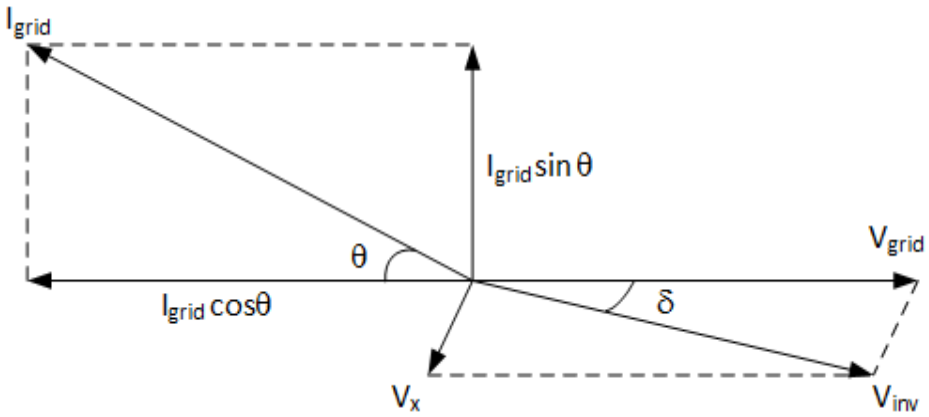

FIGURE 7.3: Real power transfer from PV module to the grid in the candidate system under lagging power factor operation on the grid side.

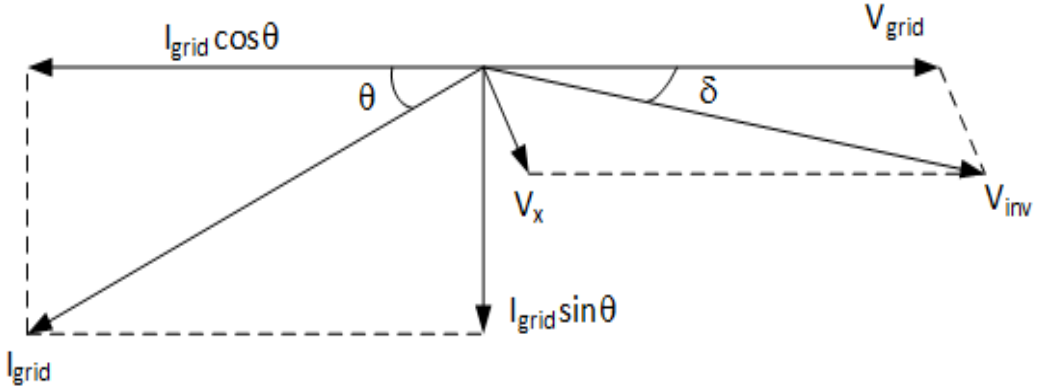

FIGURE 7.4: Real power transfer from PV module to the grid in the candidate system under leading power factor operation on the grid side.

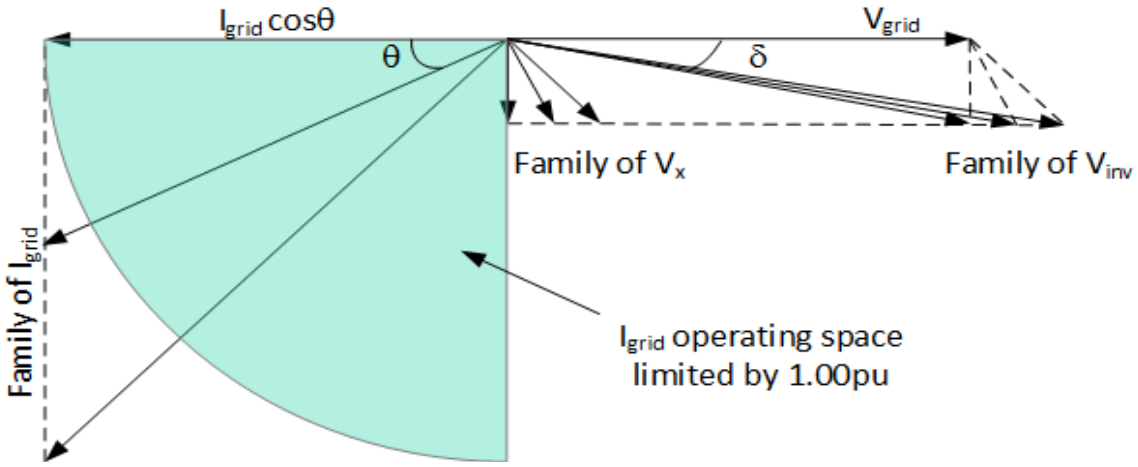

FIGURE 7.5: Various power transfer scenarios under which the real power transferred from PV module to the grid is same and reactive power flows from the inverter to the grid.

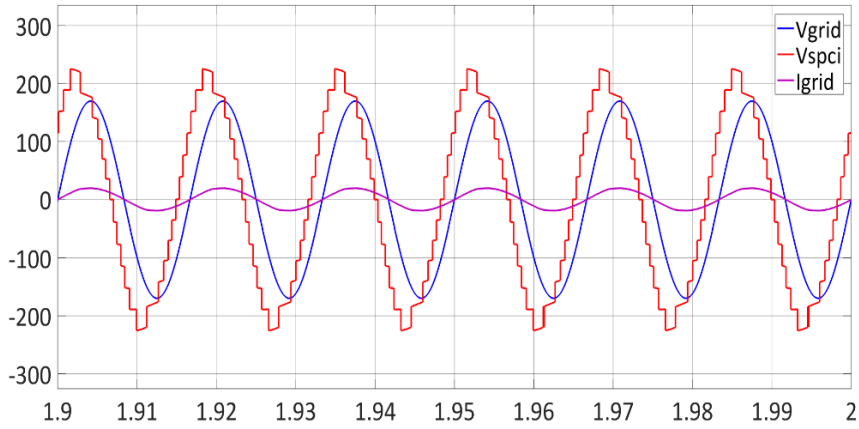

FIGURE 7.6: Waveforms of grid voltage, Vgrid, inverter output voltage, Vspci, and, grid current, Igrid when the inverters are operating under uniform irradiation of 1000W/m^2, for Sorted Stair Case Modulation (SSCM). This represents conventional case of real power transfer.

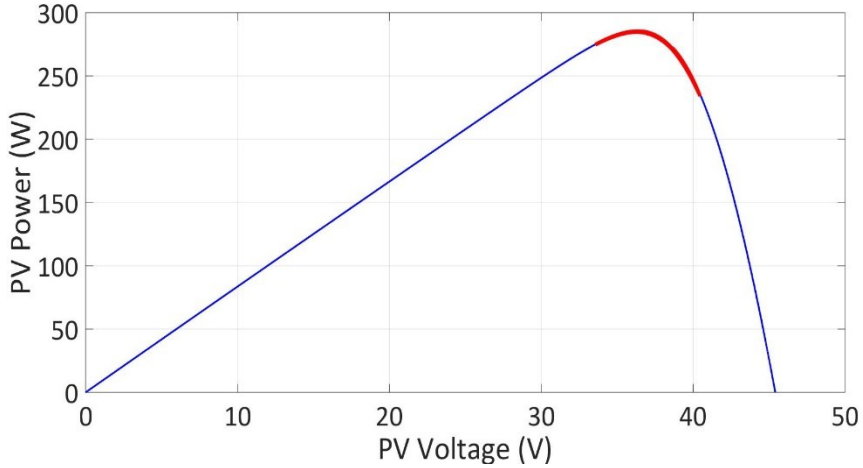

FIGURE 7.7: P-V curve showing the maximum power point operation of all the PV panels highlighted in red, operating under uniform irradiation of 1000W/m^2, for Sorted Stair Case Modulation (SSCM). This represents conventional case of real power transfer.

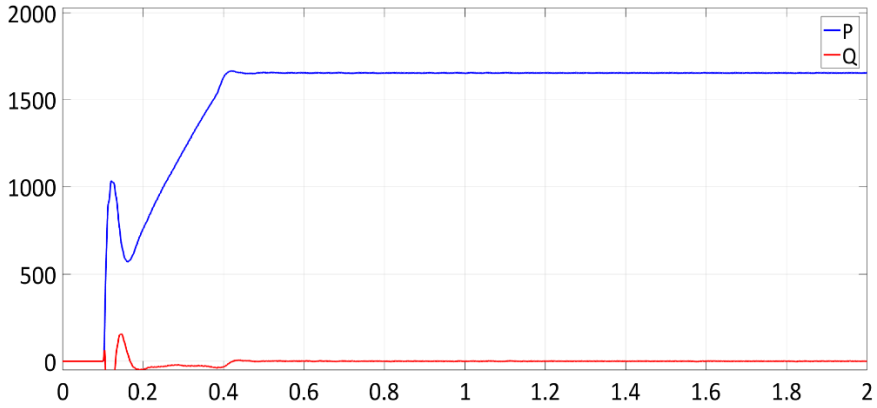

FIGURE 7.8: Waveforms of active power P (1606 W), and reactive power Q (≈ 0 Var) injected into the grid when the inverters are operating under uniform irradiation of 1000W/m^2, for Sorted Sorted Stair Case Modulation (SSCM). This represents conventional case of real power transfer.

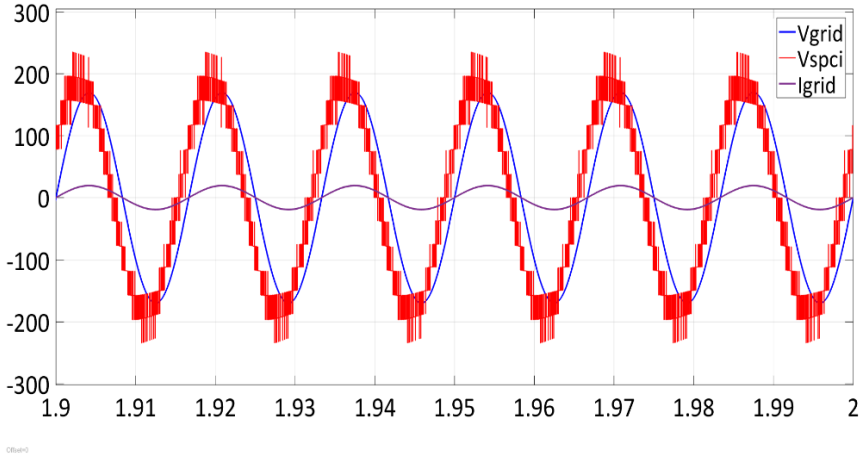

FIGURE 7.9: Waveforms of grid voltage, Vgrid, inverter output voltage, Vspci, and, grid current, Igrid when the inverters are operating under uniform irradiation of 1000W/m^2, for Sorted Pulse Width Modulation (SPWM). This represents conventional case of real power transfer.

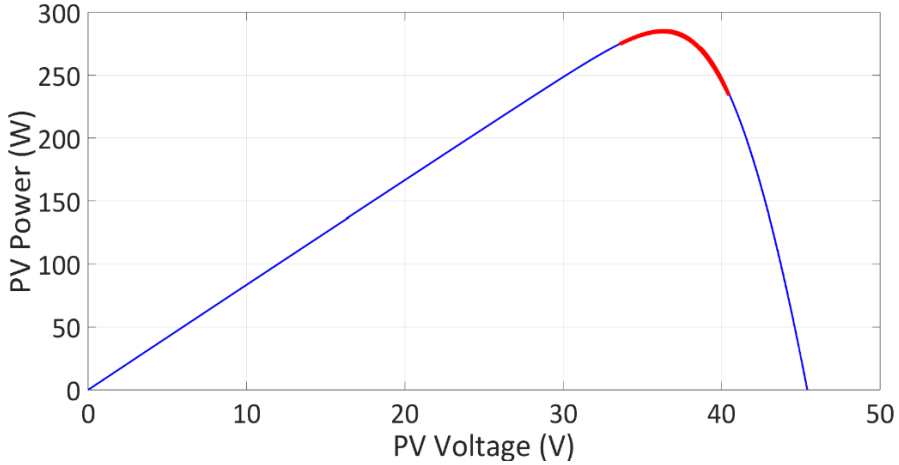

FIGURE 7.10: P-V curve showing the maximum power point operation of all the PV panels highlighted in red, operating under uniform irradiation of 1000W/m^2, for Sorted Pulse Width Modulation (SPWM). This represents conventional case of real power transfer.

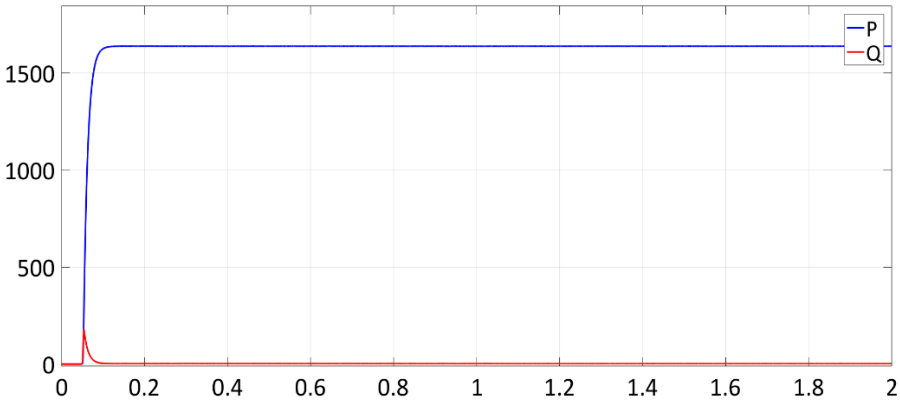

FIGURE 7.11: Waveforms of active power P (1676W), and reactive power Q (≈ 0 Var) injected into the grid when the inverters are operating under uniform irradiation of 1000W/m^2, for Sorted Pulse Width Modulation (SPWM). This represents conventional case of real power transfer.

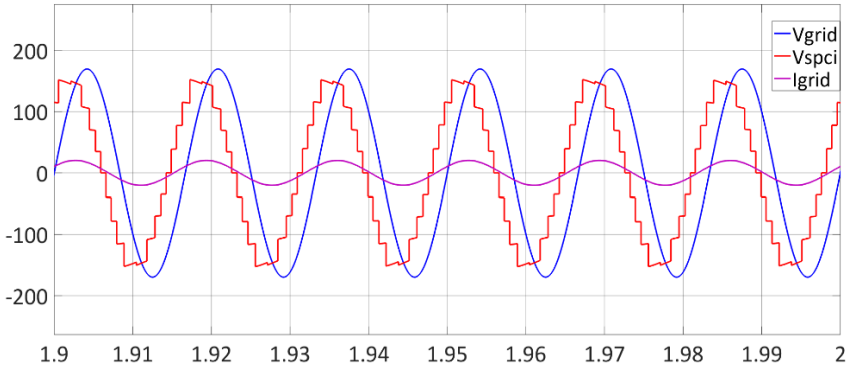

FIGURE 7.12: Waveforms of grid voltage, Vgrid, inverter output voltage, Vspci, and, grid current, Igrid when the inverters are operating under non-uniform irradiation of 1000W/m^2, 950W/m^2, 900W/m^2, 850W/m^2, 800W/m^2, 750W/m^2 for Sorted Stair Case Modulation (SSCM).

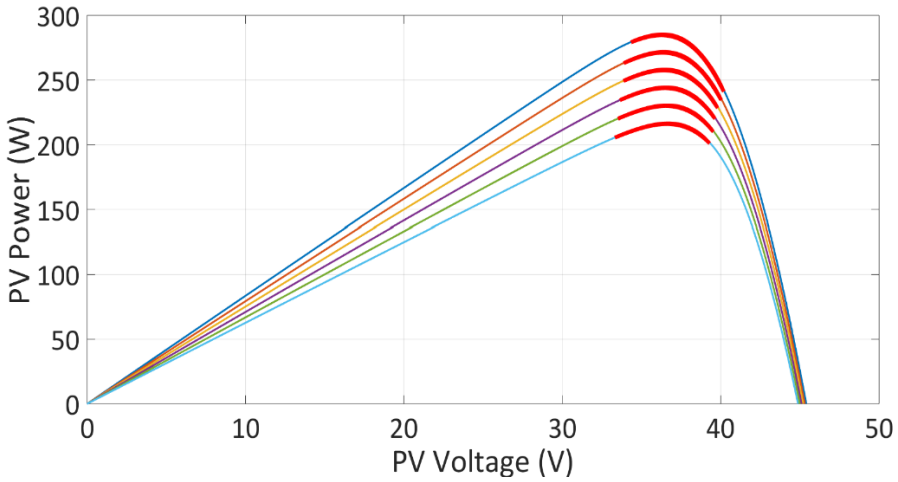

FIGURE 7.13: P-V curves showing the maximum power point operation of all the PV panels highlighted in red, operating under non-uniform irradiation of 1000W/m^2, 950W/m^2, 900W/m^2, 850W/m^2, 800W/m^2, 750W/m^2 for Sorted Stair Case Modulation (SSCM).

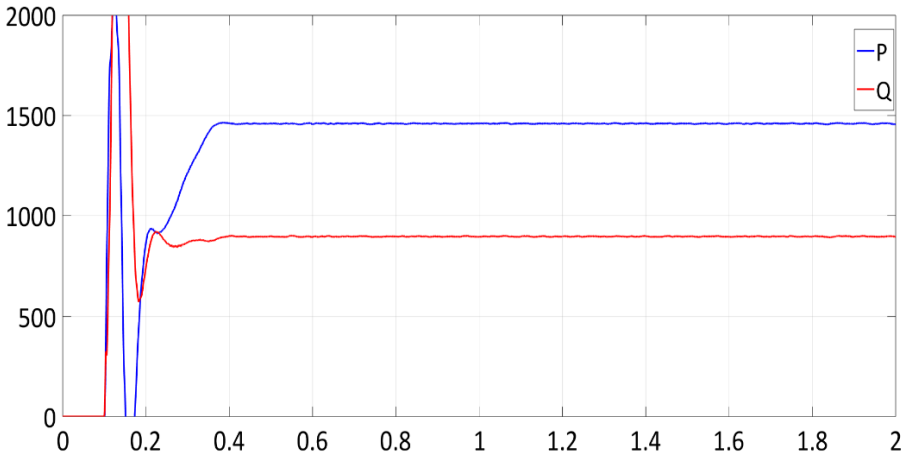

FIGURE 7.14: Waveforms of active power P (1461W), and reactive power Q (897Var) injected into the grid when the inverters are operating under non-uniform irradiation of 1000W/m^2, 950W/m^2, 900W/m^2, 850W/m^2, 800W/m^2, 750W/m^2 for Sorted Stair Case Modulation (SSCM).

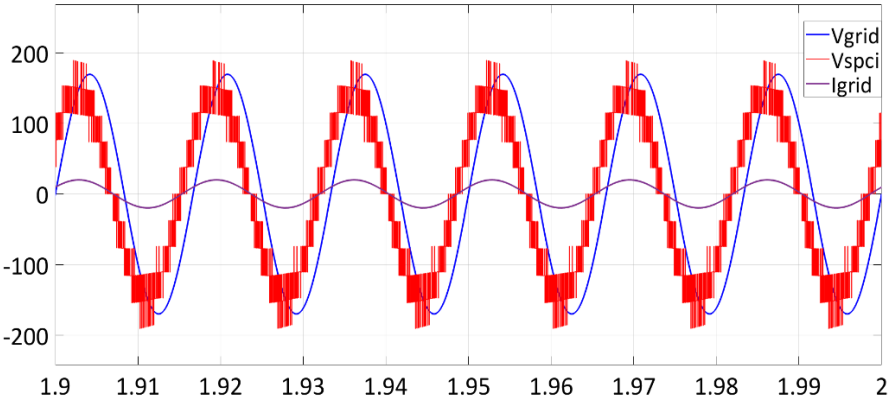

FIGURE 7.15: Waveforms of grid voltage, Vgrid, inverter output voltage, Vspci, and, grid current, Igrid when the inverters are operating under non-uniform irradiation of 1000W/m^2, 950W/m^2, 900W/m^2, 850W/m^2, 800W/m^2, 750W/m^2 for Sorted Pulse Width Modulation (SPWM).

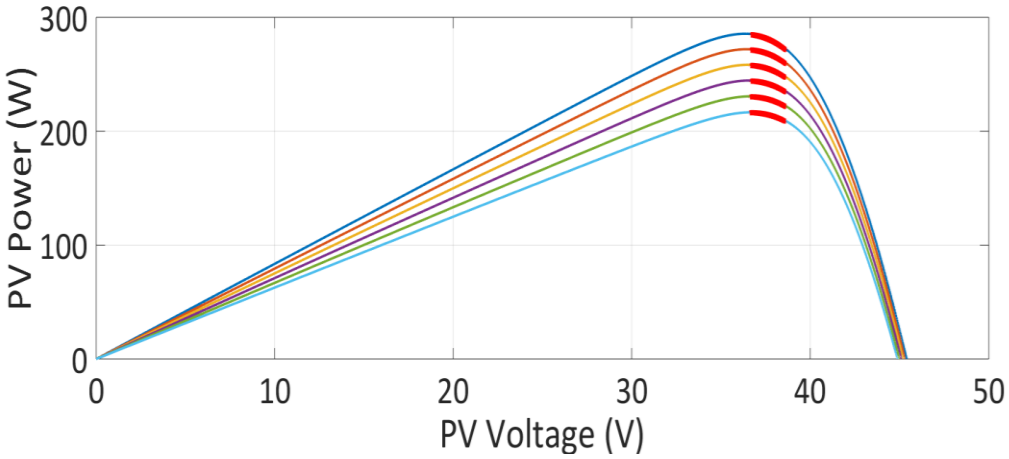

FIGURE 7.16: P-V curves showing the maximum power point operation of all the PV panels highlighted in red, operating under non-uniform irradiation of 1000W/m^2, 950W/m^2, 900W/m^2, 850W/m^2, 800W/m^2, 750W/m^2 for Sorted Pulse Width Modulation (SPWM).

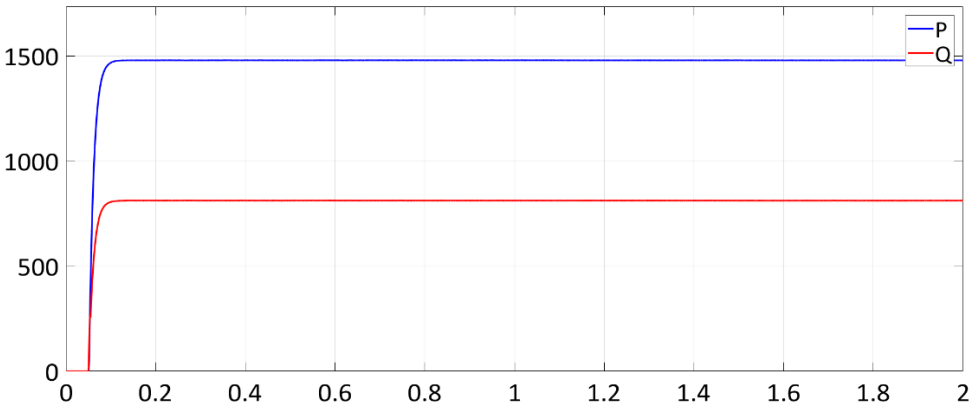

FIGURE 7.17: Waveforms of active power P (1480W), and reactive power Q (811Var) injected into the grid when the inverters are operating under non-uniform irradiation of 1000W/m^2, 950W/m^2, 900W/m^2, 850W/m^2, 800W/m^2, 750W/m^2 for Sorted Pulse Width Modulation (SPWM).

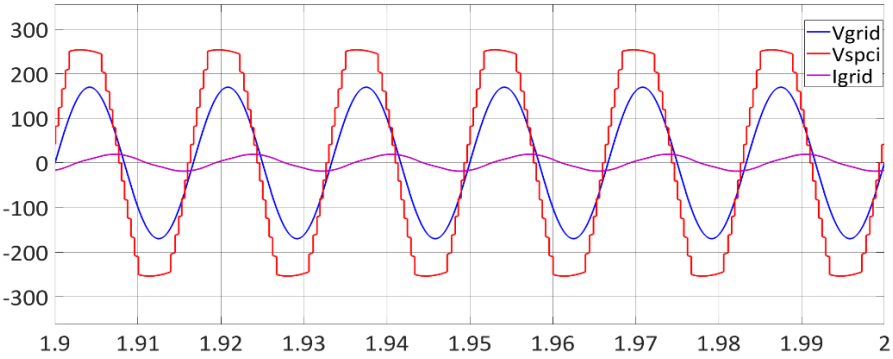

FIGURE 7.18: Waveforms of grid voltage, Vgrid, inverter output voltage, Vspci, and, grid current, Igrid when the inverters are operating under uniform irradiation of 600W/m^2 for Sorted Stair Case Modulation (SSCM).

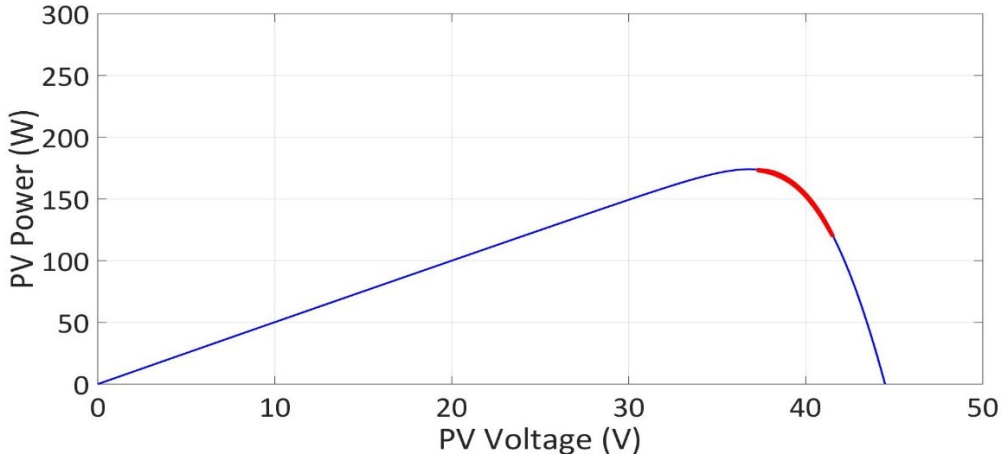

FIGURE 7.19: P-V curve showing the maximum power point operation of all the PV panels highlighted in red, operating under uniform irradiation of 600W/m^2 for Sorted Stair Case Modulation (SSCM).

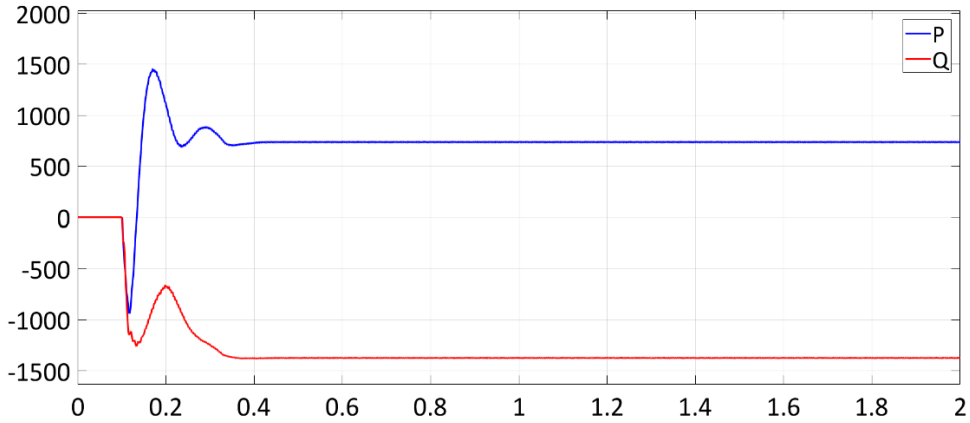

FIGURE 7.20: Waveforms of active power P (744W), and reactive power Q (-1374 Var) injected into the grid when the inverters are operating under uniform irradiation of 600W/m^2 for Sorted Stair Case Modulation (SSCM).

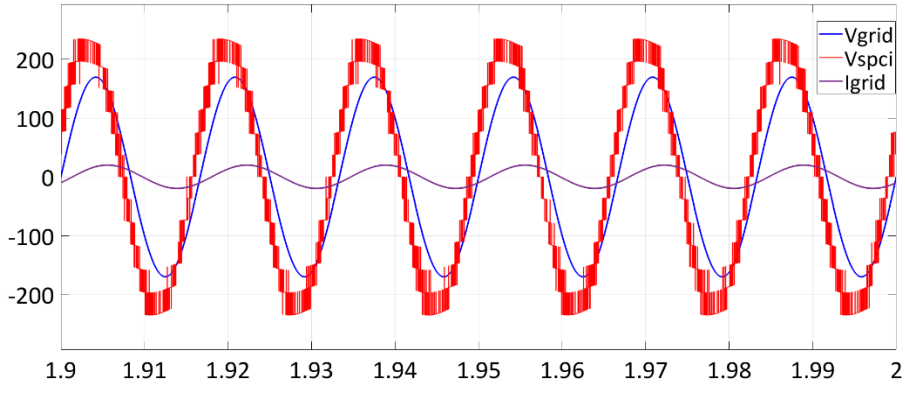

FIGURE 7.21: Waveforms of grid voltage, Vgrid, inverter output voltage, Vspci, and, grid current, Igrid when the inverters are operating under uniform irradiation of 600W/m^2 for Sorted Pulse Width Modulation (SPWM).

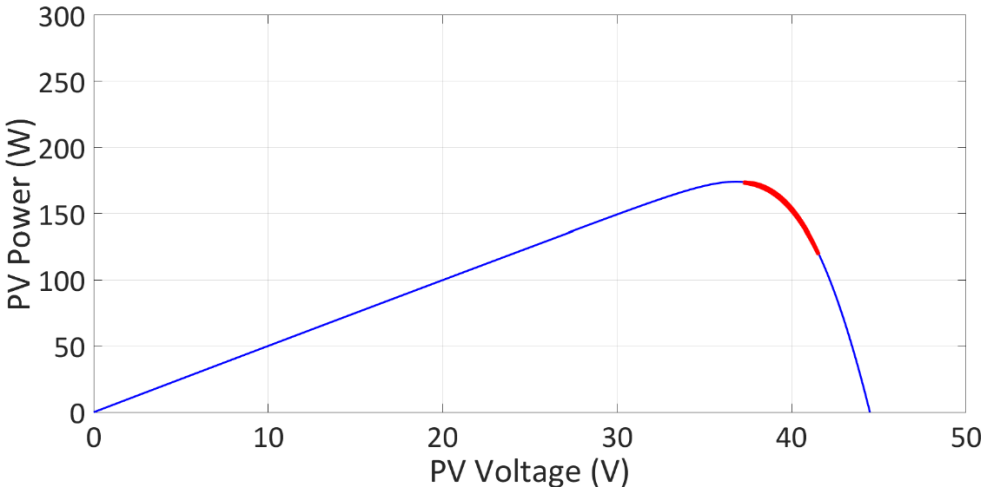

FIGURE 7.22: P-V curve showing the maximum power point operation of all the PV panels highlighted in red, operating under uniform irradiation of 600W/m^2 for Sorted Pulse Width Modulation (SPWM).

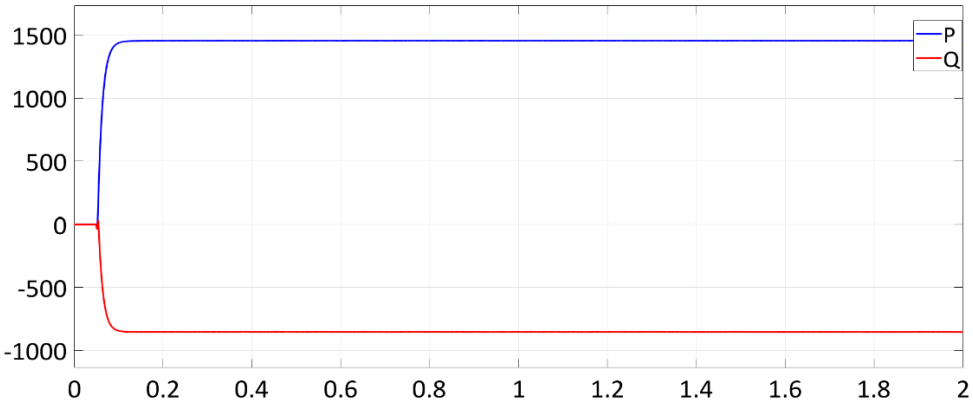

Figure 7.23: Waveforms of active power P (975W), and reactive power Q (-1363 Var) injected into the grid when the inverters are operating under uniform irradiation of 600W/m^2 for Sorted Pulse Width Modulation (SPWM).

CHAPTER 8 : PANEL LEVEL OPTIMIZATION

8.1. Introduction

In Chapter 5 and Chapter 7, Maximum Power Point Tracking (MPPT) for Solar Panel Companion Inverters (SPCI) has been performed at system level. This chapter is adapted from [64]. In this chapter, to ensure that each panel operates at maximum power, an analytical equation which defines the AC output voltage to be synthesized by each SPCI when operating at MPPT is derived in Section 8.2. Using the derived AC output equation, a control algorithm which ensures the maximum power extraction from SPCI, at panel level is presented in Section 8.3. Simulation results which demonstrate the efficacy of the proposed control scheme is demonstrated in Section 8.4. Section 8.5 ends this chapter with a brief summary.

8.2. Analysis

In this section, an analytical equation which describes the output voltage that should be synthesized by each inverter has been presented. Consider an ideal system with n number of Solar Panel Companion Inverters (SPCIs). Let V_{invi} be the rms AC output voltage across i^{th} inverter, I_{ac} be the rms AC output current of the inverter, V_{grid} be the rms AC voltage of the grid, V_{inv} be the rms AC output voltage of the inverter, ϕ be the phase of V_{inv} with respect to V_{grid}. In figure 8.1, a phasor diagram representing the voltage and current phasors when an output voltage V_{inv} is synthesized by SPCIs is shown. The active power flow into the AC grid can be written as:

$$P=V_{grid}.I_{ac} \tag{8.1}$$

Let V_{dci} be the dc bus voltage of i^{th} inverter, I_{dci} be the corresponding current at the dc bus. The active power flow contributed by each inverter can be written as:

$$P=V_{inv_i}.I_{ac}.\cos\phi = V_{dc_i}.I_{dc_i} \tag{8.2}$$

Considering the system to be lossless, from equations (8.1) and (8.2), the total average power balance equation can be written as:

$$P=\sum_{i=1}^{n} V_{inv_i}.I_{ac}.\cos\phi = \sum_{i=1}^{n} V_{dc_i}.I_{dc_i} = V_{grid}.I_{ac} \tag{8.3}$$

The equation for total AC output voltage, V_{inv} across the SPCIs can be written as sum of individual AC output voltages across each SPCI.

$$V_{inv} = \sum_{i=1}^{n} V_{inv_i} \tag{8.4}$$

From equations (8.2), (8.3), and (8.4), the equation for output voltage across each inverter can be written as:

$$V_{inv_i} = \frac{V_{dc_i}.I_{dc_i}}{\sum_{i=1}^{n} V_{dc_i}.I_{dc_i}}.V_{inv} \tag{8.5}$$

If K_i is the contribution factor of i^{th} inverter, equation (8.5) can be re-written as follows:

$$V_{inv_i}^{(pk)} = K_i.V_{inv}^{(pk)} \tag{8.6}$$

where

$$K_i = \frac{V_{dc_i}.I_{dc_i}}{\sum_{i=1}^{n} V_{dc_i}.I_{dc_i}} \tag{8.7}$$

Equations (8.5) and (8.6) show the output voltage to be synthesized across each inverter, for a given operating scenario. The total inverter output voltage, V_{inv}, that needs to be synthesized is obtained from the current control algorithm block which generates the reference voltage to be synthesized by the SPCIs. The implemented control scheme is presented in Section IV. When all the solar panels are operating at their corresponding maximum power point, $V_{dci}=V_{mppi}$, $I_{dci}=I_{mppi}$. Therefore, equations (8.5), (8.6), and (8.7) can be re-written as:

$$V_{inv_i} = \frac{V_{mppi}.I_{mppi}}{\sum_{i=1}^{n} V_{mppi}.I_{mppi}}.V_{inv} \tag{8.8}$$

$$V_{inv_i}^{(pk)} = K_i.V_{inv}^{(pk)} \tag{8.9}$$

where

$$K_i = \frac{V_{mppi}.I_{mppi}}{\sum_{i=1}^{n} V_{mppi}.I_{mppi}} \tag{8.10}$$

8.3. Control Scheme

Figure 8.2 shows the detailed block schematic of the control scheme employed for the grid connected Solar Panel Companion Inverter (SPCI) system. A Phase Locked Loop (PLL) is implemented to construct the image of grid voltage, and to obtain the phase information of the grid voltage. The Maximum Power Point Tracking (MPPT) algorithm block implements a system level MPPT [7]. This block generates reference currents I_d^*, and I_q^* which are fed as inputs to current control loop. The current control loop also takes in sensed grid current, and, output of the PLL block as inputs, and generates a reference voltage V_{ref}.

The block "Modified Sorted & Stack Algorithm, Pulse Width Modulation" shown in Figure 8.2 is used to generate gate pulses for the MOSFETs. Either Sorted Stair Case Modulation (SSCM) or Sorted Pulse Width Modulation (SPWM) technique is implemented to synthesize an AC output voltage waveform to inject power into the grid. The control scheme for power flow from Solar Panel Companion Inverter System (SPCI) into the grid is governed by the equations (8.11) and (8.12). These equations are based on direct and quadrature axis components in the rotating reference frame. If 'V_d' is the direct axis component, and 'V_q' is the quadrature axis component of the grid voltage, 'I_d' is the direct axis component, 'I_q' is the quadrature axis component of the grid current, the active power flow, 'P' into the grid in a single-phase system is given by equation (8.11).

$$P=0.5(V_d.I_d+V_q.I_q) \tag{8.11}$$

Similarly, the reactive power flow 'Q' into the grid is given by equation (8.12).

$$Q=0.5(V_q.I_d+V_d.I_q) \tag{8.12}$$

Figure 8.3 shows dq based control schematic implemented for power flow control of grid connected SPCI. Quadrature components of grid voltage and grid current are generated, and αβ-dq transformation is implemented to generate the corresponding direct axis components 'V_d', 'I_d', and the quadrature axis components 'V_q', 'I_q', in rotating reference frame. The MPPT algorithm generates a reference current along the direct axis 'I_d*', and a reference current along quadrature axis 'I_q*' [7]. The reference current 'I_d*' is compared with the actual current along the direct axis, 'I_d', and the output is fed into a PI controller. The output of the PI is fed as one of the inputs to the dq- αβ transformation block. The 'α' output of the transformation block generates a reference voltage 'V_α*'. The other input to the transformation block comes from the control loop corresponding to the quadrature axis

component of the grid current, 'I_q'. The reference current, 'I_q*' is set to zero, since the scope of this paper confines to power injection into the grid at unity power factor. The direct component of grid voltage 'V_d' is multiplied with 'V_α*', to generate the reference voltage 'V_{ref}'. This reference voltage is fed into the modified sort and stack algorithm, to generate the Pulse Width Modulation Signals to the SPCI. The reference voltage generated from this current control loop should correspond to maximum power point operation. Here, the Sort and Stack algorithm is modified as described in the next section, to maximize the power extraction from the SPCI at panel level.

8.4. Modified Sort and Stack Algorithm

For the Sort and Stack Algorithm implemented in [6], the firing angle to synthesize the quasi-square wave for inverter with highest DC bus voltage is the instance at which the reference voltage is greater than half of its DC bus voltage. The implementation of the algorithm in this paper utilizes equation (8.5) in synthesizing the quasi-square waves for all the inverters. Equation (8.5) also describes the AC output voltage to be synthesize by each inverter. This equation is used for implementing modified sort and stack algorithm, using Sorted Staircase Modulation (SSCM), and Sorted Pulse Width Modulation (SPWM).

8.4.1. Sorted Stair Case Modulation

As shown in figure 8.4, the firing angle to synthesize the AC quasi-square wave of inverter with the highest DC bus voltage is the instance at which the reference voltage of SPCI system, V_{ref}, is greater than half the reference voltage of the inverter that needs to synthesize the first quasi-sqaure wave, V_{inv1}. Similarly, the firing angle to synthesize the AC quasi-square wave of inverter with the second highest DC bus voltage is the instance at which the reference voltage of SPCI system, V_{ref}, is greater than the summation of the

reference voltage of the inverter that needs to synthesize the first quasi-square wave, V_{inv1}, and half the reference voltage of the inverter that needs to synthesize the second quasi-square wave, $V_{inv2}/2$. Simulations have been performed using modified sort and stack algorithm for SSCM strategy, and results have been demonstrated in section VI.

8.4.2. Sorted Pulse Width Modulation

As shown in figure 8.5, to synthesize the AC pulse with modulated quasi-square wave of inverter with the highest DC bus voltage, the high frequency pulse width modulation should operate at the instance at which the reference voltage of SPCI system, V_{ref}, is greater than zero. Similarly, AC pulse with modulated quasi-square wave of inverter with the second highest DC bus voltage, the high frequency pulse width modulation should operate at the instance at which the reference voltage of SPCI system, V_{ref}, is greater than the summation of the reference voltage of the inverter that needs to synthesize the first quasi-square wave, V_{inv1}. Simulations have been performed using modified sort and stack algorithm for SPWM strategy, and results have been demonstrated in section VI.

8.5. Simulation Results

The control scheme described in section 8.4 has been implemented, to ensure panel level maximum power extraction. Simulations are performed for various operating scenarios under uniform and non – uniform irradiation. Figures 8.6 through 8.11 are the simulation results performed using Sorted Stair Case Modulation strategy (SSCM). Figure 8.6 shows P-V characteristics of the solar panel model when operating at an irradiation of 1000 W/m^2 (operating scenario 1). This scenario corresponds to maximum available power, and can be considered as conditions during a bright daylight. Since all solar panels are operating under uniform irradiation, P-V characteristics of all the panels are

overlapped. The portion highlighted in red of the P-V curve in Figure 8.6 shows the steady state operating points of all the solar panels, upon reaching the maximum power point. Figure 8.9 shows the waveforms of grid voltage, V_{grid}, output voltage, V_{spci}, grid current, I_{grid}, for six cycles in when operating in scenario 1. Figure 8.7 shows the P-V characteristics of the solar panel model when operating at an irradiation of 600 W/m^2 (operating scenario 2). This scenario corresponds to moderately available power, where there is partial daylight. The portion highlighted in red of the P-V curve in Figure 8.7 shows the steady state operating points of all the solar panels, upon reaching the maximum power point. Figure 8.10 shows the waveforms of grid voltage, V_{grid}, output voltage, V_{spci}, grid current, I_{grid}, for six cycles in when operating in scenario 2. Figure 8.8 shows the P-V characteristics of the solar panels model when operating under non-uniform irradiation (operating scenario 3). The irradiation on the solar panels are set to 1000 W/m^2, 900 W/m^2, 800 W/m^2, 700 W/m^2, 600 W/m^2, and 500 W/m^2 respectively. The portion highlighted in red of the P-V curve in Figure 8.8 shows the steady state operating points of all the solar panels, upon reaching the maximum power point.

Figure 8.11 shows the waveforms of grid voltage, V_{grid}, output voltage, V_{spci}, grid current, I_{grid}, for six cycles in when operating in scenario 3. Figures 8.12 through 8.17 are the simulation results performed using Sorted Stair Case Modulation strategy (SSCM). Figure 8.13 shows P-V characteristics of all the solar panels in operating scenario 1. The portion highlighted in red of the P-V curves in Figure 8.12 shows the steady state operating points of all the solar panels, upon reaching the maximum power point. It may be seen that all the panels are operating at their corresponding maximum power points. Figure 8.15 shows the waveforms of grid voltage, V_{grid}, output voltage, V_{spci}, grid current, I_{grid}, for six

cycles when operating in scenario 1. Figure 8.13 shows P-V characteristics of all the solar panels in operating scenario 2. The portion highlighted in red of the P-V curves in Figure 8.13 shows the steady state operating points of all the solar panels, upon reaching the maximum power point. It may be seen that all the panels are operating at their corresponding maximum power points. Figure 8.16 shows the waveforms of grid voltage, V_{grid}, output voltage, V_{spci}, grid current, I_{grid}, for six cycles when operating in scenario 2. Figure 8.14 shows P-V characteristics of all the solar panels in operating scenario 3. The portion highlighted in red of the P-V curves in Figure 8.14 shows the steady state operating points of all the solar panels, upon reaching the maximum power point. It may be seen that all the panels are operating at their corresponding maximum power points. Figure 8.17 shows the waveforms of grid voltage, V_{grid}, output voltage, V_{spci}, grid current, I_{grid}, for six cycles in when operating in scenario 3.

8.6. Summary

In this chapter a scheme to ensure panel level maximum power extraction has been proposed. Analytical equation defining the output voltage to be synthesized to ensure panel level maximum power extraction has been presented. Modified sort and stack algorithm for both Sorted Stair Case Modulation (SSCM) and Sorted Pulse Width Modulation (SPWM) schemes has been proposed. Simulations demonstrating maximum power extraction at panel level have been demonstrated for both SSCM and SPWM, for both uniform and non-uniform irradiation.

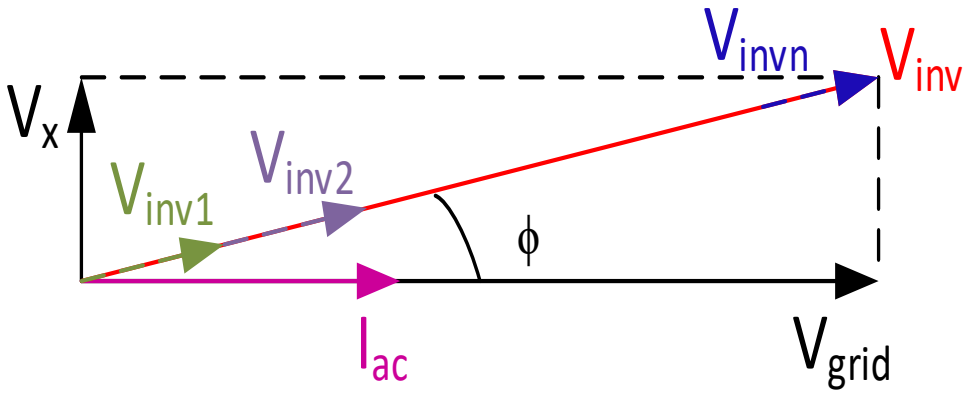

FIGURE 8.1: Schematic showing the phasor representation of voltage and current phasors of Solar Panel Companion Inverters (SPCIs).

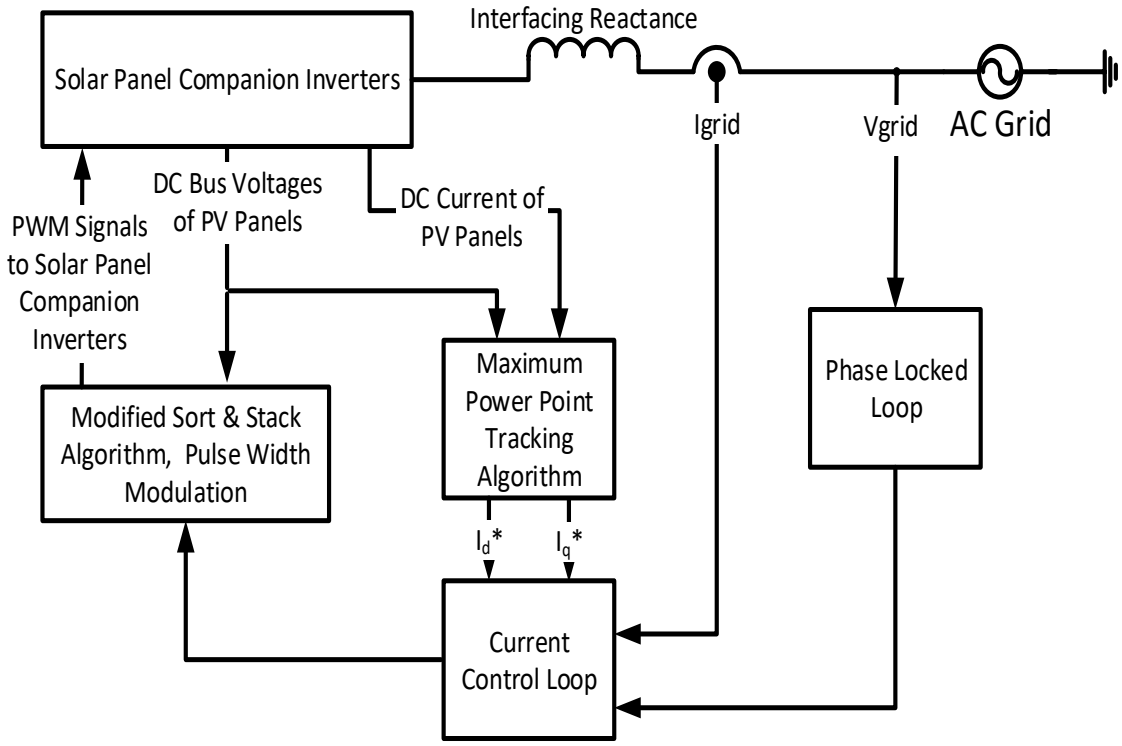

FIGURE 8.2: Detailed block schematic of the grid connected Solar Panel Companion Inverter (SPCI) system under consideration.

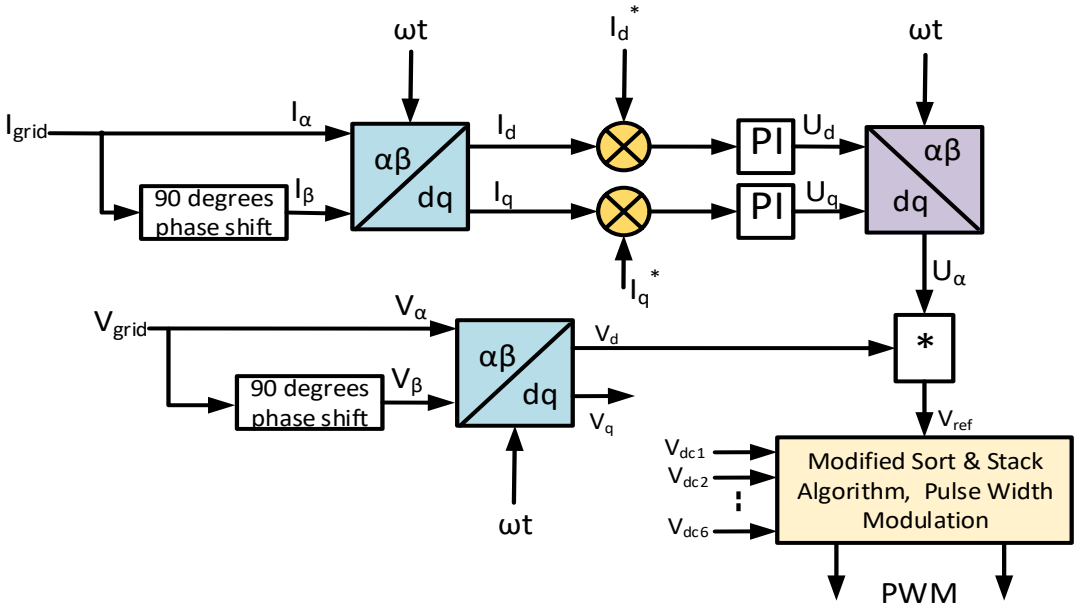

FIGURE 8.3: Block schematic of closed loop control implemented in synchronous rotating frame for the grid connected Solar Panel Companion Inverter (SPCI) system, with modified sort and stack algorithm incorporated.

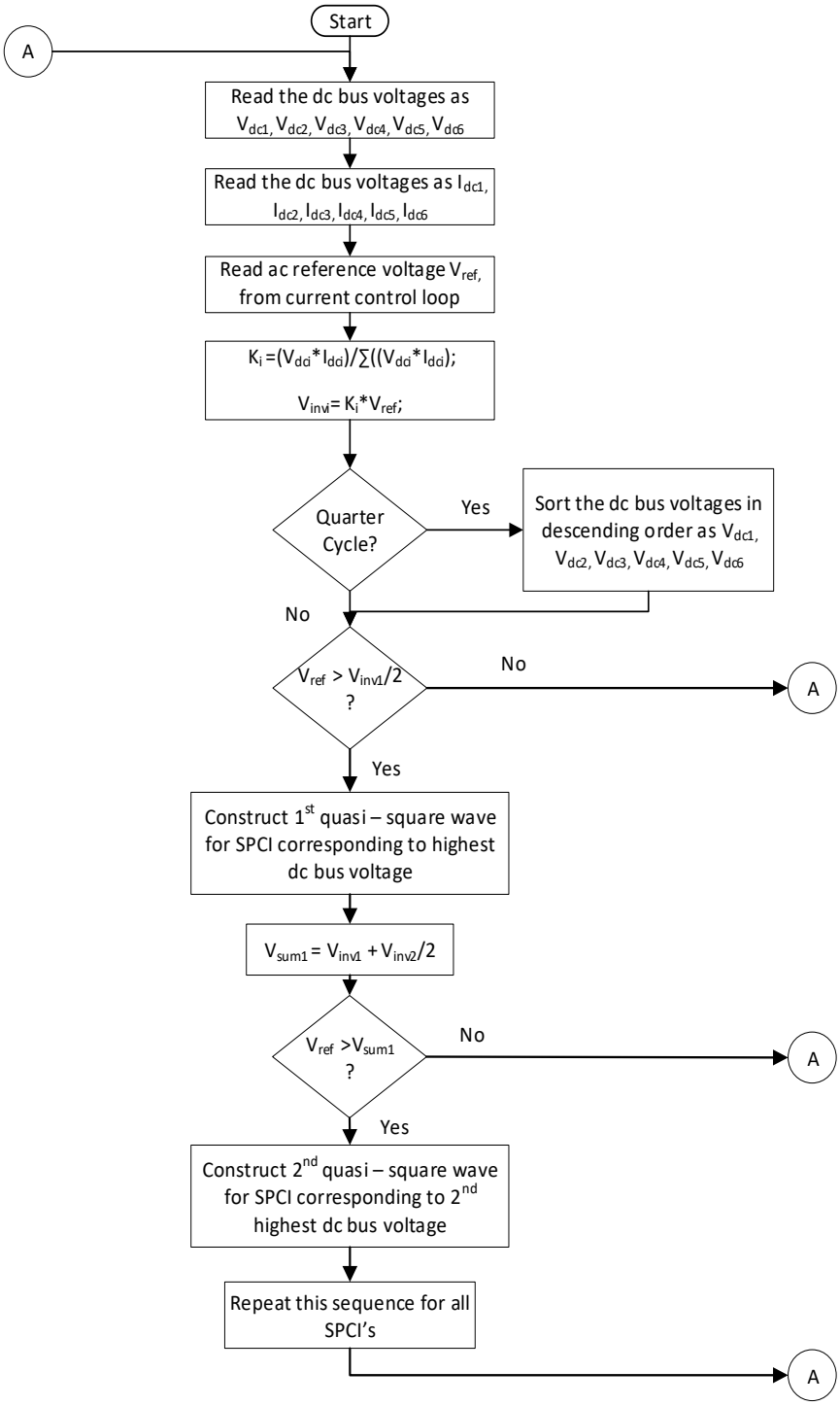

FIGURE 8.4: Simplified schematic showing the modified sort and stack algorithm for Sorted Stair Case Modulation (SSCM).

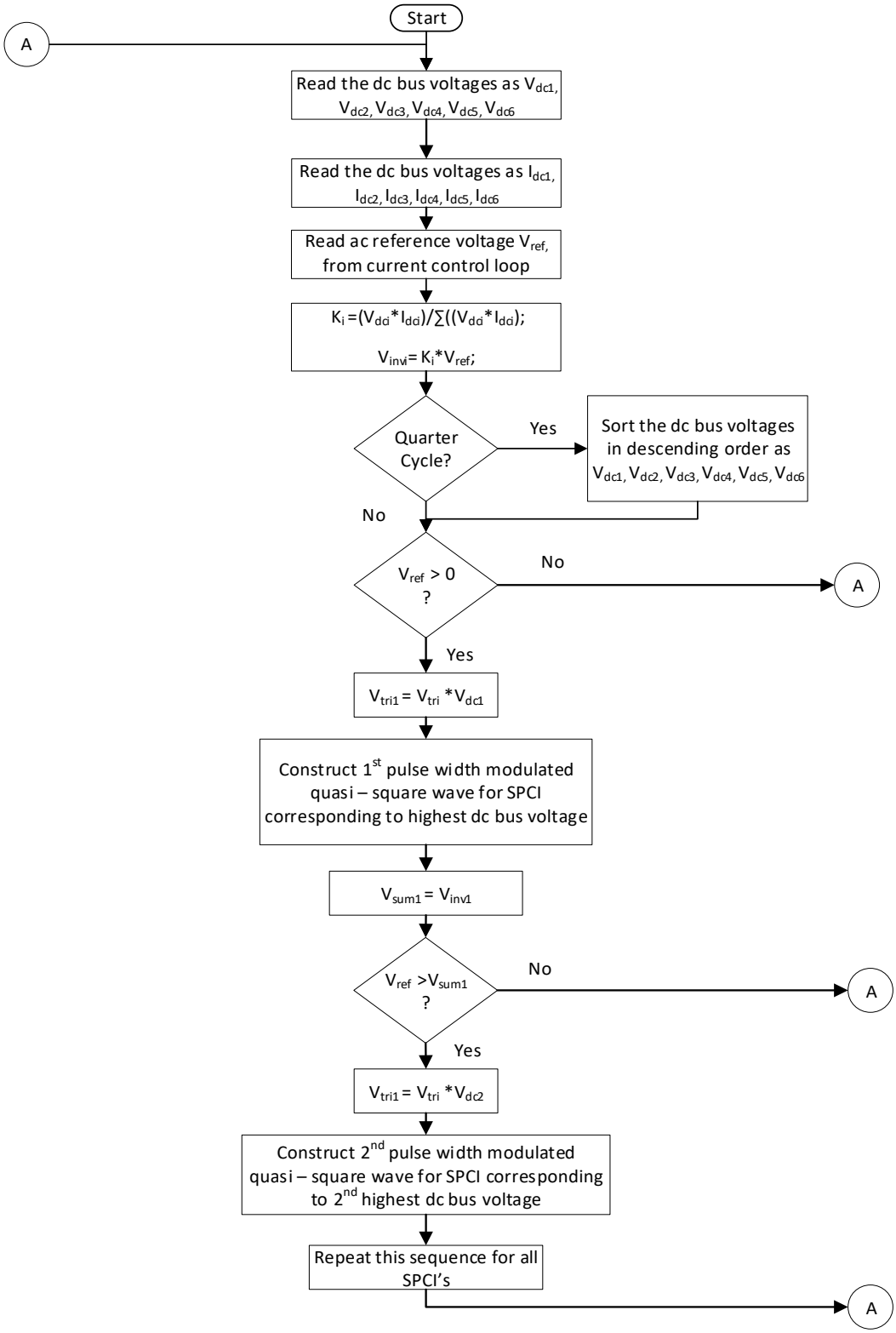

FIGURE 8.5: Simplified schematic showing the modified sort and stack algorithm for Sorted Pulse Width Modulation (SPWM).

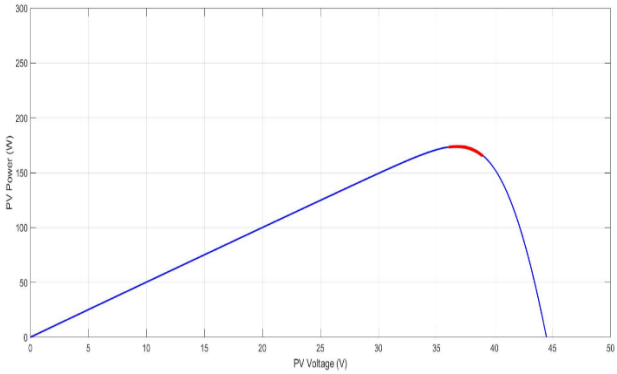

FIGURE 8.6: P-V curve showing the maximum power point operation of all the PV panels highlighted in red, operating under uniform irradiation of 600W/m^{2}with Maximum Power Point Tracking (MPPT) algorithm implemented for Sorted Staircase Modulation (SSCM).

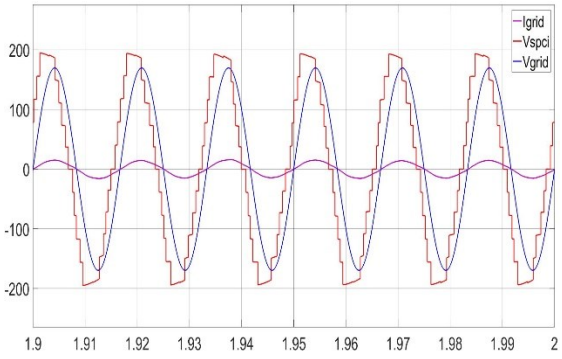

FIGURE 8.7: Simulation waveforms when the inverters are operating under uniform irradiation of 600W/m^2, with Maximum Power Point Tracking (MPPT) algorithm implemented for Sorted Staircase Modulation (SSCM).

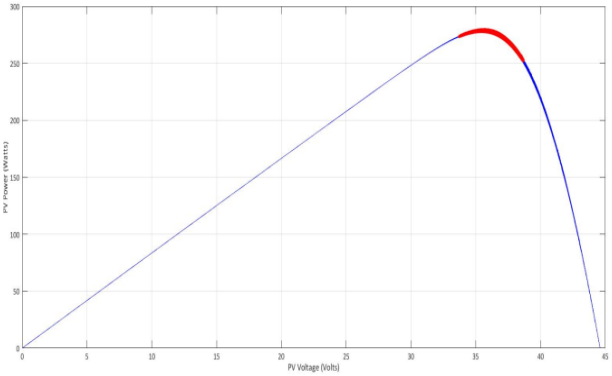

FIGURE 8.8: P-V curve showing the maximum power point operation of all the PV panels highlighted in red, operating under uniform irradiation of 1000W/m^2, with Maximum Power Point Tracking (MPPT) algorithm implemented for Sorted Staircase Modulation (SSCM).

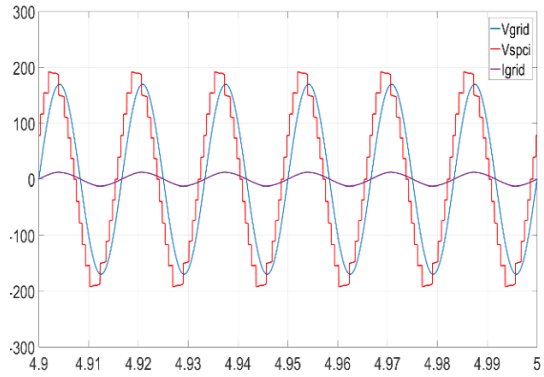

FIGURE 8.9: Simulation waveforms when the inverters are operating under uniform irradiation of 1000W/m^2, with Maximum Power Point Tracking (MPPT) algorithm implemented for Sorted Staircase Modulation (SSCM).

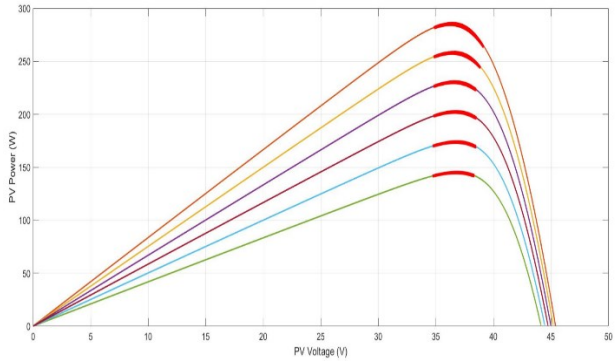

FIGURE 8.10: P-V curves showing the maximum power point operation of all the PV panels highlighted in red, operating under non - uniform irradiation. (1000W/m^2, 900W/m^2, 800W/m^2, 700W/m^2, 600W/m^2, 500W/m^2.), with Maximum Power Point Tracking (MPPT) algorithm implemented for Sorted Staircase Modulation (SSCM).

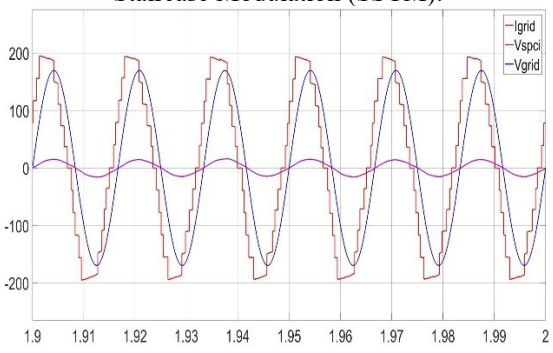

FIGURE 8.11: Simulation waveforms when the inverters are operating under non - uniform irradiation. (1000W/m^2, 900W/m^2, 800W/m^2, 700W/m^2, 600W/m^2, 500W/m^2.), with Maximum Power Point Tracking (MPPT) algorithm implemented for Sorted Staircase Modulation (SSCM).

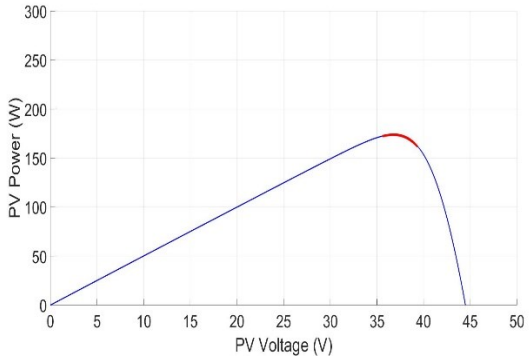

FIGURE 8.12: P-V curve showing the maximum power point operation of all the PV panels highlighted in red, operating under uniform irradiation of 600W/m^2, with Maximum Power Point Tracking (MPPT) algorithm implemented for Sorted Staircase Modulation (SPWM).

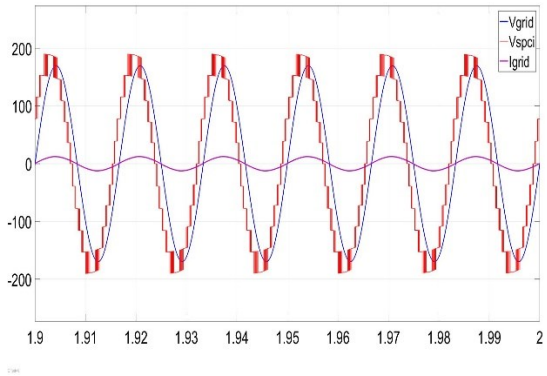

FIGURE 8.13: Simulation waveforms when the inverters are operating under uniform irradiation of 600W/m^2, with Maximum Power Point Tracking (MPPT) algorithm implemented for Sorted Staircase Modulation (SPWM).

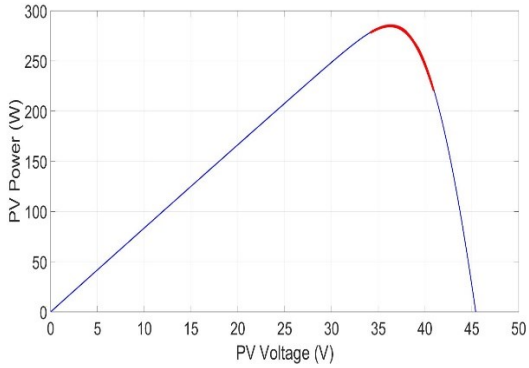

FIGURE 8.14: P-V curve showing the maximum power point operation of all the PV panels highlighted in red, operating under uniform irradiation of 1000W/m^2, with Maximum Power Point Tracking (MPPT) algorithm implemented for Sorted Staircase Modulation (SPWM).

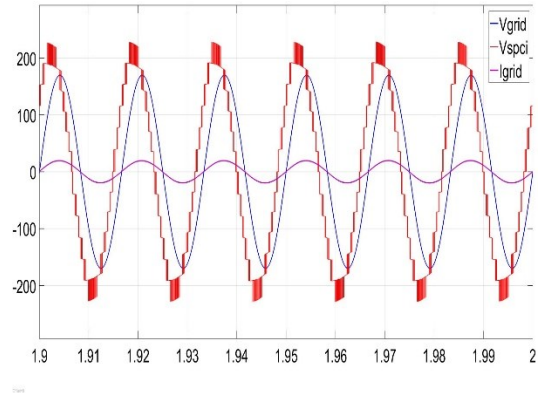

FIGURE 8.15: Simulation waveforms when the inverters are operating under uniform irradiation of 1000W/m^2, with Maximum Power Point Tracking (MPPT) algorithm implemented for Sorted Staircase Modulation (SPWM).

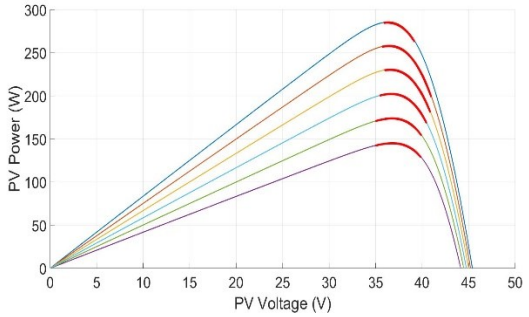

FIGURE 8.16: P-V curves showing the maximum power point operation of all the PV panels highlighted in red, operating under non - uniform irradiation. (1000W/m^2, 900W/m^2, 800W/m^2, 700W/m^2, 600W/m^2, 500W/m^2.), with Maximum Power Point Tracking (MPPT) algorithm implemented for Sorted Staircase Modulation (SPWM).

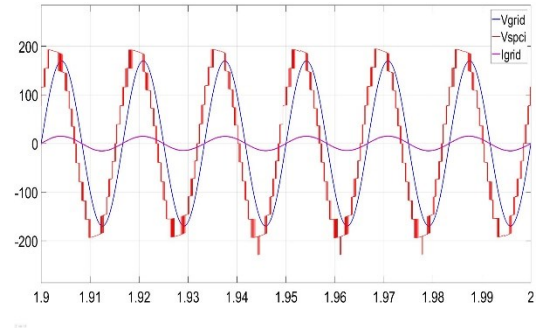

FIGURE 8.17: Simulation waveforms when the inverters are operating under non - uniform irradiation. (1000W/m^2, 900W/m^2, 800W/m^2, 700W/m^2, 600W/m^2, 500W/m^2.), with Maximum Power Point Tracking (MPPT) algorithm implemented for Sorted Staircase Modulation (SPWM).

CHAPTER 9 : EXPERIMENTAL SETUP

9.1. Introduction

In this chapter the prototype construction of Solar Panel Companion Inverters (SPCIs) and demonstration of principle of operation, grid tied operation and Maximum Power Point Tracking (MPPT) algorithm implementation is presented. Section 9.2 discussed the construction of laboratory prototype to demonstrate the working of SPCI. Grid tie operation of grid connected SPCI system is presented in Section 9.3. Section 9.4 demonstrates the MPPT implementation of grid connected SPCI, as well as the reactive power support. Section 9.5 concludes with a brief summary.

9.2. Prototype Construction

The first step involved in the construction of grid connected Solar Panel Companion Inverters (SPCIs) is establishing the setup as shown in Figure 9.1. It may be seen that each H-bridge inverter is connected to a DC power supply. Before establishing the grid tie operation, it is important to demonstrate the principle of operation of SPCI, wherein each inverter synthesizes a quasi-square wave output voltage, depending on the DC bus voltage measured across the DC terminals of each SPCI. Figure 9.2 shows the detailed circuit schematic of all the six SPCIs connected to isolated DC power supplies. Once piccolo micro controller can generate PWM signals for three SPCIs. Hence, two piccolo micro controllers are used. Each microcontroller is connected to three of the SPCIs. The analog DC bus voltage of each SPCI, measured and scaled down using a voltage sensor, is received

by both the microcontrollers. These DC bus voltage signals are utilized in the sort and stack algorithm as discussed in Chapter 3. The sort and stack algorithm executed in both the microcontrollers also generate the PWM signals to switch the corresponding SPCIs. Figure 9.3 shows the experimental prototype that has been constructed in the laboratory for realization of the proposed modulation strategies for the Solar Panel Companion Inverter SPCI. This prototype can be used to synthesize a 120V AC rms voltage. Three DC power supplies are used to connect to the DC terminals of SPCI. Each DC power supply has two channels capable of generating up to 30 V DC. Each of these channels are operated in isolated mode and are connected to each of the DC terminals of SPCI. The output voltage generated by each inverter is based on the principle of sort and stack algorithm. So, the module which has more available power would generate more power. Two F28035 Piccolo microcontrollers operating in synchronism, are used to control the six inverter bridges. Figure 9.4 shows the hardware prototype of the working SPCI system with a resistive load and an inductive (L) filter connected at the output. Figure 9.5 shows the output voltage waveforms Vinv1, Vinv2, and Vinv3, measured across first three SPCIs. Similarly, Figure 9.6 shows the output voltage waveforms Vinv4, Vinv5, and Vinv6, measured across the remaining three SPCIs. The DC bus voltage of each SPCI is set to a different value. It may be seen that the output voltage of each SPCI is an AC quasi-square wave having different widths. The SPCI with the highest measured DC bus voltage synthesizes an AC quasi-square wave with the highest width. Hence, the width of the output quasi-square wave is proportional to the DC bus voltage measured across the terminals of the SPCI. Figure 9.7 shows the aggregated AC output voltage, Vspci measured across all the SPCI. By increasing the number of SPCI modules, the quality of AC output voltage waveform can

be improved. Ispci is the load current measured at the output of SPCI. The load current is more sinusoidal because of the presence of L filter in the output.

9.3. Grid Tie Operation

The resistive load used in section 9.2 is removed, and a single-phase autotransformer is connected to emulate an AC grid. The grid voltage can be adjusted to the required voltage level using the single-phase autotransformer. Closed loop current control operation of the grid tied SPCI is performed on the experimental prototype. Firstly, the AC grid voltage is adjusted to about 97 V AC rms. The DC voltages of each power supply is gradually increased to about 30 V DC. It is made sure that the DC bus voltages across all the SPCIs are different. To inject active power into the grid, reference current along d-axis ramped up in steps to 3.5 A, and reference current along q-axis is set to zero. Experimental waveforms demonstrating active power injection into the grid may be seen in Figure 9.8. It may be seen that the grid current (Igrid) is in phase with the grid voltage (Vgrid).

9.4. Demonstration of Maximum Power Extraction using Real Solar Panels

Three of the Solar Panel Companion Inverter (SPCI) modules that have been used for the prototype described in Section 9.2 are utilized to connect to three of the PV panels as maybe seen in Figure 9.9. Three SPCIs used to demonstrate maximum power extraction from the panels maybe seen in Figure 9.10. Voltage across the PV terminals measured inside the lab, when operating at maximum power point (with full sunlight) is 23.75 V DC. Three of the panels generate a total DC voltage of 71.25 V DC. Hence, the grid voltage is chosen to be 45 V ac rms. The grid voltage is set to 45 V ac rms using the single-phase autotransformer as shown in Figure 9.11. Maximum Power Point Tracking (MPPT) algorithm has been employed together with the closed loop current control technique to

inject active power into the grid. Figure 9.12 shows the experimental waveforms captured during a sunny mid-day. Vgrid is the grid voltage, Vspci is the output voltage measured across the terminals of grid connected SPCI, Igrid is the grid current injected. An AC rms current of 8.67 A is injected into the grid, in phase with the grid voltage having an AC rms voltage of 45. This corresponds to an average power of about 396 W. The average power drawn from each of the three PV panels, assuming identical PV curves, would be 132 W. This operating point is marked on the power curve shown in Figure 9.13. The power curve is obtained by connecting a variable resistor and varying the resistance from minimum resistance to maximum resistance. The experiment is repeated later in the afternoon, when the available power is less compared to that of the mid-day. Figure 9.14 shows the experimental waveforms captured when the available power is less. It may be seen that the rms value of AC current injected into the grid is 6.54 A, which is less than the current injected during the mid-day. To demonstrate the reactive power control, the experiment is performed by injecting the reactive component of current. Figure 9.15 shows the experimental waveforms captured when the SPCI injects a component of reactive power along with the active power component. It may be seen that the grid current is not in phase with the grid voltage which shows that the SPCI is participating in reactive power injection into the grid.

9.5. Summary

This chapter presented the construction of laboratory prototype of six SPCIs for performing experiments. Closed loop current control (that has been implemented in Chapter 4 and Chapter 5) has been implemented in this chapter to demonstrate the grid tied operation of grid connected SPCI. A single-phase autotransformer has been used to adjust

the grid voltage to required level. Three of the SPCIs are connected to three solar panels, to demonstrate the maximum power extraction. The grid voltage is set to 45 V AC rms to interconnect the three SPCI system to AC grid. System level Maximum Power Point Tracking (MPPT) algorithm (that has been used in Chapter 6) has been used in this chapter as well. The operating point of the solar panels has been shown on a PV curve. Demonstration of reactive power exchange when the intensity of sunlight is less has also been presented.

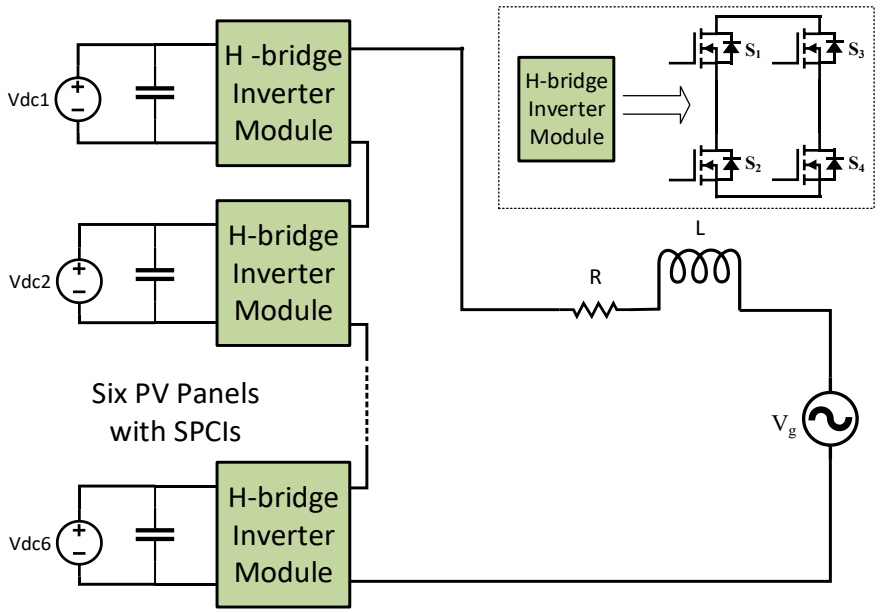

FIGURE 9.1: Simplified circuit schematic of Solar Panel Companion Inverters (SPCI), with ideal DC voltage sources on the DC terminals and connected to a 120 V AC rms distribution grid.

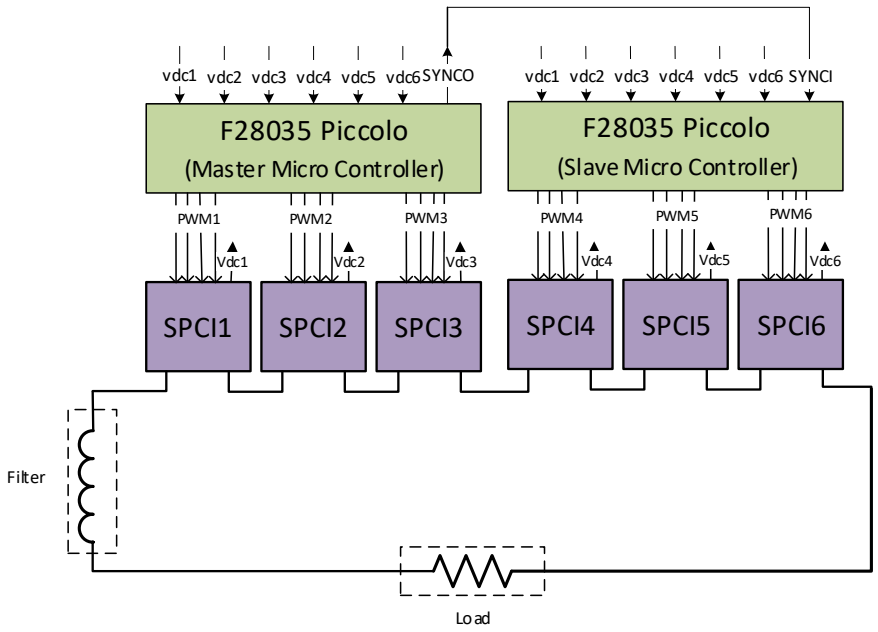

FIGURE 9.2: Detailed circuit schematic showing the Solar Panel Companion Inverters (SPCIs) connected across a resistive load, with an inductive filter.

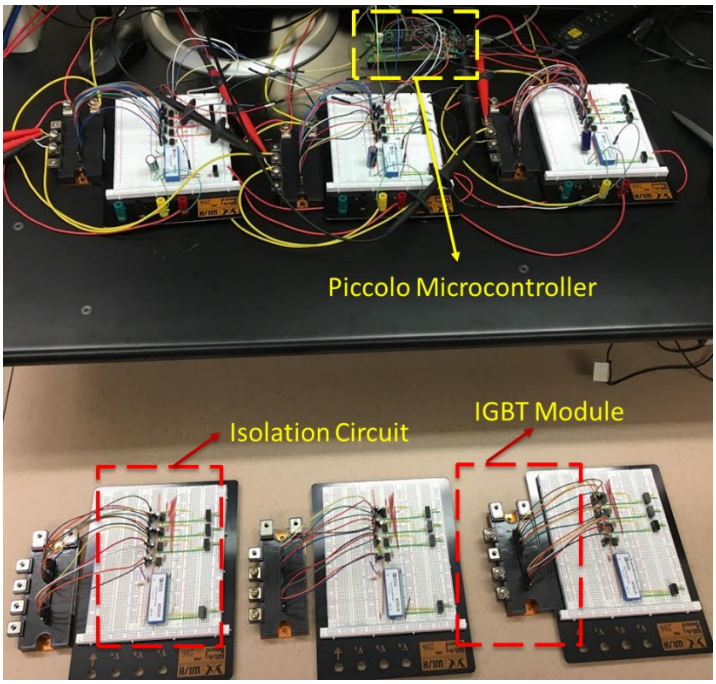

FIGURE 9.3: Hardware prototype showing piccolo microcontroller and Solar Panel Companion Inverter (SPCI) constructed using IGBT modules and isolation circuit.

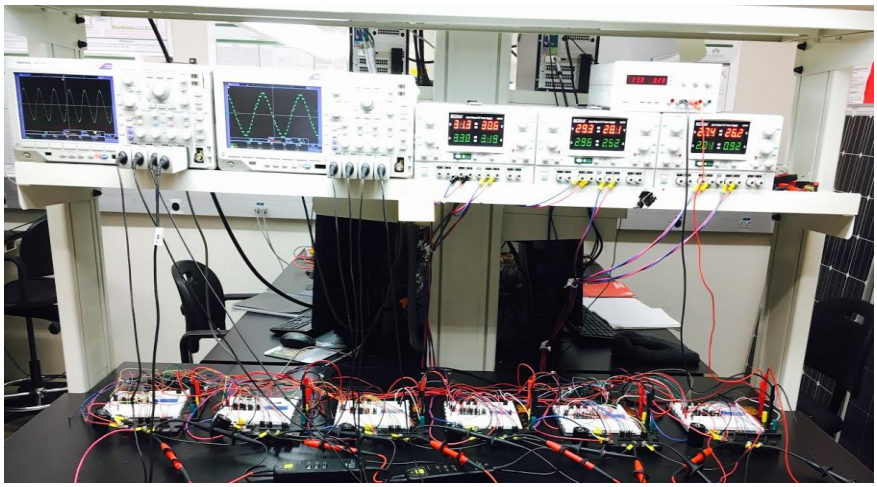

FIGURE 9.4: Working Hardware prototype showing Solar Panel Companion Inverters (SPCI) when connected across a load.

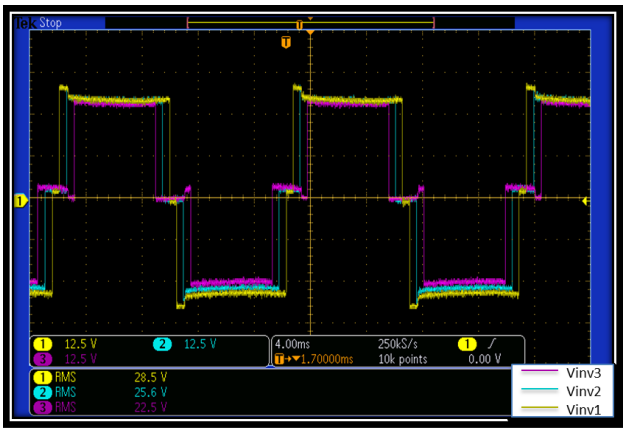

FIGURE 9.5: Experimental waveforms showing output voltages, Vinv1, Vinv2, and Vinv3 measured across first three inverters.

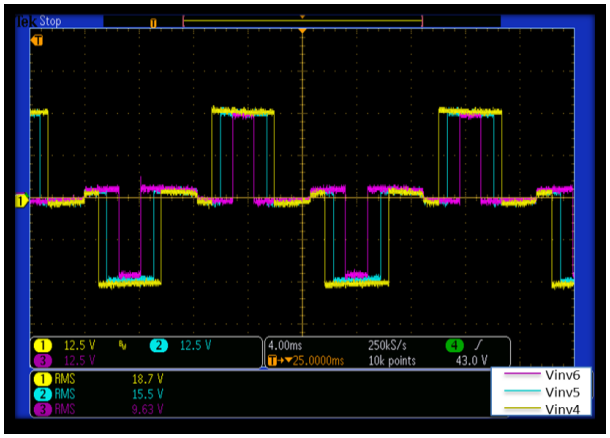

FIGURE 9.6: Experimental waveforms showing output voltages, Vinv4, Vinv5, and Vinv6 measured across last three inverters.

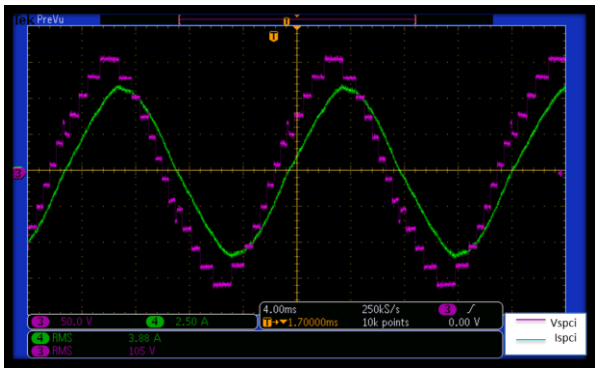

FIGURE 9.7: Experimental waveforms showing the output voltage Vspci, measured across the output of all the SPCIs, and the output current, Ispci flowing through the load.

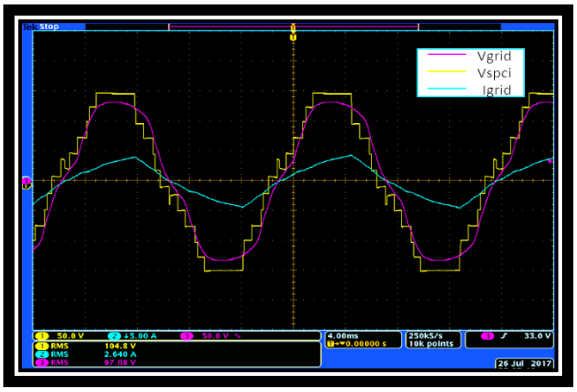

FIGURE 9.8: Experimental waveforms showing active power injection into the grid when DC power supplies are connected at the DC terminals of Solar Panel Companion Inverters and interfaced to the AC grid. Vgrid is the grid voltage, Vpsci is the output voltage of Solar Panel Companion Inverter, Igrid is the grid current injected into the grid.

FIGURE 9.9: PV panels utilized for demonstrating maximum power extraction and grid tie operation.

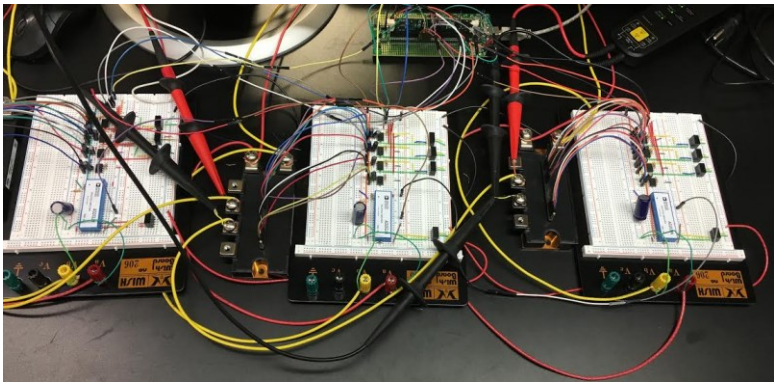

FIGURE 9.10: Hardware prototype showing piccolo microcontroller and Solar Panel Companion Inverter (SPCI) constructed using IGBT modules and isolation circuit.

FIGURE 9.11: Hardware prototype showing piccolo microcontroller and Solar Panel Companion Inverter (SPCI) constructed using IGBT modules and isolation circuit.

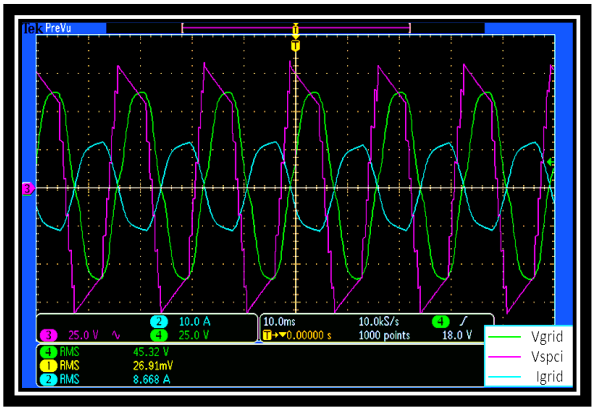

FIGURE 9.12: Experimental waveforms captured during mid-day, when available power is maximum, demonstrate active power injection into the grid from Solar Panel Companion Inverters (SPCIs).

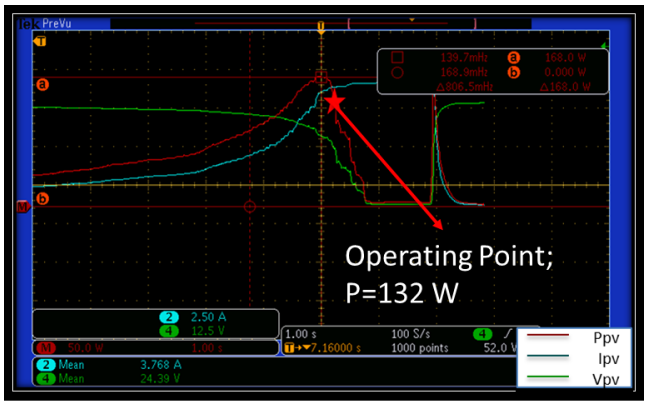

FIGURE 9.13: Power curve obtained by varying the resistance of a variable resistor connected across the terminals of a PV panel. The highlighted 'star' shows the maximum power point operation of SPCI.

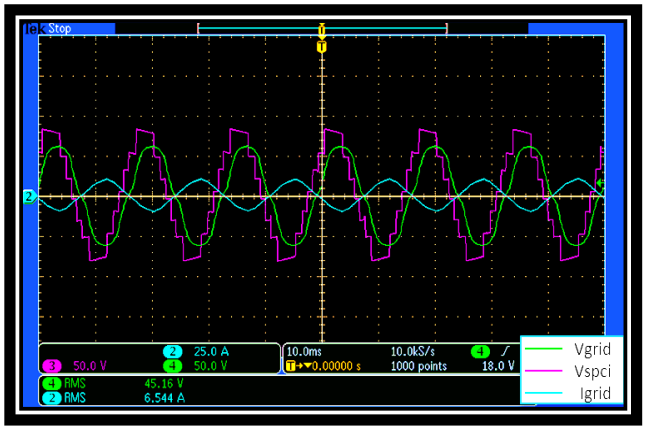

FIGURE 9.14: Experimental waveforms captured in the afternoon, when available power is less than that of mid-day, and MPPT is implemented to demonstrate active power injection into the grid from Solar Panel Companion Inverters (SPCIs).

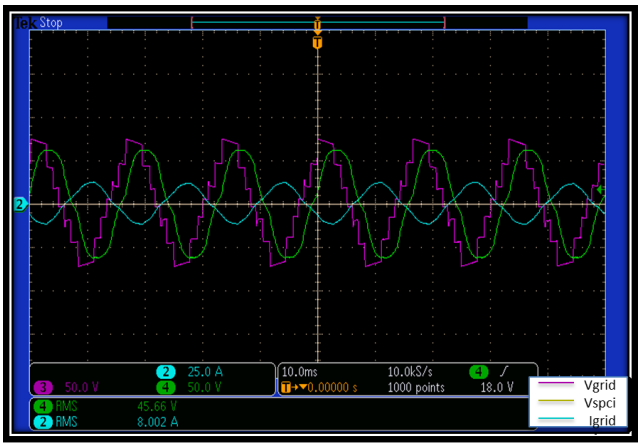

FIGURE 9.15: Experimental waveforms captured in the afternoon, when available power is less than that of mid-day, and MPPT is implemented to demonstrate reactive power injection into the grid from Solar Panel Companion Inverters (SPCIs), while maintaining the maximum power operation.

CHAPTER 10 : CONCLUSION

10.1. Summary

In this dissertation, an investigation of a unique methodology (Solar Panel Companion Inverters) that converts the conventional DC voltage output of a solar panel to switched quasi-square wave voltages with variable pulse width, which when aggregated realize a superior quality multilevel waveform that can be directly interfaced with the power grid, was performed. Dynamic analysis and closed loop control design was performed for grid connected SPCI. This closed loop control worked together with the Sort and Stack algorithm to synthesize AC power. A system level Maximum Power Point Tracking (MPPT) implementation for grid connected SPCI was proposed. It was demonstrated that the algorithm was able to extract maximum power from the system for both uniform and non-uniform irradiation. Sort and Stack algorithm in conjunction with MPPT algorithm was implemented to control active and reactive power flow into the grid and demonstrate the power transfer operating spaces of grid connected SPCI. A panel level optimization scheme was proposed and implemented to ensure maximum power extraction at panel level under all operating scenarios.

Demonstration of closed loop current control and grid tie operation was implemented in hardware. Six Solar Panel Companion Inverter Modules have been built for demonstrating the principle of operation and closed loop current control. Maximum Power Point Tracking (MPPT) algorithm has been implemented in hardware to inject maximum

power into the grid. In doing so, three of the SPCIs were connected to PV panels and the grid voltage was adjusted to 45 V AC rms using a single-phase autotransformer. Experimentally, it was demonstrated that grid connected Solar Panel Companion Inverters can participate in active and reactive power injection into the grid.

10.2. Future Work

Mitigation of DC bus voltage ripple to improve the percentage power conversion and enhance the lifetime of the DC bus capacitance maybe explored. Also, a distributed control scheme which reduces the complexity of controls and the communication wiring needs to be explored. To make the system entirely distributed, an implementation wherein the AC interfacing inductance can also be distributed along with the SPCI needs maybe explored.

REFERENCES

[1] U.S Energy Information Administration (July 1 2019). *Today in energy*.

[2] U.S Energy Information Administration "Short-term energy outlook," July 2019.

[3] Sahu, P. K. (2014). Control strategies for solar panel companion inverters (Order No. 1585388). Available from Dissertations & Theses @ University of North Carolina Charlotte; ProQuest Dissertations & Theses Global. (1666836472). Retrieved from https://librarylink.uncc.edu/login?url=https://search-proquest-com.librarylink.uncc.edu/docview/1666836472?accountid=14605

[4] US. Department of Energy "$1/W Photovoltaic Systems: White Paper to Explore a Grand Challenge for electricity from Solar."

[5] Solarfennel Corp "Solar Fennel 280W PS7A-280."

[6] M. Díez-Mediavilla, M. Dieste-Velasco, M. d. C. Rodríguez-Amigo, T. García-Calderón, and C. Alonso-Tristán, "Performance of grid-tied PV facilities based on real data in Spain: Central inverter versus string system," *Energy Conversion and Management,* vol. 86, pp. 1128-1133, 2014.

[7] H. Bergveld *et al.*, "Module-level DC/DC conversion for photovoltaic systems," in *Telecommunications Energy Conference (INTELEC), 2011 IEEE 33rd International*, 2011, pp. 1-9: IEEE.

[8] L. Hassaine, E. OLias, J. Quintero, and V. Salas, "Overview of power inverter topologies and control structures for grid connected photovoltaic systems," *Renewable and Sustainable Energy Reviews,* vol. 30, pp. 796-807, 2014.

[9] S. B. Kjaer, J. K. Pedersen, and F. Blaabjerg, "Power inverter topologies for photovoltaic modules-a review," in *Industry Applications Conference, 2002. 37th IAS Annual Meeting. Conference Record of the*, 2002, vol. 2, pp. 782-788: IEEE.

[10] S. B. Kjaer, J. K. Pedersen, and F. Blaabjerg, "A review of single-phase grid-connected inverters for photovoltaic modules," *IEEE transactions on industry applications,* vol. 41, no. 5, pp. 1292-1306, 2005.

[11] A. Elasser, M. Agamy, J. Sabate, R. Steigerwald, R. Fisher, and M. Harfman-Todorovic, "A comparative study of central and distributed MPPT architectures for megawatt utility and large scale commercial photovoltaic plants," in *IECON 2010-36th Annual Conference on IEEE Industrial Electronics Society*, 2010, pp. 2753-2758: IEEE.

[12] B. Vermulst, C. Wijnands, and J. Duarte, "Isolated high-efficiency DC/DC converter for photovoltaic applications," in *IECON 2012-38th Annual Conference on IEEE Industrial Electronics Society*, 2012, pp. 506-511: IEEE.

[13] M. Calais and V. G. Agelidis, "Multilevel converters for single-phase grid connected photovoltaic systems-an overview," in *Industrial Electronics, 1998. Proceedings. ISIE'98. IEEE International Symposium on*, 1998, vol. 1, pp. 224-229: IEEE.

[14] P. Salodkar, N. Sandeep, P. Kulkarni, and R. Udaykumar, "A comparison of seven-level inverter topologies for multilevel DC-AC power conversion," in *Power Electronics, Drives and Energy Systems (PEDES), 2014 IEEE International Conference on*, 2014, pp. 1-6: IEEE.

[15] S. Busquets-Monge, J. Rocabert, P. Rodríguez, S. Alepuz, and J. Bordonau, "Multilevel diode-clamped converter for photovoltaic generators with independent voltage control of each solar array," *IEEE Transactions on Industrial electronics,* vol. 55, no. 7, pp. 2713-2723, 2008.

[16] E. Ozdemir, S. Ozdemir, and L. M. Tolbert, "Fundamental-frequency-modulated six-level diode-clamped multilevel inverter for three-phase stand-alone photovoltaic system," *IEEE Transactions on Industrial Electronics,* vol. 56, no. 11, pp. 4407-4415, 2009.

[17] M. C. Cavalcanti, A. M. Farias, K. C. Oliveira, F. A. Neves, and J. L. Afonso, "Eliminating leakage currents in neutral point clamped inverters for photovoltaic systems," *IEEE Transactions on Industrial Electronics,* vol. 59, no. 1, pp. 435-443, 2012.

[18] L. Zhang, K. Sun, L. Feng, H. Wu, and Y. Xing, "A family of neutral point clamped full-bridge topologies for transformerless photovoltaic grid-tied inverters," *IEEE Transactions on Power Electronics,* vol. 28, no. 2, pp. 730-739, 2013.

[19] H. Xiao and S. Xie, "Transformerless split-inductor neutral point clamped three-level PV grid-connected inverter," *IEEE transactions on power electronics,* vol. 27, no. 4, pp. 1799-1808, 2012.

[20] X. Guo, M. C. Cavalcanti, A. M. Farias, and J. M. Guerrero, "Single-carrier modulation for neutral-point-clamped inverters in three-phase transformerless photovoltaic systems," *IEEE Transactions on power Electronics,* vol. 28, no. 6, pp. 2635-2637, 2013.

[21] I.-D. Kim, E.-C. Nho, H.-G. Kim, and J. S. Ko, "A generalized undeland snubber for flying capacitor multilevel inverter and converter," *IEEE transactions on industrial electronics,* vol. 51, no. 6, pp. 1290-1296, 2004.

[22] M. Khazraei, H. Sepahvand, K. Corzine, and M. Ferdowsi, "A generalized capacitor voltage balancing scheme for flying capacitor multilevel converters," in *Applied Power Electronics Conference and Exposition (APEC), 2010 Twenty-Fifth Annual IEEE*, 2010, pp. 58-62: IEEE.

[23] Y. Liang and C. Nwankpa, "A power-line conditioner based on flying-capacitor multilevel voltage-source converter with phase-shift SPWM," *IEEE Transactions on industry applications,* vol. 36, no. 4, pp. 965-971, 2000.

[24] A. Shukla, A. Ghosh, and A. Joshi, "Capacitor voltage balancing schemes in flying capacitor multilevel inverters," in *Power Electronics Specialists Conference, 2007. PESC 2007. IEEE*, 2007, pp. 2367-2372: IEEE.

[25] P. Cortés, A. Wilson, S. Kouro, J. Rodriguez, and H. Abu-Rub, "Model predictive control of multilevel cascaded H-bridge inverters," *IEEE Transactions on Industrial Electronics,* vol. 57, no. 8, pp. 2691-2699, 2010.

[26] E. Villanueva, P. Correa, J. Rodríguez, and M. Pacas, "Control of a single-phase cascaded H-bridge multilevel inverter for grid-connected photovoltaic systems," *IEEE Transactions on Industrial Electronics,* vol. 56, no. 11, pp. 4399-4406, 2009.

[27] Z. Du, L. M. Tolbert, B. Ozpineci, and J. N. Chiasson, "Fundamental frequency switching strategies of a seven-level hybrid cascaded H-bridge multilevel inverter," *IEEE Transactions on Power Electronics,* vol. 24, no. 1, pp. 25-33, 2009.

[28] B. Xiao, L. Hang, J. Mei, C. Riley, L. M. Tolbert, and B. Ozpineci, "Modular cascaded H-bridge multilevel PV inverter with distributed MPPT for grid-connected applications," *IEEE Transactions on Industry Applications,* vol. 51, no. 2, pp. 1722-1731, 2015.

[29] O. Alonso, P. Sanchis, E. Gubia, and L. Marroyo, "Cascaded H-bridge multilevel converter for grid connected photovoltaic generators with independent maximum power point tracking of each solar array," in *Power Electronics Specialist Conference, 2003. PESC'03. 2003 IEEE 34th Annual*, 2003, vol. 2, pp. 731-735: IEEE.

[30] S. Kouro, B. Wu, Á. Moya, E. Villanueva, P. Correa, and J. Rodríguez, "Control of a cascaded H-bridge multilevel converter for grid connection of photovoltaic systems," in *Industrial Electronics, 2009. IECON'09. 35th Annual Conference of IEEE*, 2009, pp. 3976-3982: IEEE.

[31] H. Sepahvand, J. Liao, and M. Ferdowsi, "Investigation on capacitor voltage regulation in cascaded H-bridge multilevel converters with fundamental frequency switching," *IEEE Transactions on industrial electronics,* vol. 58, no. 11, pp. 5102-5111, 2011.

[32] E. Guan, P. Song, M. Ye, and B. Wu, "Selective harmonic elimination techniques for multilevel cascaded H-bridge inverters," in *Power Electronics and Drives Systems, 2005. PEDS 2005. International Conference on*, 2005, vol. 2, pp. 1441-1446: IEEE.

[33] W. Zhao, H. Choi, G. Konstantinou, M. Ciobotaru, and V. G. Agelidis, "Cascaded H-bridge multilevel converter for large-scale PV grid-integration with isolated DC-DC stage," *PEDG, IEEE,* 2012.

[34] I. Ahmed and V. B. Borghate, "Simplified space vector modulation technique for seven-level cascaded H-bridge inverter," *IET Power Electronics,* vol. 7, no. 3, pp. 604-613, 2014.

[35] Y. Cao and L. M. Tolbert, "11-level cascaded H-bridge grid-tied inverter interface with solar panels," in *2010 Twenty-Fifth Annual IEEE Applied Power Electronics Conference and Exposition (APEC)*, 2010, pp. 968-972: IEEE.

[36] H. Jafarian *et al.*, "Design and implementation of distributed control architecture of an AC-stacked PV inverter," in *Energy Conversion Congress and Exposition (ECCE), 2015 IEEE*, 2015, pp. 1130-1135: IEEE.

[37] H. Jafarian, B. Parkhideh, J. Enslin, R. Cox, and S. Bhowmik, "On reactive power injection control of distributed grid-tied AC-stacked PV inverter architecture," in *Energy Conversion Congress and Exposition (ECCE), 2016 IEEE*, 2016, pp. 1-6: IEEE.

[38] H. Jafarian, S. Bhowmik, and B. Parkhideh, "Hybrid Current-/Voltage-Mode Control Scheme for Distributed AC-Stacked PV Inverter With Low-Bandwidth Communication Requirements," *IEEE Transactions on Industrial Electronics,* vol. 65, no. 1, pp. 321-330, 2018.

[39] L. Angquist and L. Lindberg, "Inner phase angle control of voltage source converter in high power applications," in *Power Electronics Specialists Conference, 1991. PESC'91 Record., 22nd Annual IEEE*, 1991, pp. 293-298: IEEE.

[40] L. Xu, V. Agelidis, and E. Acha, "Development considerations of DSP-controlled PWM VSC-based STATCOM," *IEE Proceedings-Electric Power Applications,* vol. 148, no. 5, pp. 449-455, 2001.

[41] M. C. Chandorkar, D. M. Divan, and R. Adapa, "Control of parallel connected inverters in standalone AC supply systems," *IEEE Transactions on Industry Applications,* vol. 29, no. 1, pp. 136-143, 1993.

[42] A. R. Bergen, "Power systems analysis," 1986.

[43] A. Yazdani and R. Iravani, *Voltage-sourced converters in power systems: modeling, control, and applications*. John Wiley & Sons, 2010.

[44] M. P. Kazmierkowski and L. Malesani, "Current control techniques for three-phase voltage-source PWM converters: A survey," *IEEE Transactions on industrial electronics,* vol. 45, no. 5, pp. 691-703, 1998.

[45] C. Meza, J. J. Negroni, D. Biel, and F. Guinjoan, "Energy-balance modeling and discrete control for single-phase grid-connected PV central inverters," *IEEE Transactions on industrial electronics,* vol. 55, no. 7, pp. 2734-2743, 2008.

[46] M. Ciobotaru, R. Teodorescu, and F. Blaabjerg, "Control of single-stage single-phase PV inverter," *EPE Journal,* vol. 16, no. 3, pp. 20-26, 2006.

[47] N. Femia, G. Petrone, G. Spagnuolo, and M. Vitelli, "Optimization of perturb and observe maximum power point tracking method," *IEEE transactions on power electronics,* vol. 20, no. 4, pp. 963-973, 2005.

[48] N. Fermia, D. Granozio, G. Petrone, and M. Vitelli, "Predictive & adaptive MPPT perturb and observe method," *IEEE Transactions on Aerospace and Electronic Systems,* vol. 43, no. 3, 2007.

[49] M. A. Elgendy, B. Zahawi, and D. J. Atkinson, "Assessment of perturb and observe MPPT algorithm implementation techniques for PV pumping applications," *IEEE transactions on sustainable energy,* vol. 3, no. 1, pp. 21-33, 2012.

[50] S. Alsadi and B. Alsayid, "Maximum power point tracking simulation for photovoltaic systems using perturb and observe algorithm," *International Journal of Engineering and Innovative Technology (IJEIT),* vol. 2, no. 6, pp. 80-85, 2012.

[51] B. Liu, S. Duan, F. Liu, and P. Xu, "Analysis and improvement of maximum power point tracking algorithm based on incremental conductance method for photovoltaic array," in *Power Electronics and Drive Systems, 2007. PEDS'07. 7th International Conference on*, 2007, pp. 637-641: IEEE.

[52] G. J. Kish, J. J. Lee, and P. Lehn, "Modelling and control of photovoltaic panels utilising the incremental conductance method for maximum power point tracking," *IET Renewable Power Generation,* vol. 6, no. 4, pp. 259-266, 2012.

[53] A. Safari and S. Mekhilef, "Simulation and hardware implementation of incremental conductance MPPT with direct control method using cuk converter," *IEEE transactions on industrial electronics,* vol. 58, no. 4, pp. 1154-1161, 2011.

[54] Z. Xuesong, S. Daichun, M. Youjie, and C. Deshu, "The simulation and design for MPPT of PV system based on incremental conductance method," in *information engineering (ICIE), 2010 WASE international conference on*, 2010, vol. 2, pp. 314-317: IEEE.

[55] A. Safari and S. Mekhilef, "Incremental conductance MPPT method for PV systems," in *Electrical and computer engineering (CCECE), 2011 24th Canadian Conference on*, 2011, pp. 000345-000347: IEEE.

[56] T. Esram and P. L. Chapman, "Comparison of photovoltaic array maximum power point tracking techniques," *IEEE Transactions on energy conversion,* vol. 22, no. 2, pp. 439-449, 2007.

[57] F. He, Z. Zhao, L. Yuan, and S. Lu, "A DC-link voltage control scheme for single-phase grid-connected PV inverters," in *Energy Conversion Congress and Exposition (ECCE), 2011 IEEE*, 2011, pp. 3941-3945: IEEE.

[58] S. Golestan, M. Monfared, J. M. Guerrero, and M. Joorabian, "A DQ synchronous frame controller for single-phase inverters," in *Power Electronics, Drive Systems and Technologies Conference (PEDSTC), 2011 2nd*, 2011, pp. 317-323: IEEE.

[59] H. Cha, T.-K. Vu, and J.-E. Kim, "Design and control of Proportional-Resonant controller based Photovoltaic power conditioning system," in *Energy Conversion Congress and Exposition, 2009. ECCE 2009. IEEE*, 2009, pp. 2198-2205: IEEE.

[60] P. K. Sahu and M. Manjrekar, "Control strategies for solar panel companion inverters," in *2015 IEEE Applied Power Electronics Conference and Exposition (APEC)*, 2015, pp. 3075-3082: IEEE.

[61] U. d. A. Miranda, L. Rolim, and M. Aredes, "A DQ synchronous reference frame current control for single-phase converters," in *Power Electronics Specialists Conference, 2005. PESC'05. IEEE 36th*, 2005, pp. 1377-1381: IEEE.

[62] Sahu, Prasanth Kumar, Madhav Manjrekar, and Ronak Bhatt. "Maximum power point tracking for solar panel companion inverters." In *2017 IEEE 18th Workshop on Control and Modeling for Power Electronics (COMPEL)*, pp. 1-7. IEEE, 2017.

[63] Sahu, Prasanth Kumar, and Madhav Manjrekar. "Investigations on Power Transfer Operating Spaces of Solar Panel Companion Inverters." In *2018 9th IEEE International Symposium on Power Electronics for Distributed Generation Systems (PEDG)*, pp. 1-8. IEEE, 2018.

[64] Sahu, Prasanth Kumar, and Madhav Manjrekar. "A Control Scheme for Panel Level Maximum Power Extraction of Solar Panel Companion Inverters." In *2018 IEEE Energy Conversion Congress and Exposition (ECCE)*, pp. 2524-2530. IEEE, 2018.